I.O.S.

MEASUREMENTS OF SEDIMENT TEMPERATURES, CONDUCTIVITY AND HEAT FLOW IN THE NORTH ATLANTIC AND THEIR RELEVANCE TO RADIOACTIVE WASTE DISPOSAL

BY

M.J. NOEL

REPORT NO. 172

1984

OCEAN DISPOSAL OF HIGH LEVEL RADIACTIVE WASTE
A RESEARCH REPORT PREPARED FOR THE DEPARTMENT OF THE ENVIRONMENT

NATURAL ENVIRONMENT RESEARCH COUNCIL

INSTITUTE OF OCEANOGRAPHIC SCIENCES

INSTITUTE OF OCEANOGRAPHIC SCIENCES

Wormley, Godalming,
Surrey, GU8 5UB.
(0428 - 79 - 4141)

(Director: Dr. A.S. Laughton FRS)

Bidston Observatory,
Birkenhead,
Merseyside, L43 7RA.
(051 - 653 - 8633)

(Assistant Director: Dr. D.E. Cartwright)

Crossway,
Taunton,
Somerset, TA1 2DW.
(0823 - 86211)

(Assistant Director: M.J. Tucker)

When citing this document in a bibliography the reference should be given as

NOEL, M.J. 1984 Measurements of sediment temperatures, conductivity and heat flow in the North Atlantic and their relevance to radioactive waste disposal. *Institute of Oceanographic Sciences, Report*, No. 172, 92pp.

INSTITUTE OF OCEANOGRAPHIC SCIENCES

WORMLEY

Measurements of sediment temperatures, conductivity and heat flow in the North Atlantic and their relevance to radioactive waste disposal

by

*M.J. Noel

I.O.S. Report No. 172

1984

**Present address:*

Department of Geology
Beaumont Building
University of Sheffield
SHEFFIELD, S3 7HF

DEPARTMENT OF THE ENVIRONMENT
RADIOACTIVE WASTE MANAGEMENT
RESEARCH PROGRAMME 1983/84

DoE Report No.: DoE/RW 84.019

Contract Title: The properties of ocean sediments in relation to the disposal of radioactive waste.

DoE Reference: DGR 481/177

Report Title: Measurements of sediment temperatures, conductivity and heat flow in the North Atlantic and their relevance to radioactive waste disposal.

Author: NOEL, M.J.

Date of submission to DoE: 25 January 1984

ABSTRACT

This report describes the methods which were used to measure sediment temperatures, conductivity and heat flow at ten stations in the northeast Atlantic. These have yielded data from a total of 53 individual penetrations. Surface heat fluxes are compared to the values predicted by crustal cooling models while sediment temperature profiles are examined for evidence of vertical pore water advection. No thermal evidence was found for advection through sediments in the Great Meteor East study area. However, non-linear temperature profiles may be evidence for rapid pore water advection at several locations within the King's Trough Flank study region. These results are critically assessed in terms of other factors which may give rise to the observed non-linear temperature profiles.

Keywords

299	DoE sponsored research	94	Disposal under deep ocean bed
		104	Site selection
		114	Thermal aspects
		117	Rock/sediment structure (porosity, fissuring, permeability)
		131	Soils/sediments

This work has been commissioned by the Department of the Environment as part of its radioactive waste management research programme. The results will be used in the formulation of Government policy but, at this stage, they do not necessarily represent Government policy.

CONTENTS

INTRODUCTION

This report describes some measurements of sediment temperature, conductivity and heat flow in a region of the northeast Atlantic shown in Figure 1. The programme of research has involved four cruises extending from February 1981 (Discovery CR118) to March 1983 (Discovery CR134) and attention has concentrated on two areas earmarked for a detailed assessment of the feasibility of the sub-seabed disposal of high-level radioactive waste (Searle, 1979). These are the King's Trough Flank region (KTF) and the area to the east of Great Meteor Seamount (GME) outlined in Figure 1.

It has been shown from previous studies that disturbances to the geothermal gradient in permeable media can indicate the presence of pore-water circulation (Mansure and Reiter, 1979; Bredehoeft and Papadopulos, 1965). Vertical advection at even very low rates would pose a major threat to the integrity of the sediment barrier with regard to the containment of buried radionuclides. For this reason it was felt that detailed thermal measurements could form an important component of the site selection programme.

Knowledge of the mechanisms and rate by which heat is released from the earth's crust is of fundamental importance to an understanding of geotectonic processes (Parsons and Sclater, 1977). In the oceans, new crust is created at active spreading centres by the accretion of cooling magma to the edges of diverging lithospheric plates (Figure 2). Consequently, the temperature distribution depends on the temperature and rate of supply of the source material coupled with the eventual mode of heat loss. Thermal models which treat the oceanic lithosphere as a semi-infinite solid, cooling by conduction, (Davis and Lister, 1974) successfully predict the depth versus $(\text{age})^{\frac{1}{2}}$ relationship observed for the ocean floor but cannot account for the anomalously low measured values of conductive heat flux in areas close to the active spreading centres (Lister, 1972). It is now generally accepted that in these regions the 'missing heat' is being dissipated by hydrothermal circulation through the crust and into the ocean, a process which is aided by the high permeability of young crustal material (Williams et al., 1974; Anderson et al., 1979; Becker et al., 1982; Strens and Cann, 1982). Spatial variations in the magnitude and direction of the hydrothermal circulation could then also explain the scatter in heat flow values adjacent to spreading centres (c.f. Figure 2).

Evidence for hydrothermal circulation in the oceanic crust has been found from direct observations of hot springs on the Galapagos Spreading Centre (Corliss et al., 1979), the East Pacific Rise (RISE, 1980; Macdonald and

Luyendyk, 1981) and in rapid downhole flow at DSDP site 504B (Anderson et al., 1982). With increasing age, the permeability of the basaltic crust probably diminishes due to the precipitation of hydrothermal minerals from solution and this factor, together with the steady accumulation of overlying, low permeability sediments, forces the general convection pattern to change, as shown schematically in Figure 3. It seems likely that, for a time, while the sediments are still thin, the general circulation pattern can penetrate this layer and communicate with the ocean. However, when the hydraulic impedence imposed by the thickening sediments becomes sufficiently high the convection pattern is eventually confined to the basement (Figure 3).

Evidence for the changing convection regime shown in Figure 3 has emerged from detailed measurements of sediment temperature profiles and surface heat flux. Convection beneath a sedimentary blanket with very low permeability should produce an oscillatory heat flow distribution. This has been found in recent, closely-spaced measurements over young oceanic crust near the Galapagos Spreading Centre (Green et al., 1981; Williams et al., 1974), the East Pacific Rise (Becker and Von Herzen, 1983) and the Juan de Fuca Ridge System (Davis et al., 1980).

In the younger transition zone shown in Figure 3, the heat flow distribution will also be oscillatory but, in areas of upwelling, the temperature gradient will decrease with depth due to an advective component of heat transport through the sediment (Mansure and Reiter, 1979). Conversely, where there is downward porewater flow, the gradient will increase with depth. This is explained in more detail below. Anderson et al. (1979) have reported non-linear sediment temperature profiles as evidence for this form of convection in the Crozet and Madagascar Basins. Curved temperature profiles have been suggested as evidence of pore water advection through sediments at other localities including the Sohm Abyssal Plain (Burgess and Judge, 1981), Brazil Basin (Langseth and Herman, 1981), the Galapagos Rift (Becker and Von Herzen, 1983; Williams et al., 1979) and the Mariana Trough (Abbot et al., 1983). In these reports, calculated advection velocities are typically 1m y^{-1}.

The following sections outline the theoretical basis for estimating pore water advection velocities from sediment temperature profiles and the instruments and methods used and then conclude with a summary and appraisal of the results, particularly with regard to the specific radioactive waste disposal study areas.

THERMAL EFFECTS OF POREWATER ADVECTION

If a deep sea sediment is regarded as an immobile medium of uniform conductivity, K, then the conductive heat flux, q, is given by the linear steady state equation,

$$q = -K\frac{dT}{dz} \tag{1}$$

where dT/dz is the vertical temperature gradient. For a linear temperature profile in the absence of advection K must clearly be constant. If the conductivity varies with depth then (1) is rewritten as

$$T(z) = T_o + q\int_{z=0}^{D}\frac{dz}{K(z)} \tag{2}$$

where T_o is the surface temperature and T(z) is the temperature at depth z (Bullard, 1939).

Both the heat flux and sediment temperatures are sensitive to mass movement of either the solid or liquid phases. This effect was first recognised by Bullard et al. (1956) who considered the thermal effects of the churning caused by burrowing organisms. They showed that if q is the actual heat flow and q_e is the heat flow estimated from the temperature gradient and thermal diffusivity κ then,

$$\frac{q - q_e}{q_e} = \pi\left(\frac{VR}{\kappa}\right)^2$$

where V is the vertical velocity component of the sediment movement and R is the radius of the convecting columns. To change the heat flow by as much as 10% in a sediment of diffusivity 2.5 x 10^{-7} m^2s^{-1} requires burrowing to a depth 2R of 10 cm (Peng et al., 1977) at the improbable velocity of ~8 cm per day. This suggests that the mass movement due to burrowing would have a negligible effect on heat flow and sediment temperatures. These conclusions were also drawn by Von Herzen and Uyeda (1963) on the basis of a similar model.

In contrast to shallow burrowing the vertical movement of pore water throughout the sediment column has a greater effect on the temperature distribution. If the heat and fluid flow are in the vertical, z, direction then the sediment temperatures can be obtained from the simplified differential equation

$$\frac{d^2T}{dz^2} - \frac{c\rho v}{K}\frac{dT}{dz} = 0$$

(de Vries, 1958; Stallman, 1963; Mansure and Reiter, 1979) where c, ρ and v are

the specific heat, density and mean velocity of the moving incompressible fluid and K is the thermal conductivity of the sediment-fluid mixture. With boundary conditions $T(z) = T_o$ at $z = 0$ and $T(z) = T_L$ at depth $z = L$, Bredehoeft and Papadopulos (1965) obtain the following solution,

$$\frac{T(z) - T_o}{T_L - T_o} = \frac{e^{\beta z/L} - 1}{e^{\beta} - 1} \text{ where } \beta = \frac{c\rho v L}{K} \qquad (3)$$

Advection causes the temperature profile to become convex in the direction of fluid motion. This effect has been verified experimentally by Kunii and Smith (1961) and Cartwright (1979). In a medium of uniform thermal conductivity the advection velocity can be estimated by varying β in (3) until the best fit is obtained to the temperature profile (e.g. Langseth and Herman, 1981). If the sediment conductivity is not constant, then depths must first be adjusted using (2) such that the integral of the thermal resistance (reciprocal conductivity) increases linearly with depth (Bullard, 1939; Becker and Von Herzen, 1983).

In the presence of advection the total heat flow, q, becomes

$$q = -K \frac{dT}{dz} + c\rho v(T - T_r) \qquad (4)$$

where T_r is a reference temperature at which the energy carried by advection is zero. An alternative method of analysing the temperature profile for advection is given by Mansure and Reiter (1979) who rearrange (4) to obtain

$$\frac{dT}{dz} = \frac{\beta}{L}(T - T_r) - \frac{q}{K}$$

Thus, a plot of dT/dz versus T yields a straight line, slope β/L, from which the advection velocity, v, can be determined. Stallman (1967) has suggested that a more sensitive method is to plot z/L versus $z/L - (T_z - T_o)$ and then to compare this with type curves of z/L versus $z/L - [\exp(\beta z/L) - 1]/[\exp\beta - 1]$. This method is appropriate for $v < 30$ cm y^{-1} (Sorey, 1971; Cartwright, 1979).

In general, when analysing the sediment temperature profiles presented in this report, it has proved satisfactory to estimate β by modelling a temperature profile using equation (3) using the method of least squares. A comprehensive review of theoretical studies relating groundwater movement and temperature distribution is given by Smith and Chapman (1983).

INSTRUMENTATION

The results presented in this report were gathered using two heat probes of a novel design (originally suggested by C.R.B. Lister [see: Hyndman et al., 1978]) based on the 'violin bow' configuration (Figures 4, 5). In this design,

the conflicting requirements of short thermal time constant and high mechanical strength are reconciled by separating the sensing elements from the strength member. The former are thus housed in a slender steel tube which is held taut beside a solid steel lance. The instrument is hence far sturdier than Bullard-type probes which comprise a single, slender lance (Bullard and Day, 1961) and also provides for a closer sensor spacing than is feasible, for example, when placing outriggers on a corer, as in the Ewing method (e.g. Gerard et al., 1962). The short thermal time constant of the bowstring (~1 minute) also enables a rapid approach to thermal equilibrium which, in turn, allows for 'pogo stick'or multiple penetration deployment on a single lowering.

1. Applied Microsystems Probe

Construction of this instrument is shown in Figure 4. The probe was developed from a Pacific Geoscience Center design (Hyndman et al., 1979) and constructed by Applied Microsystems Ltd., Victoria, British Columbia. After initial trials in Loch Etive, the probe was deployed on Discovery Cruise 118.

The instrument head consists of three pressure cases clamped between circular endplates. The cases contain, in turn: a data logger, acoustics and heat pulse electronics, rechargeable batteries. Extending below the head is the 6-cm diameter, 6m-long solid steel strength member in three sections, terminating in a support fin and nose cone. A 0.95-cm diameter steel tube is held taut between the fin and logger housing and at a distance of 8 cm from the strength member. The tube contains an array of thermistors for measuring the sediment temperature. Their resistance values are periodically scanned and recorded by the data logger to give an equivalent temperature resolution of 0.008°C. Also within the tube are lengths of resistance wire which serve as a heater for producing the calibrated heat pulse used in conductivity determinations.

The data logger is a 0.25 inch reel-to-reel type with a capacity for 60,000 ten-bit samples and set to scan once every 15s. Synchronous with the scanning, the logger passes coded information to the acoustics unit which then transmits each of the ten-bit words serially as 12.4 kHz and 11.6 kHz pulses from an ITT ring transducer.

A geophone within the instrument is designed to sense the motion of the probe on the ship's wire and continuously reset an internal clock. After sediment penetration this process ceases and the clock counts a 7.5 min period after which a current is passed through the heater wires to produce a thermal pulse of 15s duration. This releases a nominal energy of 500 joules/m causing a

temperature rise of ~5°C. Temperatures are then logged for about another 7 minutes in order to estimate the sediment conductivity (see below).

This instrument revealed a number of major weaknesses when operated in the deep sea. The main limitation was insufficient weight for full penetration but this was overcome by bolting lead weights onto the strength member. Lack of compliance in the tensioning mechanism of the thermistor string caused it to break during oblique pullouts. The instrument was also troubled by pressure leaks and problems in servicing. This led to the design of an improved probe.

2. The IOS/Cambridge HEAT PROBE*

This instrument (Figure 5) represents a combination of the A.M. temperature logging circuitry, IOS acoustics and a mechanical design by Bullard Laboratories, Cambridge.

The strength member is shorter (4.6m) and coupled to the massive weight stand by a collar and nut arrangement. This head has provision for adding extra weights. The thermistor string attachment at the upper end incorporates a spring-tensioning mechanism which permits about 3 cm of extension to allow for flexure of the strength member.

Two pressure cases house the data logger, heat pulse and acoustics circuitry and rechargeable cells. The data logger has a temperature resolution of 0.008°C. The acoustics are of the pulse delay type for transmission of temperature, near-bottom depth (from an echo sounder) and tilt. The latter is derived from a vertically-mounted accelerometer within the instrument. A typical P.E.S. echogram is shown in Figure 6. The new probe was deployed on Discovery Cruises 126, 131 and 134.

3. Needle Probe

A needle probe was built to measure thermal conductivities of core samples. The theory of the method is presented by Jaeger (1956, 1958). The needle probe approximates a continuous, infinite line source of heat immersed in a material of unknown thermal diffusivity, κ, and conductivity, K. It can thus be shown that the rise in temperature, T, of the probe with time, t, is given to a good approximation by

$$T = \frac{Q}{4K\pi} \cdot \ln\left(\frac{4\kappa t}{Ba^2}\right) \qquad (5)$$

---

* Hydrothermal Enthalpy And Temperature Penetrometer for Repeated Observations in the Benthic Environment

where Q is the heat output per unit length per unit time, a is the probe radius and B = 1.7811. The relationship is valid when $t \gg \frac{a^2}{\kappa}$, the thermal time constant of the probe. In this case, a plot of ΔT versus ln(t) will give a straight line, the slope of which is proportional to K.

Several needle probe designs have been published most of which embody a thermistor temperature sensor and separate heater wires within a hypodermic needle (e.g. Von Herzen and Maxwell, 1959; Bloomer and Ward, 1979). This complex construction limits the minimum needle diameter and hence the thermal time constant to typically 1s.

In an effort to simplify the needle construction, several alternative designs were explored. It was found that adequate temperature resolution (0.01°C) could be obtained over the desired temperature rise (~5°C) by simply monitoring the change in electrical resistance of the stainless steel needle. This concept led to the simple design shown in Figure 7. The probe consists of a 7-cm long, 22-s.w.g. hypodermic tube containing a quartz tube. A 0.18-mm diameter stainless steel wire passes through this tube and is welded to the outer sheath at the tip. The needle is then vacuum impregnated with oil to ensure good thermal contact. The resulting (calculated) thermal time constant is 0.25s.

A four-terminal method is used to monitor changes in needle resistance (2.67Ω) which would otherwise be comparable to changes occurring in the copper leads (1.6Ω). The probe is heated by a 30-Hz, 470-mA square waveform and the resistance monitored by a modified current meter circuit (design by C. Clayson).

A further feature of the instrument is the provision for a logarithmic timebase voltage. Equation (5) can thus be plotted in real time on an XY recorder. Calibration is achieved using a solution of gelatine in water (Hyndman et al., 1979).

DATA PROCESSING

When the heat probe enters the sediments there is a frictional temperature rise which is comparable to the temperature differences which it is required to measure (over 5m). Although the short thermal time constant of the thermistor string accelerates the approach to thermal equilibrium it is, nevertheless, necessary to use a theoretical method to estimate the true in-situ temperature prior to the heat pulse or pullout.

The method employed is described by Bullard (1954) and has been implemented in the program THEQ (Appendix I). The decay in temperature θ, from the initial

frictional heating can be written as,

$$\theta = \theta_{eq} + \theta_{ex} \cdot F(\alpha,\tau) \qquad (6)$$

where θ_{ex} is the initial excess temperature above the required equilibrium temperature θ_{eq}. $F(\alpha,\tau)$ is the cooling function shown in Figure 8 where α is twice the ratio of the thermal capacity of the sediment to that of the probe material, viz.:

$$\alpha = \frac{2\pi a^2 p\sigma}{m}$$

where a = probe radius
p = sediment density
σ = sediment specific heat
m = probe's thermal water equivalent per unit length

For the Applied Microsystems thermistor string $\alpha \simeq 2$. τ is a dimensionless measure of time given by

$$\tau = \frac{\kappa t}{a^2}$$

where κ = sediment thermal diffusivity

The thermal time constant for the probe = $\frac{a^2}{\kappa} \simeq 60$s in this case. The function $F(\alpha,\tau)$ has been tabulated for a range of α,τ by Lister (1979) and is used in THEQ.

In principle, the equilibrium temperature for each thermistor can thus be estimated by adjusting θ_{eq} and θ_{ex} in (6) until the optimum fit of θ to the measured temperatures is obtained . However, the method is unnecessarily tedious and a simpler technique is to choose some time, t_1, near the end of the cooling record and then to find, by reverse interpolation, times t_2 and t_3 at which the temperature correction is twice and three times the correction at t_1. In this way, three estimates can be made of the equilibrium temperature (Bullard, 1954). If τ_1, τ_2 and τ_3 are the corresponding dimensionless times, then from (6)

$$\theta_1 = \theta_{eq} + \theta_{ex} \cdot F(\alpha,\tau_1)$$
$$\theta_2 = \theta_{eq} + \theta_{ex} \cdot F(\alpha,\tau_2)$$
$$\text{and} \quad \theta_3 = \theta_{eq} + \theta_{ex} \cdot F(\alpha,\tau_3)$$

From the average of all possible solutions we find that

$$\theta_{eq} = \frac{7\theta_1 - 5\theta_3 + 4\theta_2}{6}$$

$$\text{and} \quad \theta_{ex} = \frac{5\theta_3 - \theta_1 - 4\theta_2}{6F(\alpha,\tau_1)}$$

This is implemented in THEQ. An additional complication is the unknown origin time of the frictional heat pulse. To overcome this problem, the cooling

profile for the lowest thermistor is first approximated by (6) using values of θ_{eq} and θ_{ex} computed with zero time delay. The procedure is then repeated with delays increasing by one second until the best RMS fit is obtained. This defines an optimum delay which is assumed to be the same for all remaining thermistors for which θ_{eq} and θ_{ex} can then be calculated.

THEQ initially converts the data logger number into real temperatures using a calibration polynomial. The procedure also makes use of the short term stability of the bottom-water temperature to cross-calibrate the thermistor readings. Offsets are calculated from the thermistor temperature immediately prior to penetration and these offsets then added to each subsequent reading such that the temperature scales (while in the sediment) are closely matched. Changes in offset values from penetration to penetration are listed in the data tables and are a good indication of thermistor stability during a station.

CONDUCTIVITY DETERMINATION

Values of in-situ thermal conductivity were determined from the decay of a calibrated heat pulse. The theory of the method is given by Jaeger (1956), Bullard (1954) and Carslaw and Jaeger (1959). Detailed tables of temperatures versus time are given by Huppert and Sclater (1968) and Lister (1979). For times which are long compared to the thermal time constant of the probe the temperature, T, falls as the reciprocal of time, t, viz.:

$$T = \frac{Q}{4\pi K t} \qquad (7)$$

where Q is the energy of the heat pulse per unit length of the probe and K is the sediment thermal conductivity. For shorter times the probe temperature also depends on the sediment thermal diffusivity, κ, and on the probe's heat capacity and diameter and this causes it to depart from the above law. A convenient approach for the determination of the sediment conductivity for short times is to multiply the measured temperatures by a correction factor $C(\alpha,\tau)$, where α and τ were defined earlier. Hyndman et al. (1979) show that

$$C(\alpha,\tau) = \frac{1}{2\alpha\tau F(\alpha,\tau)}$$

When temperatures are corrected in this way it is possible to use (7) to determine conductivity from a cooling period as short as 5 minutes. An example of a cooling profile is given in Figure 9.

Thermal conductivity was determined using program COND (Appendix II) which computes the gradient of a plot of corrected temperatures against 1/t. The program also varies the origin time of the heat pulse in order to optimise the

linearity of the plot. Figure 10 shows the variation in the gradient with changing origin time for some CR134 data. It was found that the continuation of the frictional cooling correction during the heat pulse decay had a negligible effect on the conductivity estimate and the effect has, therefore, been neglected.

Figure 11 summarises a typical temperature record from a penetration which includes a heat pulse. The diagram also indicates the appropriate steps in the data analysis.

RESULTS

The following sections describe the results obtained from four cruises. The data are then discussed in relation to those areas selected as study sites to determine the feasibility of disposal in the sediments of high-level radioactive waste.

Discovery Cruise 118

This cruise provided the first opportunity to test the Applied Microsystems heat probe in water depths up to 6000m and to carry out some initial measurements in the Great Meteor East and King's Trough Flank study areas. Further details of the cruise programme are given in IOS Cruise Report 177 (1981). Five stations were occupied at the locations shown in Figure 1. Three of these were successful. At the first sucessful station (10301) ten penetrations were made by the probe along a 3 nautical miles transect on the northern Madeira Abyssal Plain. However, the temperature data clearly show that the probe had penetrated to depths of only one or two metres (Figures 12, 13). The mean geothermal gradient from these results is 0.076°C/m. No in-situ measurements of thermal conductivity were made. Assuming a typical thermal conductivity value for deep sea sediments of 2×10^{-3} cal cm^{-1} s^{-1} $°C^{-1}$, this gives a mean heat flow of 1.52μ cal cm^{-2} s^{-1} (Table 1).

Station 10318 was located east of Great Meteor Seamount in the Madeira Abyssal Plain (Figure 1). 500 lb. of lead weights were attached to the probe and this ensured a full 5m penetration on four successive 'dips'. The data (Figures 14, 15) show temperature profiles which are linear within the resolution of the instrument. Again, assuming a sediment thermal conductivity of 2×10^{-3} cal cm^{-1} s^{-1} $°C^{-1}$, the mean heat flux for the station is 1.47μ cal cm^{-2} s^{-1} (Table 2).

A third transect was made on the King's Trough Flank study area during

station 10335 (Figure 1). Two penetrations revealed linear temperature profiles within the measurement resolution (Figure 16). However, at the third, a highly non-linear profile was recorded (Figure 17). The sense of curvature implies upward porewater advection. The significance of this result is discussed more fully below. The results for this station are summarised in Table 3.

Experience acquired during this cruise revealed the weaknesses inherent in the Applied Microsystems heat probe.

Discovery/Shackleton Cruise 126

The new IOS/Cambridge heat probe was successfully deployed at three locations in or near the Great Meteor East study area during this cruise (Figure 1). Further details are given in IOS Cruise Report 141. Unfortunately, due to failure of the heat pulse circuitry, no measurements of in-situ thermal conductivity were made. The temperature profiles are shown in Figures 18-21.

At station 10405 six penetrations were made along an approximately 4 nm N-S transect. The results from Dips 1 and 3 reveal smooth, non-linear temperature profiles whose sense of curvature implies downward porewater advection. This is discussed below. The remaining temperature profiles at this station are either linear within the measurement resolution (Dip 2) or show irregularities due to excessive thermistor drift (Dips 4, 5 and 6). This is confirmed by the changeable offsets seen in Table 4. The reason for the drift is unclear.

At the coincident stations S126.3 and S126.5 to the southwest (Figure 22) the sediment temperature profiles were all linear within the resolution of the instrument. The mean geothermal gradient is 0.066°C/m (6 Dips, Tables 5 and 6). Assuming a thermal conductivity of 2×10^{-3} cal cm^{-1} $°C^{-1}$ this gives a mean heat flux of 1.32μcal cm^{-2} s^{-1}.

During this cruise an attempt was made to make simultaneous in-situ measurements of pore pressure by replacing the probe nosepiece with a version containing a porous plate connected to a pressure transducer. Unfortunately, the experiment failed owing to the loss of the apparatus.

Needle-probe measurements of thermal conductivity were made on Kastenlot core 10406 the stratigraphy of which is shown in Figure 23. To test for the presence of thermal conductivity anisotropy, two measurements were made at each level in the core, viz: with the needle vertical and horizontal. Significant differences were found between most pairs of measurements. An example is shown in Figure 24 in which the differing gradients in the T versus log(t) plot is evidence for a conductivity anisotropy.

When the probe is inserted normal to the bedding it measures the geometric average, A_1, of the principal conductivities in the bedding plane, K_x and K_y. When inserted horizontally in the x direction, A_2 is measured as the geometric average of K_z and K_y. Similarly, $A_3 = (K_z \cdot K_x)^{\frac{1}{2}}$. Thus the principal conductivities can be calculated from

$$K_x = \frac{A_1 \cdot A_3}{A_2}, \qquad K_y = \frac{A_1 \cdot A_2}{A_3}, \qquad K_z = \frac{A_2 \cdot A_3}{A_1}$$

This method assumes prior knowledge of the directions x, y and z (principal conductivity directions) and, without this, the method cannot be applied to determine the shape of the conductivity ellipsoid. However, in a deep sea sediment, the lineation in the conductivity is likely to be very small and the main difference in conductivity will be between the horizontal plane and the vertical. Then,

$$K_x = K_y = A_1, \qquad \text{and} \qquad K_z = \frac{(A_2)^2}{A_1}$$

and the % anisotropy is simply, $\frac{2(K_x - K_z)}{K_x + K_z} \times 100$

This has been used to calculate the anisotropy values shown in Figure 23. The maximum value is about 30% with no evidence for a correlation between enhanced anisotropy and lithostratigraphy. It is possible that the anisotropy reflects varying concentrations of platey minerals which are not necessarily confined to the marl or carbonate layers. In the absence of clear trends in the anisotropy profile, it seems very unlikely that a significant thermal conductivity anisotropy change with depth is in some way responsible for the non-linear temperature profiles recorded at the neighbouring station 10405.

Discovery Cruise 131

Two heat flow stations were occupied during the cruise (Figure 1). Station 10601 was situated approximately 120 nm north of King's Trough and station 10606 was located on the NE-end of the southern fragment of the Charlie Gibbs Fracture Zone. Further details are given in IOS Cruise Report 137.

At station 10601 eight penetrations were made along an approximately 3 nm, S-N transect. Unfortunately, the temperature data are of very poor quality because of unstable thermistor calibrations (Figures 25, 26). This is evident from the drifts in offset values seen in Table 7. However, linear temperature profiles are seen at two of the dips (3 and 4) but in isolation this cannot be

taken as evidence for a lack of pore water advection. Correct operation of the heat pulse circuitry has enabled thermal conductivity estimates to be made for dips 1, 2 and 6. The data are given in Table 7.

At station 10606 three dips were attempted but only two were successful. These show linear temperature profiles with the exceptionally high mean geothermal gradient of 0.136°C/m (Figure 27, Table 8). Assuming a typical conductivity (2×10^{-3} cal cm^{-1} s^{-1} $°C^{-1}$) this gives mean heat flux of 272 μcal cm^{-2} s^{-1} which presumably reflects the youth of this site.

Discovery Cruise 134

Two successful stations were occupied during this cruise resulting in a total of 14 good quality temperature records (Figure 1). Furthermore, conductivity measurements were made at each penetration. The results are shown in Figures 28 to 30 and listed in Tables 9 and 10.

Station 10662 was located approximately 180 nautical miles SW of King's Trough. Ten penetrations were made along a transect extending five nautical miles in an approximately SW direction. All the profiles, with the exception of dip 2, were linear within the accuracy of the instrument.

Station 10674 was situated in the vicinity of the Plato and Atlantis seamounts, north of Great Meteor Seamount. Four dips were made along a 1.5 nm transect trending SE. The temperature records indicate partial penetration in each case to a depth of about 3m. However, the temperature profiles show consistent evidence for a gradient which decreases with depth which may imply upward porewater flow. This is discussed further below. Heat flow values at both stations are given in Tables 9 and 10.

Figure 31 shows the vertical sediment conductivity profile for each of the four dips of station 10674. There appears to be a consistent trend of decreasing thermal conductivity with depth, the total change amounting to about 40%. Studies of core samples have shown that the water content of deep sea sediments is highly variable to depths of 10m or more. Since thermal conductivity is inversely related to water content (e.g. Ratcliffe, 1960) these results could thus be explained by a rapid increase in sediment porosity in the first 4m. Alternatively, it is possible that the penetration of the probe has in some way increased the water content of the deeper (disturbed) material by dragging down bottom water and surface material.

DISCUSSION

King's Trough Flank

King's Trough Flank is situated approximately 300 miles northeast of the Azores and 600 miles west of northern Spain in water depths of 3500-4000m (Figures 1, 32). The region is characterised by a relatively rugged terrain with hills and scarps 10-30 km apart and slopes around the hills ranging from 18° to 30°. However, there are also regions of relatively smooth seafloor up to 35 km across where slopes are more subdued (about 2°). The area is mantled by pelagic carbonate sediments whose thickness typically ranges from 0.5-1 km, as revealed by seismic reflection profiling. Although the area was a marginal choice with regard to waste disposal in terms of the selection criteria outlined by Hollister et al. (1976) it was felt that a more detailed assessment was, nevertheless, justified (Searle, 1979). The area selected for close study extends from 41° to 43°N; 20° to 24.5°W. The results of geological and geophysical investigations up to December 1982 are given by Kidd et al. (1983).

Two heat flow stations were occupied in the King's Trough Flank area, as seen in Figure 33, viz. 10335 (CR118) and 10662 (CR134). No other measurements are reported in the World Heat Flow Data Collection (Jessop et al., 1976). Three full penetrations were obtained at the first station in a water depth of 4050m. The mean heat flow value of 1.1μ cal cm^{-2} s^{-1} is close to the expected theoretical value based on the half-plate cooling model of Parsons and Sclater (1977). Significant curvature is present in the temperature profile at the third penetration (Figure 17), the gradient changing by 96% over a depth of 3m. The sense of curvature could imply upward porewater advection since no corresponding curvature is seen in the thermal conductivity profile (Table 3). When the data are modelled using the conduction convection equation (3) the suggested velocity is 52 cm/y. This would be sufficient to raise dissolved waste materials from a depth of, say, 30m to the surface in only 58 years.

However, as previously discussed in Kidd et al. (1983) the data could also be explained by several alternative mechanisms. For example, if changes in bottom water temperature had occurred then a temperature wave could be present in the sediment. The station is close to the base of an abyssal hill where enhanced current velocities may have been the cause of variable bottom water temperature. The curvature in the temperature profile would then reflect the amplitude and phase of the surface disturbance (Noel, in press). The non-linear profile discussed here can be explained by a sudden drop in surface temperature of 0.17°C, 120 days prior to the measurement. However, this temperature change

seems improbable when compared to the far smaller variations recorded by long-term current meters in the northeast Atlantic (Müller, 1981). Similarly, the curvature is unlikely to be due to any regular, seasonal changes in bottom-water temperature which are only important in high latitudes.

The curvature could also be explained by a continuous heat production in the sediment. Possible mechanisms include exothermic chemical reactions during diagenesis or biological activity; the conversion of potential energy into heat during compaction; the attenuation of continuous microseismic noise or the heat released by radioactive decay. Modelling studies show that the curvature present in this profile (Figure 17) would require heat production at the rate of 0.1 cal cm^{-3} y^{-1}. It is difficult to account for such a continuous, high production in a sediment which is accumulating at only 1-2 cm/1000y.

Other explanations include the disturbance caused by rapid sedimentation or erosion, or by uneven topography which can be particularly important when the topographic scale is comparable to the probe length. The insertion of the probe into the sediment may also disrupt the original temperature distribution. These and other factors have been discussed in detail by Noel (in press). In the present context it seems unlikely that unstable sedimentation has been responsible for the non-linearity since the probability of the measurement occurring soon after an erosional event such as a slump is very low. However, the influence of large topographic features such as furrows or sandwaves cannot be ruled out without further detailed mapping. Hence this estimate of the rate of pore-water advection should remain tentative.

Great Meteor East

The general locations of heat-flow stations in the vicinity of Great Meteor Seamount are shown in Figure 22 and in more detail in Figure 34. The world Heat Flow Data Collection (Jessop et al., 1976) lists no previous measurements in this study area.

Station 10674 was situated in a small sedimentary basin at a water depth of about 3400m. The results show consistent non-linear temperature profiles for Dips 2, 3 and 4 whose gradients decrease with depth. At Dip 1 the suggestion of a non-linearity is based on a single temperature reading and is, therefore, best discounted (Figure 30). Assuming, initially, that the curvature is due to advection, the flow rates for Dips 2-4 have been calculated using equation (3) and are listed in Table 10. The mean velocity is 112 cm/y and would be sufficient to raise buried waste materials in solution from a depth of 30m to the

surface in only 27y.

As discussed above, the curvature in these profiles could be explained by a number of alternative mechanisms. It does seem possible that, in this region of relatively shallow water, an increased instability in bottom water temperature could have caused these curved temperature profiles.

Station 10318 is located on the western extremity and 126.3/5 is near the centre of the Madeira Abyssal Plain. Water depths are around 5400m. Both stations record remarkably linear temperature profiles from a total of eight penetrations. This reflects either the absence of pore water movement in the sediment or an increased stability of bottom water temperatures in this deep water basin.

In contrast, although similar physical conditions prevailed at Station 10405, two measurements (Dips 1, 3) recorded the largest departures from linearity of all the temperature profiles described in this report. When the results are modelled using equation (3), downward advection velocities of around 6 m/y are suggested (Table 4). This extreme result seems rather improbable in view of the large differential pore pressures which would be required to drive the pore water through the low permeability underlying sediments. Similarly, it is also difficult to explain these results in terms of a change in bottom water temperature since the required fluctuation is excessive (>1°C) when compared with deep-ocean mooring data from the same area of the Atlantic (Müller, 1981). Alternatively, the curvature may have arisen from a very large conductivity contrast in the surface sediments (rather unlikely), topographic features with wavelengths and heights of several metres or by a slump or turbidity flow less than a year before the measurements were made (Noel, in press).

All dips at Station 10301 (Figures 12, 13) lacked sufficient penetration to assess accurately the probability of pore-water advection from the temperature data.

CONCLUSIONS

The results presented in this report demonstrate the possibility of making rapid, accurate and repeated measurements of sediment temperatures, conductivity and heat flow in the deep ocean using a 'pogostick' method of heat probe deployment.

The non-linear temperature profile recorded in the King's Trough Flank region (10335) may be regarded as possible evidence for a rapid upward advection of porewater. It would be interesting to repeat this measurement as part of a

longer transect intended to discover the overall pattern of porewater circulation.

Two stations (10674, 10405) near the Great Meteor East study area again present possible evidence of rapid pore water advection which should be checked by repeat measurements and by estimates based on other methods. These include O^{18}/O^{16} analyses of porewater linked to micropalaeontological studies, geochemical measurements and by recording directly the sediment pore pressure gradient.

ACKNOWLEDGEMENTS

I am very grateful for the assistance given by the Masters, Officers and crew of the RRS "Discovery" and RRS "Shackleton". I am also grateful to many shipboard scientists who helped with the deployment and operation of the heat flow probes, often under trying conditions.

The final mechanical design of the heat flow probe evolved from discussions with P. Wood and colleagues at Bullard Laboratories, Cambridge, while the circuitry was designed by E. Darlington. M. Harris persuaded it to function at sea. C. Clayson collaborated in the design of the needle probe.

I would also like to thank Gabrielle Mabley for accurately typing the manuscript.

REFERENCES

Abbot, D.H., Menke, W. and Morin, R., 1983. Constraints upon water advection in sediments of the Mariana Trough. J. Geophys. Res., 88, 1075-1093.

Anderson, R.N., Hobart, M.A. and Langseth, M.G., 1979. Geothermal convection through oceanic crust and sediments in the Indian Ocean. Science, 204, 828-832.

Anderson, R.N., Honnorez, J., Becker, K., Adamson, A.C., Alt, J.C., Emmerman, R., Kempton, P.D., Kinoshita, H., Laverne, C., Mottl, M.J. and Newmark, R.L., 1982. DSDP Hole 504B, the first reference section over 1 km through Layer 2 of the oceanic crust. Nature, 300, 589-594.

Becker, K., Von Herzen, R.P., Francis, T.J.G., Anderson, R.N., Honnorez, J., Adamson, A.C., Alt, J.C., Emmerman, R., Kempton, P.D., Kinoshita, H., Laverne, C., Mottle, M.J. and Newmark, R.L., 1982. In-situ electrical resistivity and bulk porosity of the oceanic crust Costa Rica Rift, Nature, 300, 594-598.

Becker, K. and Von Herzen, R.P., 1983. Heat flow on the western flank of the East Pacific Rise at 21°N. J. Geophys. Res., 88, 1057-1066.

Bloomer, J.R. and Ward, J., 1979. A semi-automatic field apparatus for the measurement of thermal conductivities of sedimentary rocks. J. Phys. E. Sci. Instrum., 12, 1033-1035.

Bredehoeft, J.D. and Papadopulos, I.S., 1965. Rates of vertical groundwater movement estimated from the earth's thermal profile. Water Resour. Res., 1, 325-328.

Bullard, E.C., 1939. Heat flow in South Africa. Proc. Roy. Soc., London, A, 173, 474-502.

Bullard, E.C., 1954. The flow of heat through the floor of the Atlantic Ocean. Proc. R. Soc., London, A, 222, 408-429.

Bullard, E.C., Maxwell, A.E. and Revelle, R., 1956. Heat flow through the deep sea floor. Adv. Geophys., 3, 153-181.

Bullard, E.C. and Day, A., 1961. The flow of heat through the floor of the Atlantic Ocean. Geophys. J., 4, 282-292.

Burgess, M. and Judge, A., 1981. Heat flow studies in the Sohm Abyssal Plain and their relevance to nuclear waste disposal investigations. Report to the Div. of Seismology and Geothermal Studies. Energy Mines and Resources, Canada.

Carslaw, H.S. and Jaeger, J.C., 1959. Conduction of heat in solids. Oxford University Press.

Cartwright, K., 1979. Measurement of fluid velocity using temperature profiles: experimental vertification. J. Hydrology, 43, 185-194.

Corliss, J.B., Dymond, J., Gordon, L.I., Edmond, J.M., Von Herzen, R.P., Ballard, R.D., Green, K., Williams, D.L., Bainbridge, A., Crane, K. and Van Andel, T.H., 1979. Submarine thermal springs on the Galapagos Rift. Science, 203, 1073-1083.

Davis, E.E. and Lister, C.R.B., 1974. Fundamentals of ridge crest topography. Earth Planet Sci. Lett., 21, 405-413.

Davis, E.E., Lister, C.R.B., Wade, U.S. and Hyndman, R.D., 1980. Detailed heat flow measurements over the Juan de Fuca Ridge System. J. Geophys Res., 85, 299-310.

De Vries, D.A., 1958. Simultaneous transfer of heat and moisture in porous media. EOS, Trans. AGU, 39, 909-916.

Gerard, R., Langseth, M.G. and Ewing, M., 1962. Thermal gradient measurements in the water and bottom sediments of the western Atlantic. J. Geophys. Res., 67, 785-803.

Green, K.E., Von Herzen, R.P. and Williams, D.L., 1981. The Galapagos Spreading Centre at 86°W: A detailed field study. J. Geophys. Res., 86, 979-986.

Hollister, C.D., Anderson, D.R. and Talbert, D.M., 1976. The first international workshop on seabed disposal of high-level wastes. Proceedings of the International Symposium on the Management of Waste from the LWR Fuel Cycle, 11-16 July 1976, Denver, Colorado, 637-657.

Huppert, H.E. and Sclater, J.G., 1968. On the in-situ measurement of the thermal conductivity of deep-sea sediments. Scripps Inst. Oceanog. Tech. Rept. MPL-U-20/68, La Jolla, California.

Hyndman, R.D., Rogers, G.C., Bone, M.N., Lister, C.R.B., Wade, U.S., Barrett, D.L., Davis, E.E., Lewis, T., Lynch, S. and Seemann, D., 1978. Geophysical measurements in the region of the Explorer Ridge of Western Canada. Can. J. Earth Sci., 15, 1508-1525.

Hyndman, R.D., Davis, E.E. and Wright, J.A., 1979. The measurement of marine geothermal heat flow by a multipenetration probe with digital acoustic telemetry and in-situ thermal conductivity. Mar. Geophys. Res., 4, 181-205.

Jaeger, J.C., 1956. Conduction of heat in an infinite region bounded internally by a circular cylinder of a perfect conductor. Australian J. Phys., 9, 167-179.

Jaeger, J.C., 1958. The measurement of thermal conductivity and diffusivity

with cylindrical probes. Trans. Am. Geophys. Union, 39, 708-710.

Jessop, A.M., Hobart, M.A. and Sclater, J.G., 1976. The world heat flow data collection, 1975. Geothermal series No. 5. Energy, Mines and Resources.

Kidd, R.B., Searle, R.C., Weaver, P.P.E., Jacobs, C.L., Huggett, Q.J., Noel, M.J. and Schultheiss, P.J., 1983. King's Trough Flank: Geological and geophysical investigations of its suitability for high-level radioactive waste disposal. IOS Report (in prep.).

Kunii, D. and Smith, J.M., 1961. Heat transfer characteristics of porous rocks - II. Thermal conductivities of unconsolidated particles with flowing fluid. J. Am. Inst., Chem. Eng., 7(1), 29-34.

Langseth, M.G. and Herman, B.M., 1981. Heat Transfer in the Oceanic Crust of the Brazil Basin. J. Geophys. Res., 86, 10805-10819.

Lister, C.R.B., 1972. On the thermal balance of a mid-ocean ridge. Geophys. J. R. astr. Soc., 26, 515-535.

Lister, C.R.B., 1979. The pulse-probe method of conductivity measurement. Geophys. J. Roy. astr. Soc., 57, 451-461.

Macdonald, K.C. and Luyendyk, B.P., 1981. The crest of the East Pacific Rise. Earth Planet. Sci. Lett., 48, 1-7.

Mansure, A.J. and Reiter, M., 1979. A vertical groundwater movement correction for heat flow. J. Geophys. Res., 84, 3490-3496.

Müller, T.J., 1981. Current and temperature measurements in the northeast Atlantic during NEADS. Berichte aus dem Institut für Meereskunde. Christian-Albrechts-Universität, Kiel, No. 90.

Noel, M.J. (in press). Origins and significance of non-linear temperature profiles in deep-sea sediments. Geophys. J. R. astr. Soc.

Parsons, B. and Sclater, J.G., 1977. An analysis of the variation of ocean floor bathymetry and heat flow with age. J. Geophys. Res., 82, 803-827.

Peng, T-H., Broecker, W.S., Kipphut, G. and Shackleton, N., 1977. Benthic mixing in deep sea cores as determined by C14-dating and its implications regarding climate stratigraphy and the fate of fossil fuel CO_2. In: The fate of fossil fuel CO_2 in the oceans, N.R. Anderson and A. Mallahoff (Eds.), Plenum Press, New York.

Ratcliffe, E.H., 1960. The thermal conductivities of ocean sediments. J. Geophys. Res., 65, 1535-1541.

RISE Project Group, 1980. Hot springs and geophysical experiments on the East Pacific Rise. Science, 207, 1421-1433.

Searle, R.C., 1979. Guidelines for the selection of sites for the disposal of

radioactive waste on or beneath the ocean floor. Institute of Oceanographic Sciences, Report No. 91, 44 pp. (Unpublished manuscript).

Smith, L. and Chapman, D.S., 1983. On the thermal effects of groundwater flow - I. Regional Scale systems. J. Geophys. Res., 88, 593-608.

Sorey, M.L., 1971. Measurement of vertical groundwater velocity from temperature profiles in wells. Water Resour. Res., 7(4), 963-970.

Stallman, R.W., 1963. Computation of groundwater velocity from temperature data. U.S. Geol. Surv. Water Supply Pap., 1544-H, 36-46.

Stallman, R.W., 1967. Flow in the zone of aeration. In: V.T. Chow (Ed.), Advances in Hydroscience, 4, Academic Press, New York.

Strens, M.R. and Cann, J.R., 1982. A model of hydrothermal circulation in fault zones at mid-ocean ridge crests. Geophys. J. R. astr. Soc., 71, 225-240.

Von Herzen, R.P. and Uyeda, S., 1963. Heat flow through the eastern Pacific Ocean floor. J. Geophys. Res., 68, 4219-4250.

Von Herzen, R. and Maxwell, A.E., 1959. The measurement of thermal conductivity of deep-sea sediments by a needle-probe method. J. Geophys. Res., 64, 1557-1563.

Williams, D.L., Von Herzen, R.P., Sclater, J.G. and Anderson, R.N., 1974. The Galapagos spreading centre: Lithospheric cooling and hydrothermal circulation. Geophys. J. R. astr. Soc., 38, 587-6-8.

Williams, D.L., Green, K., Van Andel, T.H., Von Herzen, R.P., Dymond, J.R. and Crane, K., 1979,. The hydrothermal mounds of the Galapagos Rift: Observations with DSRV Alvin and detailed heat flow studies. J. Geophys Res., 84, 7467-7484.

APPENDIX 1 - Computer Program "THEQ"

Description

This computer program is used to estimate the equilibrium sediment temperatures by subtracting the frictional temperature rise caused by the penetration of the heat probe. The method used is that described by Bullard (1954). Further details of the theory are given in the text.

The program begins by calculating the offsets of each of the thermistors from their mean resistance values immediately prior to penetration. This figure is then added to the resistance in order to compensate for resistance drift between stations. The resistance values are then converted to temperature readings using a polynomial supplied by Applied Microsystems Ltd.

The equilibrium temperature is then estimated for the lowest thermistor with no origin time delay. Values for θ_{eq} and θ_{ex} (see text) are then used to reconstruct the cooling curve and compute the RMS misfit to the actual cooling record. This procedure is repeated for increasing delays and the optimum fit (and hence the optimum θ_{eq}) computed. θ_{eq} is then found for the remaining thermistors using the same delay.

Input Parameters

Fourteen uncalibrated data logger readings per line, any number of lines. Format 14 F6.0. Comprising T1, T2, A1, T3, A2, T4, A3, T5, A4, T6, DUMMY, DUMMY, Reference Resistor, Time Code.

The first NOFF lines correspond to data acquired immediately prior to penetration (used for offset calculation).

The program requests 'NO. LINES TO BE USED FOR CALCULATING OFFSETS?' Enter NOFF.

The offsets are then listed.

The program then asks if lines are to be missed. This permits the offset calculation to be based on stable data before the probe is run in.

The program then requests the number of data lines corresponding to the dip. These should not include data obtained during pullout otherwise the computed equilibrium temperature will be in error.

Output Data

1. The program outputs the thermistor offsets for the station.
2. The bottom water temperature.

3. A listing of RMS residual versus delay in the estimation of θ_{eq} for T6.
4. The final measured temperatures and the estimated equilibrium temperatures for each of the thermistors.

Language

Honeywell Fortran.

```
10*#FRN * = #/DATA,R"01"
20      FUNCTION FAT(T)
30C     THIS FUNCTION ROUTINE COMPUTES THE FUNCTION F(ALPHA,TAU) BY
40C     INTERPOLATING FROM LISTERS TABLE ASSUMING ALPHA = 2
50      DIMENSION B(50,2)
60      B(1,1)  = 0.00
70      B(2,1)  = 0.20
80      B(3,1)  = 0.40
90      B(4,1)  = 0.60
100     B(5,1)  = 0.75
110     B(6,1)  = 1.00
120     B(7,1)  = 1.25
130     B(8,1)  = 1.50
140     B(9,1)  = 1.75
150     B(10,1) = 2.00
160     B(11,1) = 2.25
170     B(12,1) = 2.50
180     B(13,1) = 2.75
190     B(14,1) = 3.00
200     B(15,1) = 3.25
210     B(16,1) = 3.50
220     B(17,1) = 3.75
230     B(18,1) = 4.00
240     B(19,1) = 4.25
250     B(20,1) = 4.50
260     B(21,1) = 4.75
270     B(22,1) = 5.00
280     B(23,1) = 5.25
```

```
290     B(24,1) =  5.50
300     B(25,1) =  5.75
310     B(26,1) =  6.00
320     B(27,1) =  6.25
330     B(28,1) =  6.50
340     B(29,1) =  6.75
350     B(30,1) =  7.00
360     B(31,1) =  7.25
370     B(32,1) =  7.50
380     B(33,1) =  7.75
390     B(34,1) =  8.00
400     B(35,1) =  8.25
410     B(36,1) =  8.50
420     B(37,1) =  8.75
430     B(38,1) =  9.00
440     B(39,1) =  9.25
450     B(40,1) =  9.50
460     B(41,1) =  9.75
470     B(42,1) = 10.00
480     B(43,1) = 10.25
490     B(44,1) = 10.50
500     B(45,1) = 10.75
510     B(46,1) = 11.00
520     B(47,1) = 11.25
530     B(48,1) = 11.50
540     B(49,1) = 11.75
550     B(50,1) = 12.00
560     B(1,2)  =  1.00000
570     B(2,2)  =  0.40100
580     B(3,2)  =  0.29020
590     B(4,2)  =  0.231100
600     B(5,2)  =  0.20120
610     B(6,2)  =  0.16630
620     B(7,2)  =  0.14195
630     B(8,2)  =  0.12403
640     B(9,2)  =  0.11012
650     B(10,2) =  0.09910
```

```
660     B(11,2) = 0.09014
670     B(12,2) = 0.08266
680     B(13,2) = 0.07634
690     B(14,2) = 0.07088
700     B(15,2) = 0.6626
710     B(16,2) = 0.06218
720     B(17,2) = 0.05853
730     B(18,2) = 0.05521
740     B(19,2) = 0.05233
750     B(20,2) = 0.04974
760     B(21,2) = 0.04738
770     B(22,2) = 0.04523
780     B(23,2) = 0.04328
790     B(24,2) = 0.04148
800     B(25,2) = 0.03983
810     B(26,2) = 0.03830
820     B(27,2) = 0.03689
830     B(28,2) = 0.03558
840     B(29,2) = 0.03436
850     B(30,2) = 0.03322
860     B(31,2) = 0.03215
870     B(32,2) = 0.03116
880     B(33,2) = 0.03022
890     B(34,2) = 0.02933
900     B(35,2) = 0.02849
910     B(36,2) = 0.02770
920     B(37,2) = 0.02696
930     B(38,2) = 0.02625
940     B(39,2) = 0.02558
950     B(40,2) = 0.02494
960     B(41,2) = 0.02434
970     B(42,2) = 0.02376
980     B(43,2) = 0.02321
990     B(44,2) = 0.02268
1000    B(45,2) = 0.02217
1010    B(46,2) = 0.02169
1020    B(47,2) = 0.02123
```

```
1030        B(48,2) = 0.02079
1040        B(49,2) = 0.02037
1050        B(50,2) = 0.01998
1060C       THE ARGUMENT T IS NON-DIMENSIONAL TIME = TIME (SECS)/TIME CONST
1061C       FIRST CHECK THAT T IS NOT TOO LARGE
1062        IF (T.GT.12.0) PRINT, "T TOO LARGE FOR FAT(T)"
1070C       NOW SEARCH FOR THE TWO VALUES OF TAU FLANKING ARGUMENT T.
1080        ISTEP = 1
1090  100   IF (T.GE.B(ISTEP,1)) AND (T.LE.B(ISTEP + 1,1)) GO TO 120
1100        ISTEP = ISTEP + 1
1110        GO TO 100
1120  120   X1 = B(ISTEP,1)
1130        X2 = B(ISTEP + 1,1)
1140        Y1 = B(ISTEP,2)
1150        Y2 = B(ISTEP + 1,2)
1160        GRAD = (Y2 - Y1)/(X2 - X1)
1170        X = T - B(ISTEP,1)
1180        FAT = Y1 + GRAD*X
1190        RETURN
1200        END
1210C       ------------------------------------------------------------------
1220        FUNCTION FATINV(FALFATAU)
1230C       THIS FUNCTION IS THE INVERSE OF FAT
1240        ISTEP = 1
1250  10    TAU = ISTEP - 1
1260        TAU = TAU*0.1
1270        IF (FALFATAU.GE.FAT(TAU + 0.1).AND.FALFATAU.LE.FAT(TAU)) GO TO 20
1280        ISTEP = ISTEP + 1
1290        IF (ISTEP.GT.10000) PRINT,"ISTEP(FATINV)",ISTEP,FALFATAU,FAT(TAU + 0.1)
1300        GO TO 10
1310  20    Y = FALFATAU - FAT(TAU)
1320        GRAD = (FAT(TAU + 0.1) 0 FAT(TAU))/0.1
1330        TAU = TAU + Y/GRAD
1340        FATINV = TAU
1350        RETURN
1360        END
1370C       ------------------------------------------------------------------
```

```
1380        FUNCTION CNVT(DPT)
1390C       THIS FUNCTION CONVERTS DIGIPRINTER NUMBERS INTO TEMPERATURES
1400        A =  2.78307E - 4
1410        B =  7.59484
1420        C =  1.32108
1430        D = -0.943184
1440        T = A + (B*(DPT/1023.)) + (C*(DPT/1023.)**2.) + (D*(DPT/1023)**3.)
1450        CNVT = T
1460        RETURN
1470        END
1480C       ------------------------------------------------------------------
1490        SUBROUTINE TEQ (THERM,TIME,NTHERM,NDATA,TEQUIL,TEXCESS)
1500C       THIS SUBROUTINE FINDS THE EQUILIBRIUM TEMPERATURE FOR THE THERMISTOR
1510C       IN COLUMN NTHERM OF ARRAY THERM
1520        DIMENSION THERM(100,10)
1530        DIMENSION TIME(100)
1540C       THIS ARRAY CONTAINS CORRESPONDING TIMES
1550        TEMP1 = THERM(NDATA, NTHERM)
1560        TIME1 = TIME(NDATA)
1570        F = FAT(TIME1)
1580        TIME2 = FATINV(2.0*F)
1590        TIME3 = FATINV(3.0*F)
1600        X2 = (TIME2/0.25 - AINT(TIME2/0.25))*0.25
1610        GRAD2=(THERM(INT(TIME2/0.25)+2,NTHERM)-
1620       &              THERM(INT(TIME2/0.25)+1,NTHERM))/0.25
1630        TEMP2 = THERM(INT(TIME2/0.25) + 1,NTHERM) + X2*GRAD2
1640        X3 = (TIME3/0.25 - AINT(TIME3/0.25))*0.25
1650        GRAD3=(THERM(INT(TIME3/0.25)+2,NTHERM)-
1660       &            THERM(INT(TIMES3/0.25)+1,NTHERM))/0.25
1670        TEMP3 = THERM(INT(TIME3/0.25) + 1,NTHERM) + X3*GRAD3
1680        TEQUIL = (7*TEMP1-5*TEMP3+4*TEMP2)/6.0
1690        TEXCESS = (5*TEMP3-4*TEMP2-TEMP1)/(6.0*F)
1700 90     FORMAT(1H ,F7.3,'  ',F7.3,'  ',F7.3)
1710        RETURN
1720        END
1730C       ------------------------------------------------------------------
```

```
1740C         NOW READ IN DATA
1750          DIMENSION THERM(100,10),WORK(100,10),CORR(10)
1760          DIMENSION TIME(100),OFFWK(20,10)
1770C         FIRST READ IN NUMBER OF DATA LINES FOR CALCULATION OF OFFSETS
1780          WRITE(6,199)
1790 199      FORMAT(1H ,"NO LINES TO BE USED FOR CALCULATING OFFSETS?")
1800          READ(5,30)NOFF
1810          DO 8 I=1,NOFF
1820          READ(1,60) (OFFWK(I,N),N=1,10),DISCON1,DISCON2,RR,LINENUM
1830 8        CONTINUE
1840          GTOT = 0.0
1850          DO 9 I=1,10
1860          TOT = 0.0
1870          DO 11 J=1,NOFF
1880          TOT = TOT + OFFWK(J,I)
1890          GTOT = GTOT + OFFWK(J,I)
1900 11       CONTINUE
1910          CORR(I) = TOT/FLOAT(NOFF)
1920 9        CONTINUE
1930          GAV = GTOT/(FLOAT(NOFF)*10.0)
1940          BOTTEMP = CNVT(GAV)
1950          WRITE(6,63)BOTTEMP
1960 63       FORMAT(1H,"BOTTOM WATER TEMPERATURE=",1F5.3
1970          DO 64 I = 1,10
1980          CORR(I) = GAV - CORR(I)
1990 64       CONTINUE
2000          WRITE(6,65)
2010 65       FORMAT(1H ,"THESE ARE THE THERMISTOR OFFSETS FOR THIS STN.")
2020          WRITE(6,66)(CORR(I),I=1,10)
2030 66       FORMAT(10F6.1)
2040          WRITE(6,67)
2050 67       FORMAT(1H ,"HOW MANY LINES TO BE MISSED?")
2060          READ(5,30)NMISS
2070          IF(NMISS.EQ.0) go to 499
2080          DO 69 I=1,NMISS
2090          READ(1,30) TOOSOON
2100 69       CONTINUE
```

```
2110 499      WRITE(6,500)
2120 500      FORMAT(1H ,"INPUT NUMBER OF DATA LINES ")
2130          READ(5,30) ND
2140 30       FORMAT(V)
2150          DO 35 I=1,ND
2160          READ(1,60) (WORK(I,N),N=1,10),DISCON1,DISCON1,RR,LINENUM
2170 60       FORMAT(14F6.0)
2180 35       CONTINUE
2200C         ------------------------------------------------------------------
2210C         FIND THE BEST DELAY FOR THERMISTOR T6
2220C         THE BEST DELAY IS THE ONE WHICH GIVES THE MIN. ROOT MEAN SQUARE
2230C         RESIDUAL
2240          PRESID = 1000.0
2250          DO 999 IDLY = 1,41
2260          IDELAY = IDLY - 1
2270          ISKIP = 0
2280          IF(DELAY.EQ.O) GO TO 39
2290          ISKIP = 1 + (DELAY - 1)/15
2300 39       ISHIFT = ISKIP*15 -IDELAY
2310          SHIFT = FLOAT(ISHIFT)/60.0
2320          DO 40 I = 1,ND - SKIP
2330          RI = I - 1
2340          TIME(I) = RI*0.25 + SHIFT
2350 40       CONTINUE
2360          DO 333 I = 1,ND - SKIP
2370          DO 334 N = 1,10
2380          THERM(I,N) = CNVT(WORK(I + ISKIP,N) + CORR(N))
2390 334      CONTINUE
2391C         WRITE(6,30) (THERM(I,NNN),NNN = 1,10)
2400 333      CONTINUE
2410C         THERM NOW CONTAINS CORRECTED THERMISTOR TEMPERATURES
2420          CALL TEQ(THERM,TIME,10,ND - ISKIP,TEQUIL,TEXCESS)
2430C         CALCULATE THE RESIDUAL OF THE FIT TO THE DATA
2440          RESID = 0.0
2450          DO 200 I = 3,ND - SKIP
2460          THETA = TEQUIL + EXCESS*FAT(TIME(I))
2470          RESID = RESID + (THETA - THERM(I,10))**2
```

```
2480 200      CONTINUE
2490          RESID = SQRT(RESID/ND - ISKIP))
2500          WRITE(6,150) IDELAY,RESID
2510 150      FORMAT(1H ,12,'  ',F14.5)
2520C         CHOOSE THE DELAY TIME WHICH GIVES THE BEST FIT
2530          IF(RESID.GE.PRESTO) GO TO 888
2540          PRESID = RESID
2550          IBESTDLY = IDELAY
2560 888      CONTINUE
2570 999      CONTINUE
2571          WRITE(6,699) IBESTDLY
2572 699      FORMAT(1H ,"BEST DELAY=",I2)
2580C         ------------------------------------------------------------------------
2590C         USING THE BEST DELAY FOR T6 AS THE BEST DELAY FOR ALL THERMISTORS
2600C         CALCULATE THE EQUILIBRIUM TEMPERATURES
2610          ISKIP = 0
2620          IF(IBESTDLY.EQ.0) GO TO 777
2630          ISKIP = 1 + (IBESTDLY - 1)/15
2640 777      ISHIFT = ISKIP*15 - IBESTDLY
2650          SHIFT = FLOAT(ISHIFT)/60.0
2660          DO 700 I = 1,ND - SKIP
2670          RI = I - 1
2680          TIME(I) = RI*0.25 + SHIFT
2690 700      CONTINUE
2700          DO 666 N = 1,10
2701          NN = N
2710          CALL TEQ(THERM,TIME,NN,ND- SKIP,TEQUIL,TEXCESS)
2720          WRITE(6,250) N,THERM(ND - ISKIP,N),TEQUIL
2730 250      FORMAT(1H ,12,3H   ,F7.4,3H   ,F7.4)
2740 666      CONTINUE
2750          STOP
2760          END
```

APPENDIX II - Computer Program "COND"

Description

This program computes the sediment thermal conductivity from the decay of a calibrated heat pulse, using the method of Hyndman et al. (1979). As in 'THEQ', the thermistor readings are corrected for offsets and calibrated.

The program is structured to then run in interactive mode: trial values of time delay (with respect to the heat pulse origin time) and probe thermal time constant are entered and the gradient of a plot of temperature versus 1/t(s) is calculated; the temperatures having been corrected using the $C(\alpha,\tau)$ function as described in the text. The RMS residual in the fit of the decay curve to the regression line is then computed and the user then minimises this figure by iterations involving origin time and time constant (typically 60s). This approach was chosen because it is possible to monitor the nature of the convergence to the solution to the conductivity. The procedure is repeated for each of the conductivity array thermistors.

Input Parameters

Fourteen uncalibrated logger readings per line, any number of lines. Format 14F6.0. Comprising T1, T2, A1, T3, A2, T4, A3, T5, A4, T6, DUMMY, DUMMY, Reference Resistor, Time Code.

The first line of data should correspond to the onset of the heat pulse.

The program requests the number of data lines followed by the offset values for the 'A' thermistors.

The iteration then commences with the program requesting the first values for DELAY, TIMECONSTANT, and CHANNEL, NO. The latter is 1, 2, 3, 4 or 5. The program responds with the conductivity value (MKS units) and the RMS residual.

Output Data

As described, after each iteration the program responds with the conductivity and residual. Iteration is terminated by entering DELAY>1000.

Language

Honeywell Fortran.

```
10*#FRN *=#/DATA1,R"01";/OUT,W"02"
20      FUNCTION FAT(T)
30C     THIS FUNCTION ROUTINE COMPUTES THE FUNCTION F (ALPHA,TAU) BY
40C     INTERPOLATING FROM LISTERS TABLE ASSUMING ALPHA = 2
50      DIMENSION B(50,2)
60      B( 1,1) = 0.
70      B( 2,1) = 0.20000
80      B( 3,1) = 0.40000
90      B( 4,1) = 0.60000
100     B( 5,1) = 0.75000
110     B( 6,1) = 1.00000
120     B( 7,1) = 1.25000
130     B( 8,1) = 1.50000
140     B( 9,1) = 1.75000
150     B(10,1) = 2.00000
160     B(11,1) = 2.25000
170     B(12,1) = 2.50000
180     B(13,1) = 2.75000
190     B(14,1) = 3.00000
200     B(15,1) = 3.25000
210     B(16,1) = 3.50000
220     B(17,1) = 3.75000
230     B(18,1) = 4.00000
240     B(19,1) = 4.25000
250     B(20,1) = 4.50000
260     B(21,1) = 4.75000
270     B(22,1) = 5.00000
280     B(23,1) = 5.25000
290     B(24,1) = 5.50000
300     B(25,1) = 5.75000
310     B(26,1) = 6.00000
320     B(27,1) = 6.25000
330     B(28,1) = 6.50000
340     B(29,1) = 6.75000
350     B(30,1) = 7.00000
360     B(31,1) = 7.25000
370     B(32,1) = 7.50000
```

```
380     B(33,1) =  7.75000
390     B(34,1) =  8.00000
400     B(35,1) =  8.25000
410     B(36,1) =  8.50000
420     B(37,1) =  8.75000
430     B(38,1) =  9.00000
440     B(39,1) =  9.25000
450     B(40,1) =  9.50000
460     B(41,1) =  9.75000
470     B(42,1) = 10.00000
480     B(43,1) = 10.25000
490     B(44,1) = 10.50000
500     B(45,1) = 10.75000
510     B(46,1) = 11.00000
520     B(47,1) = 11.25000
530     B(48,1) = 11.50000
540     B(49,1) = 11.75000
550     B(50,1) = 12.00000
560     B( 1,2) =  1.00000
570     B( 2,2) =  0.40100
580     B( 3,2) =  0.29020
590     B( 4,2) =  0.23110
600     B( 5,2) =  0.20120
610     B( 6,2) =  0.16630
620     B( 7,2) =  0.14195
630     B( 8,2) =  0.12403
640     B( 9,2) =  0.11012
650     B(10,2) =  0.09910
660     B(11,2) =  0.09014
670     B(12,2) =  0.08266
680     B(13,2) =  0.07634
690     B(14,2) =  0.07088
700     B(15,2) =  0.06626
710     B(16,2) =  0.06218
720     B(17,2) =  0.05853
730     B(18,2) =  0.05521
740     B(19,2) =  0.05233
```

```
750           B(20,2) = 0.04974
760           B(21,2) = 0.04738
770           B(22,2) = 0.04523
780           B(23,2) = 0.04328
790           B(24,2) = 0.04148
800           B(25,2) = 0.03983
810           B(26,2) = 0.03830
820           B(27,2) = 0.03689
830           B(28,2) = 0.03558
840           B(29,2) = 0.03436
850           B(30,2) = 0.03322
860           B(31,2) = 0.03215
870           B(32,2) = 0.03116
880           B(33,2) = 0.03022
890           B(34,2) = 0.02933
900           B(35,2) = 0.02849
910           B(36,2) = 0.02770
920           B(37,2) = 0.02696
930           B(38,2) = 0.02625
940           B(39,2) = 0.02558
950           B(40,2) = 0.02494
960           B(41,2) = 0.02434
970           B(42,2) = 0.02376
980           B(43,2) = 0.02321
990           B(44,2) = 0.02268
1000          B(45,2) = 0.02217
1010          B(46,2) = 0.02169
1020          B(47,2) = 0.02123
1030          B(48,2) = 0.02079
1040          B(49,2) = 0.02037
1050          B(50,2) = 0.01998
1060C         THE ARGUMENT T IS NON-DIMENSIONAL TIME = TIME (SECS)/TIME CONST
1070C         NOW SEARCH FOR THE TWO VALUES OF TAU FLANKING ARGUMENT T
1080          ISTEP = 1
1090  100     IF (T.GE.B(ISTEP,1).AND.T.LE.B(ISTEP + 1,1) GO TO 120
1100          ISTEP = ISTEP + 1
1110          GO TO 100
```

```
1120 120      X1 = B(ISTEP,1)
1130          X2 = B(ISTEP + 1,1)
1140          Y1 = B(ISTEP,2)
1150          Y2 = B(ISTEP + 1,2)
1160          GRAD = (Y2 - Y1)/(X2 - X1)
1170          X = T - B(ISTEP,1)
1180          FAT = Y1 + GRAD*X
1190          RETURN
1200          END
1210          FUNCTION CAT(T)
1220C         THIS FUNCTION ROUTINE COMPUTES THE FUNCTION C (ALPHA,T) OF HYNDMAN
1230C         ET AL.
1240          ALPHA = 2.0
1250          CAT = 1.0/(2.0*ALPHA*T*FAT(T))
1260          RETURN
1270          END
1280          FUNCTION CNVT(DPT)
1290C         THIS FUNCTION CONVERTS DIGIPRINTER NUMBERS INTO TEMPERATURES
1300          A = 2.78307E - 4
1310          B = 7.59484
1320          C = 1.32108
1330          D = -0.943184
1340          T = A + (B*(DPT/1023.)) + (C*(DPT/1023.)**2.) + (D*(DPT/1023.)**3)
1350          CNVT = T
1360          RETURN
1370          END
1380          SUBROUTINE LSF (ARRAY,N1,N2,CONST,GRAD,RMSRESID)
1390          DIMENSION ARRAY (100,2)
1400C         THIS SUBROUTINE FINDS THE LEAST SQUARES FIT TO A STRAIGHT LINE OF
1410C         THE DATA CONTAINED IN ARRAY, WHERE XN = ARRAY (N,2) AND
1420C         YN = ARRAY (N,1)
1430          AVX = 0.0
1440          AVY = 0.0
1450          RNUM = 0.0
1460          RDEN = 0.0
1470          RMSR = 0.0
1480          DO 10 I = N1,N2
```

```
1490          AVX = AVX + ARRAY (I,2)
1500          AVY = AVY + ARRAY (I,1)
1510  10      CONTINUE
1520          T = N2 - N1 + 1
1530          AVX = AVX/T
1540          AVY = AVY/T
1550          DO 20 I = N1,N2
1560          RNUM = RNUM + ARRAY (I,1)*(ARRAY(I,2) - AVX)
1570          RDEN = RDEN + (ARRAY(I,2) - AVX)**2
1580  20      CONTINUE
150           GRAD = RNUM/RDEN
1600          CONST = AVY - GRAD*AVX
1610          DO 30 I = N1,N2
1620          RMSR = RMSR + (ARRAY(I,1) - CONST - GRAD*ARRAY (I,2))**2
1630  30      CONTINUE
1640          RMSRESID = SQRT (RNSR/T)
1650          RETURN
1660          END
1670          SUBROUTINE CONDIFF (TEMPS,TIMES,DIFFIN,NDATA,DIFFOUT,COND,RESID)
1680C         THIS SUBROUTINE CALCULATES SEDIMENT THERMAL CONDUCTIVITY FROM THE
1690C         SLOPE OF A GRAPH OF CORRECTED TEMPERATURES VERSUS 1/TIME(SECS) BY
1700C         THE METHOD OF HYNDMAN ET AL., INPUT PARAMETERS:
1710C         TEMPS = TEMPERATURES (DEG C) OF THERMISTOR CHAIN
1720C         TIMES = DELAYED TIMES FROM ESTIMATED ORIGIN OF H.P. IGNORING 1ST MIN
1730C         DIFFIN = INPUT VALUE OF DIFFUSIVITY TO CALCULATE PROBE TIME CONST
1740C         DIFFOUT = OUTPUT DIFFUSIVITY CALCULATED FROM CONDUCTIVITY
1750C         RESID = RMS RESIDUAL IN FIT TO STRAIGHT LINE
1760C         NDATA = NUMBER OF DATA LINES
1770          DIMENSION TEMPS (100),TIMES(100),WORK (100,2)
1780          Q = 434.0
1790          A = (3.0/16.0) + 0.0254
1800          TCONST = A*A/DIFFIN
1810          DO 10 I = 1,NDATA
1820          TAU = TIMES (I)/TCONST
1830          WORK(I,1) = TEMPS(I)*CAT(TAU)
1840          WORK(1,2) = 1.0/TIMES(I)
1850  10      CONTINUE
```

```
1860          CALL LSF (WORK,1,NDATA,C,G,R)
1870          COND = Q/(4.0*3.14159*G)
1880          DIFFOUT = COND*10.E - 6/(5.79 - (3.67*COND) + (1.106*(COND*COND)))
1890          RESID = R
1900          RETURN
1910          END
1920          DIMENSION A2(100),A3(100),A4(100),A5(100),TIME(100),TIMES(100)
1930          WRITE (6,15)
1940 15       FORMAT (1H ,' INPUT NUMBER OF DATA LINES')
1950          READ (5,20) NDATA
1960 20       FORMAT (V)
1970          NDATA = NDATA - 8
1980          DOI 30 I = 1,8
1990          READ (1,50) BOGUS
2000 30       CONTINUE
2010C         THIS IGNORES THE FIRST MINUTE AND 45 SECONDS OF DATA
2020          DO 40 I = 1,NDATA
2030          R = I
2040          TIME(I) = (R + 7.0)*15.0
2050          READ (1,50) A2(I),A3(I),A4(I),A5(I)
2060          A2(I) = CNVT (A2(I))
2070          A3(I) = CNVT (A3(I))
2080          A4(I) = CNVT (A4(I))
2090          A5(I) = CNVT (A5(I))
2100 50       FORMAT (V)
2110 40       CONTINUE
2120C         NOW FIND THE OPTIMUM DELAY
2130          R2 = 100000.0
2140          A = (3.0/16.0)*0.0254
2150          DELAY = -1.0
2160          DIFFIN = A*A/60.0
2170 99       DELAY = DELAY + 1.0
2180          DO 60 I = 1,NDATA
2190          TIMES (I) = TIME (I) - DELAY
2200 60       CONTINUE
2210          CALL CONDIFF (A3,TIMES,DIFFIN,NDATA,DIFFOUT,C,R1)
2220          IF (R1.GE.R2) GO TO 101
```

```
2230          R2 = R1
2240          GO TO 99
2250 101      WRITE (6,500) DELAY
2260 500      FORMAT (7H DELAY = ,F4.0)
2261          DO 700 I = 1,NDATA
2262          WRITE (2,750) 1/TIMES (I), A5(I)*CAT(ATIMES(I)/60.0)
2263 750      FORMAT (1H ,F6.4,3H   ,F7.4)
2264 700      CONTINUE
2270C         ARRAY TIMES NOW CONTAINS TIMES CORRECTED FOR OPTIMUM DELAY
2280C         ASSUMED OPTIMUM FOR FOUR OTHER THERMISTOR CHAINS
2290C         NOW DETERMINE CONDUCTIVITY FROM 3 ITERATIONS INVOLVING DIFFUSIVITY
2300          WRITE (6,77)
2310 77       FORMAT (2H ,'     CONDUCTIVITY   RMSRESID')
2320          WRITE (6,511)
2330 511      FORMAT (1H ,'THERMISTOR A2')
2340          DO 80 I = 1,3
2350          CALL CONDIFF (A2, TIMES,DIFFIN,NDATA,DIFFOUT,C,R)
2360          WRITE (6,90) C,R
2370 90       FORMAT (5H     ,F12.4,3H   ,F7.3)
2380          DIFFIN = DIFFOUT
2390 80       CONTINUE
2400          DIFFIN = A*A/60.0
2410          WRITE (6,512)
2420 512      FORMAT (1H ,'THERMISTOR A3')
2430          DO 100 I = 1,3
1440          CALL CONDIFF (A3,TIMES,DIFFIN,NDATA,DIFFOUT,C,R)
2450          WRITE (6,90) C,R
2460          DIFFIN = DIFFOUT
2470 100      CONTINUE
2480          DIFFIN = A*A/60.0
2490          WRITE (6,513)
2500 513      FORMAT (1H ,'THERMISTOR A4')
2510          DO 110 I = 1,3
2520          CALL CONDIFF (A4,TIMES,DIFFIN,NDATA,DIFFOUT,C,R)
2530          WRITE (6.90) C,R
2540          DIFFIN = DIFFOUT
2550 110      CONTINUE
```

```
2560          DIFFIN = A*A/60.0
2570          WRITE (6,520)
2580 520      FORMAT (1H ,'THERMISTOR A5'))
2590          DO 120 I = 1,3
2600          CALL CONDIFF (A5,TIMES,DIFFIN,NDATA,DIFFOUT,C,R)
2610          WRITE (6,90) C,R
2620          DIFFIN = DIFFOUT
2630 120      CONTINUE
2640          STOP
2650          END
```

TABLE 1

Station: 10301 (CR118)
Mean latitude: 34°27'N
Mean longitude: 21°41'W
Duration: 8.5h
Mean water depth: 5210m
Total no. of dips: 11
No. of successful dips: 11
Comments: A.M. Probe. Only 1-2m penetration due to lack of weight. No conductivity determination.

DIP	THERMISTOR OFFSETS												GRADIENT °C/m	BOTTOM WATER TEMP.	HEAT FLOW μ cal cm^{-2} s^{-1}
	T1	T2	A1	T3	A2	T4	A3	T5	A4	T6	A5	T7			
1	9.3	-3.6	3.7	2.5	2.0	-0.8	-1.5	-3.4	-1.2	2.0	5.0	-14.0	0.0741	2.448	1.48
2	9.1	-3.5	4.4	2.4	2.3	-0.6	-2.7	-3.6	-0.5	2.4	4.7	-14.1	0.0554	2.442	1.11
3	9.1	-3.9	4.5	2.3	2.3	-0.5	-2.7	-3.8	-0.4	2.1	4.9	-14.2	0.0697	2.446	1.39
4	9.1	-3.9	4.4	2.3	2.2	-0.6	-3.0	-3.7	-0.3	2.2	5.1	-14.0	0.0933	2.445	1.87
5	9.3	-3.8	4.3	2.3	2.3	-0.8	-2.8	-3.8	-0.7	2.3	5.3	-13.8	0.0810	2.447	1.62
6	9.2	-3.7	4.3	2.3	2.3	-0.7	-2.7	-3.8	-0.7	2.2	5.1	-14.1	0.0850	2.447	1.70
7	9.0	-4.1	4.5	2.0	2.4	-0.1	-2.5	-3.9	-0.1	2.4	4.9	-14.1	0.0863	2.451	1.73
8	9.5	-4.0	4.3	2.3	2.0	-0.8	-3.3	-4.0	0.0	2.3	5.1	-13.7	0.0364	2.461	0.73
9	QUICK DIP. DATA NOT PROCESSED.														
10	9.4	-4.1	4.4	2.4	2.1	-0.6	-2.6	-3.6	-0.6	2.4	4.9	-13.6	0.0925	2.455	1.85
11	9.2	-3.8	4.2	2.2	2.2	-0.8	-2.8	-3.8	-0.2	2.2	5.2	-13.8	0.0867	2.454	1.73

Notes: These comments apply to this and subsequent tables. The thermistor offsets represent the deviation from the mean logger 'temperature' immediately prior to penetration and are an indication of thermistor stability. The logger numbers are subsequently calibrated to give real temperatures. Thermistors 'T' are used in measuring the sediment temperature profile and are at depths of 0.1, 0.2, 1.0, 2.0, 3.0, 4.0 and 5.0 metres (T1 to T7 respectively). Thermistors 'A' comprise groups of four thermistors wired in series and parallel (over 1m length) to resemble one single, but extended, thermistor. These arrays are used in measuring the sediment conductivity. The centres of the 'A' arrays are at depths of 0.5, 1.5, 2.5, 3.5 and 4.5 metres. The IOS/Cambridge probe is shorter and omits sensors A5 and T7.

TABLE 2

Station: 10318 (CR118)
Mean latitude: 31°15'N
Mean longitude: 25°43'W
Duration: 8h
Mean water depth: 5433m
Total no. of dips: 10
No. of successful dips: 4
Comments: A.M. Probe. Full penetration due to added weight. No conductivity determination. End of thermistor string found broken on recovery. Heat flow values assume $K = 2 \times 10^{-3}$ cal s^{-1} $°C^{-1}$ cm^{-1}.

DIP	THERMISTOR OFFSETS												GRADIENT °C/m	BOTTOM WATER TEMP.	HEAT FLOW μ cal cm^{-2} s^{-1}
	T1	T2	A1	T3	A2	T4	A3	T5	A4	T6	A5	T7			
1	-1.4	1.6	-0.4	-1.8	-1.4	0.6	-0.4	3.6	1.6	-3.4	1.6	-0.4	0.0781	2.132	1.56
2	-0.7	1.7	-0.5	-1.8	-1.6	0.4	0.0	3.4	1.5	-2.8	1.4	-0.7	0.0754	2.133	1.51
3	-1.2	1.7	-0.4	-1.9	-1.6	0.5	-0.3	3.5	1.6	-3.3	1.5	-0.6	0.0724	2.134	1.45
4	-0.9	1.8	-0.5	-1.8	-1.3	0.3	-0.1	3.6	1.5	-3.0	1.5	-0.9	0.0669	2.140	1.34

TABLE 3

Station: 10335 (CR118)
Mean latitude: 42°07'N
Mean longitude: 21°48'W
Duration: 7.3h
Mean water depth: 4060m
Total no. of dips: 8
No. of successful dips: 3
Comments: A.M. Probe. Full penetration due to added weight. Top end of thermistor string found broken on recovery.

DIP	THERMISTOR OFFSETS												GRADIENT °C/m	BOTTOM WATER TEMP.	HEAT* FLOW μ cal cm^{-2} s^{-1}
	T1	T2	A1*	T3	A2	T4	A3	T5	A4	T6	A5	T7			
1	-0.1	0.9	-	-0.6	-2.4	-0.1	-2.4	2.0	-1.6	3.9	1.7	-0.8	0.0769	2.603	1.54+
2	-0.1	0.9	-	-0.6	-2.4	-0.1	-2.4	2.0	-1.6	3.9	1.7	-0.8	0.0696	2.603	1.20
3	1.1	-0.1	-	-3.9	-2.7	-1.3	-2.1	3.1	-1.2	4.3	2.5	-0.2	0.0600	2.621	0.51

* Faulty channel

DIP	CONDUCTIVITY FOR GIVEN ARRAY, cal s^{-1} $°C^{-1}$ x 10^{-3}					
	A1*	A2	A3	A4	A5	MEAN
2	-	1.963	1.756	1.620	1.548	1.722
3	-	1.147	0.867	0.796	0.603	0.853

* Faulty channel

+ assumes K = 2.0 x 10-3 cal s-1 °C-1 cm-1

TABLE 4

Station: 10405 (CR126)
Mean latitude: 33°30'N
Mean longitude: 22°59'W
Duration: 8h
Mean water depth: 5410m
Total no. of dips: 8
No. of successful dips: 6
Comments: IOS/Cambridge probe. Thermistor string broken and pressure transducer and electronics lost. No conductivity determination.

DIP	THERMISTOR OFFSETS										GRADIENT °C/m	BOTTOM WATER TEMP.	HEAT* FLOW μ cal cm^{-2} s^{-1}	ADVECTION*+ VELOCITY $cm\ y^{-1}$
	T1	T2	A1	T3	A2	T4	A3	T5	A4	T6				
1	72.9	81.9	-44.1	44.9	-114.1	83.9	-184.1	-50.1	17.9	90.6	0.0312	2.851	0.62	687
2	71.5	80.3	-43.4	43.4	-111.4	82.6	-181.4	-50.6	20.6	88.3	0.1208	2.840	2.42	
3	70.7	79.7	-43.5	42.2	-111.3	81.7	-182.3	-47.1	23.0	86.7	0.0920	2.833	1.84	550
4	69.7	78.3	-43.7	42.2	-107.9	80.3	-182.7	-45.9	23.7	86.0	0.0683	2.822	1.37	
5	19.2	25.2	-17.8	14.6	- 62.2	25.0	- 46.0	10.0	4.3	28.1	0.0410	2.486	0.82	
6	13.8	24.5	-17.2	10.4	- 57.2	22.8	- 30.2	8.8	2.4	21.8	0.0428	2.427	0.86	

+ from equation (3)

* assumes $K = 2.0 \times 10^{-3}$ cal $°C^{-1}$ cm^{-1} s^{-1}

TABLE 5

Station: S126.3 (CR 126)
Mean latitude: 31°31'N
Mean longitude: 24°28'W
Duration: 4.8h
Mean water depth: 5447m
Total no. of dips: 3
No. of successful dips: 3
Comments: IOS/Cambridge probe. Station terminated because no heat pulses.

DIP	THERMISTOR OFFSETS										GRADIENT °C/m	BOTTOM WATER TEMP.	HEAT* FLOW μ cal cm^{-2} s^{-1}
	T1	T2	A1	T3	A2	T4	A3	T5	A4	T6			
1	2.5	-1.9	0.5	6.5	-3.2	4.7	0.4	2.1	-2.5	-9.3	0.0680	2.168	1.36
2	2.2	-1.1	0.2	6.2	-3.7	4.2	1.2	2.2	-2.8	-8.8	0.0663	2.176	1.33
3	2.7	-1.3	-0.3	6.7	-3.3	4.7	0.7	1.7	-2.3	-9.3	0.0582	2.172	1.16

* assumes K = 2.0 x 10^{-3} cal cm^{-1} °C^{-1} s^{-1}

TABLE 6

Station: S126.5 (CR 126)
Mean latitude: 31°30'N
Mean longitude: 24°28.5'W
Duration: 5h
Mean water depth: 5444m
Total no. of dips: 3
No. of successful dips: 3
Comments: IOS/Cambridge probe. Station terminated because no heat pulses.

DIP	THERMISTOR OFFSETS										GRADIENT °C/m	BOTTOM WATER TEMP	HEAT* FLOW μ cal cm^{-2} s^{-1}
	T1	T2	A1	T3	A2	T4	A3	T5	A4	T6			
1	2.7	-1.7	0.6	6.6	-3.2	4.9	0.2	1.9	-2.6	-9.0	0.0654	2.169	1.31
2	2.3	-1.8	0.3	6.3	-2.9	5.3	0.3	1.3	-2.7	-8.8	0.0675	2.169	1.35
3	2.2	-1.7	0.6	6.3	-3.1	5.2	0.2	1.6	-2.8	-8.9	0.0677	2.168	1.35

* assumes $K = 2.0 \times 10^{-3}$ cal $°C^{-1}$ cm^{-1} s^{-1}

TABLE 7

Station: 10601 (CR 131)
Mean latitude: 46°30'N
Mean longitude: 23°28'W
Duration: 9h
Mean water depth: 4000m
Total no. of dips: 8
No. of successful dips: 8
Comments: IOS/Cambridge probe. Three conductivity measurements. Poor thermistor performance.

DIP	THERMISTOR OFFSETS										GRADIENT °C/m	BOTTOM WATER TEMP	HEAT* FLOW μ cal cm^{-2} s^{-1}
	T1	T2	A1	T3	A2	T4	A3	T5	A4*	T6			
1	7.0	4.0	3.6	10.2	5.0	-39.0	5.0	6.3	-	-2.0	0.0639	2.317	0.81
2	3.4	2.4	0.9	7.8	-3.2	-10.9	0.6	3.6	-	-4.6	0.0691	2.344	0.87
3	1.9	-2.1	-1.1	5.9	-1.1	2.9	-1.1	0.9	-	-6.1	0.0680	2.269	0.89+
4	1.6	-1.6	-0.6	4.9	-0.6	3.5	-0.6	0.7	-	-7.6	0.0526	2.273	0.69+
5	1.0	-1.3	-1.7	4.9	-0.3	3.8	-0.3	0.9	-	-7.3	0.0493	2.276	0.65+
6	1.1	-1.9	-1.9	5.1	0.1	4.1	0.1	0.2	-	-6.9	0.0461	2.278	0.64
7	2.0	-2.0	-1.0	6.0	-1.0	4.0	-1.0	1.0	-	-7.6	0.0419	2.269	0.55+
8	1.0	-1.9	-1.8	5.0	0.0	4.0	0.0	0.3	-	-7.0	0.0493	2.278	0.65+

DIP	CONDUCTIVITY FOR GIVEN ARRAY x 10^{-3} cal $°C^{-1}$ cm^{-1} s^{-1}				MEAN
	A1	A2	A3	A4*	
1	1.258	1.316	1.247	-	1.274
2	1.290	1.326	1.173	-	1.263
6	1.350	1.429	1.407	-	1.395

Overall mean 1.311

\+ uses overall conductivity mean
* Faulty Channel

TABLE 8

Station: 10606 (CR 131)
Mean latitude: 52°21'N
Mean longitude: 30°00'W
Duration: 10h
Mean water depth: 4150m
Total no. of dips: 4
No. of successful dips: 2
Comments: IOS/Cambridge probe. Station terminated by winch problems.

DIP	THERMISTOR OFFSETS										GRADIENT °C/m	BOTTOM WATER TEMP.	HEAT* FLOW μ cal cm^{-2} s^{-1}
	T1	T2	A1	T3	A2	T4	A3	T5	A4*	T6			
1	1.5	1.9	-1.1	7.9	-6.5	4.2	-1.1	1.3	-	-8.1	0.1122	2.547	2.24
2	-0.6	2.4	-0.6	8.4	-6.6	4.6	-0.6	0.9	-	-7.6	0.1594	2.551	3.19

* Faulty channel

+ assumes $K = 2.0 \times 10^{-3}$ cal $°C^{-1}$ cm^{-1} s^{-1}

TABLE 9

Station: 10662 (CR 134)
Mean latitude: 41°48'N
Mean longitude: 23°51'W
Duration: 8h
Mean water depth: 3780m
Total no. of dips: 10
No. of successful dips: 10
Comments: IOS/Cambridge probe. Good station with conductivity measurements.

DIP	THERMISTOR OFFSETS										GRADIENT °C/m	BOTTOM WATER TEMP.	HEAT FLOW μ cal cm^{-2} s^{-1}
	T1	T2	A1	T3	A2	T4	A3	T5	A4	T6			
1	8.8	-12.4	-2.4	-0.6	5.8	4.6	-4.4	-2.4	4.6	-1.4	0.0832	2.378	0.96
2	9.3	-12.7	-2.5	-0.7	7.3	4.3	-4.7	-2.7	4.3	-1.7	0.0721	2.375	0.90
3	9.3	-12.7	-2.7	-0.7	7.3	4.3	-4.7	-2.7	4.3	-1.7	0.0657	2.375	0.84
4	8.9	-12.4	-2.4	-1.0	5.9	4.6	-4.4	-2.4	4.6	-1.4	0.0734	2.378	0.91
5	9.5	-12.5	-2.5	-0.5	7.1	4.5	-4.5	-2.7	3.8	-1.9	0.0635	2.377	0.79
6	8.8	-13.3	-2.3	-1.0	5.9	4.7	-4.3	-2.3	4.7	-1.3	0.0600	2.379	0.76
7	9.1	-13.9	-1.9	-0.9	6.1	5.1	-3.9	-2.9	3.8	-0.9	0.0598	2.382	0.75
8	9.3	-12.7	-1.7	-0.8	6.8	2.3	-2.8	-2.6	3.3	-1.3	0.0546	2.392	0.69
9	9.3	-13.1	-1.7	-0.8	6.3	3.3	-3.7	-2.5	3.8	-1.3	0.0524	2.384	0.64
10	9.0	-12.8	-2.0	-0.8	6.4	3.8	-3.6	-2.6	4.2	-1.4	0.0492	2.379	0.64

DIP	CONDUCTIVITY FOR GIVEN ARRAY cal $°C^{-1}$ cm^{-1} s^{-1} x 10^{-3}				MEAN
	A1	A2	A3	A4	
1	1.163	1.161	1.123	1.151	1.150
2	1.211	1.288	1.264	1.240	1.251
3	1.295	1.288	1.316	1.199	1.275
4	1.230	1.280	1.259	1.175	1.236
5	1.276	1.283	1.242	1.175	1.244
6	1.304	1.395	1.209	1.166	1.269
7	1.307	1.331	1.175	1.171	1.246
8	1.304	1.340	1.194	1.209	1.262
9	1.304	1.304	1.161	1.101	1.218
10	1.338	1.433	1.235	1.180	1.297

TABLE 10

Station: 10674 (CR 134)
Mean latitude: 33°56'N
Mean longitude: 29°20'W
Duration: 8h
Mean water depth: 3350m
Total no. of dips: 10
No. of successful dips: 4
Comments: IOS/Cambridge probe. Thermistor string broken on fifth dip.

DIP	THERMISTOR OFFSETS										GRADIENT* °C/m	BOTTOM WATER TEMP.	HEAT FLOW μ cal cm^{-2} s^{-1}	ADVECTION VELOCITY cm/y
	T1	T2	A1	T3	A2	T4	A3	T5	A4	T6				
1	6.8	-3.6	-4.2	-2.3	4.0	3.4	-2.6	-4.2	4.2	-1.6	0.0874	2.511	1.17	-
2	6.7	-3.9	-3.9	-2.3	4.3	3.1	-2.9	-3.9	5.1	-1.9	0.0901	2.509	1.18	97.6
3	6.8	-4.0	-4.0	-2.4	4.2	3.0	-3.0	-4.0	5.0	-2.0	0.0841	2.509	1.16	126.7
4	6.6	-3.6	-4.1	-2.2	4.2	3.4	-2.6	-4.2	4.2	-1.6	0.0760	2.511	1.07	111.2

* Limited penetration. Gradient based on 3m T3 to T6.

DIP	CONDUCTIVITY FOR GIVEN ARRAY cal $°C^{-1}$ s^{-1} x 10^{-3}				MEAN
	A1	A2	A3	A4	
1	1.660	1.362	1.240	1.075	1.334
2	1.799	1.280	1.233	0.913	1.306
3	1.835	1.254	1.266	1.142	1.374
4	1.882	1.321	1.269	1.142	1.404

FIGURE CAPTIONS

Figure 1. Location of all heat flow stations described in this report. 'KTF' and 'GME' are the King's Trough Flank and Great Meteor East study areas respectively. KTF extends from 41° to 43°N, 20° to 24.5°W while GME extends from 30.5° to 32.5°N, 24° to 26°W.

Figure 2. Simplified model which considers the ocean crust to be a semi-infinite solid cooling by conduction. Lower graph shows the theoretical variation of heat flow with age compared to measured values (dots from Parsons and Sclater, 1977).

Figure 3. Schematic section through spreading centre and ageing ocean crust showing the postulated changes in hydrothermal circulation brought about by overlying sedimentation and reduction in basalt permeability. Graphs show predicted sediment temperature profiles.

Figure 4. The original heat probe supplied by Applied Microsystems.

Figure 5. The improved heat probe. The mechanical design is by Bullard Laboratories, Cambridge, while the acoustic telemetry system was designed by IOS. The probe weighs approximately one ton in air.

Figure 6. A typical station record received from the IOS/Cambridge heat probe on the precision echosounder unit (P.E.S.). Each line is built up from a series of points printed by a stylus which traverses the paper from left to right every two seconds. The points correspond to the detection of a 10-kHz pulse from the probe and as the paper is drawn slowly upwards the points merge into the lines seen here. The lines represent plots of probe temperature (T1 to T4), tilt and elchosounder height. The pulses corresponding to these items are transmitted after a reference pulse with a delay proportional to the data value. Thus the temperature rise during the heat pulse can be seen together with the cooling on pullout. 'Beacon' corresponds to a signal from an independent 'pinger' clamped up-wire from the probe.

Figure 7. Section through the IOS needle probe showing details of the internal construction. The probe is inserted into a sediment sample and heated by an alternating current. The rise in

temperature of the needle then gives a measure of the thermal conductivity of the material.

Figure 8. The function $F(\alpha, \tau)$ versus dimensionless time τ, for various values of α, (from Bullard, 1954). This function describes the cooling of a heat pulse within the probe and is used to subtract the effects of frictional heating. In a modified form, the function is also used in the estimation of sediment conductivity by the heat pulse method.

Figure 9. A typical linear plot of corrected temperatures (°C) versus the reciprocal of time (seconds) for a typical heat pulse decay in sediment.

Figure 10. Variation in the gradient of a plot of corrected temperature versus reciprocal time for changing heat pulse origin time (+). The RMS residual in the fit to a straight line is also shown, (□). The graphs illustrate how the computer program 'COND'is used to estimate the gradient corresponding to the optimum apparent 'origin time' of the heat pulse.

Figure 11. A typical temperature record during a heat probe station together with the appropriate stages in the data analysis.

Figure 12. Sediment temperature profiles measured at Station 10301. It is evident that the probe has penetrated to a depth of only 1-2 metres.

Figure 13. Sediment temperature profiles measured at Station 10301. It is evident that the probe has penetrated to a depth of only 1-2 metres.

Figure 14. Sediment temperature profiles measured at Station 10318.

Figure 15. Sediment temperature profiles measured at Station 10318.

Figure 16. Sediment temperature profiles measured at the first two dips of Station 10335.

Figure 17. Sediment temperature profile measured at the final dip of Station 10335.

Figure 18. Sediment temperature profiles measured at the first three dips of Station 10405.

Figure 19. Sediment temperature profiles measured at the final three dips of Station 10405.

Figure 20. Sediment temperature profiles measured at the three dips of Station S126/3.

Figure 21. Sediment temperature profiles measured at the three dips of Station S126/5.

Figure 22. Heat flow stations, described in this report, in the vicinity of Great Meteor Seamount. The region designated as a Study Area is enclosed by the box.

Figure 23. Lithostratigraphy and thermal conductivity measurements on Kastenlot core 10406 (32°35'N, 22°27'W). Two orthogonal measurements have been combined to estimate the percentage anisotropy.

Figure 24. A pair of orthogonal needle probe measurements at a single level in Kastenlot core 10406 (32°35'N, 22°27'W). Plots are of temperature rise versus log (time). The differences in gradient reflect conductivity anisotropy in the sediment.

Figure 25. Sediment temperature profiles measured at the first four penetrations of Station 10601.

Figure 26. Sediment temperature profiles measured at the final four penetrations of Station 10601.

Figure 27. Sediment temperature profiles measured at the two dips of Station 10606.

Figure 28. Sediment temperature profiles measured at the first six dips of Station 10662.

Figure 29. Sediment temperature profiles measured at the final four dips of Station 10662.

Figure 30. Sediment temperature profiles measured at the four dips of Station 10674. The penetration in each case is approximately only 3m.

Figure 31. Sediment thermal conductivity profiles for the four dips of station 10674.

Figure 32. Location of the King's Trough Flank (KTF) study area (shaded box). Bathymetric contours at 1000m intervals.

Figure 33. Location of heat flow stations in relation to the bathymetry of the KTF study area. Contours in 100m intervals. Outline of GLORIA coverage is shown by the thin box-shaped outline.

Figure 34. The study area to the east of Great Meteor Seamount shown in greater detail. The location of heat flow stations described in this report are also shown.

FIG. 1

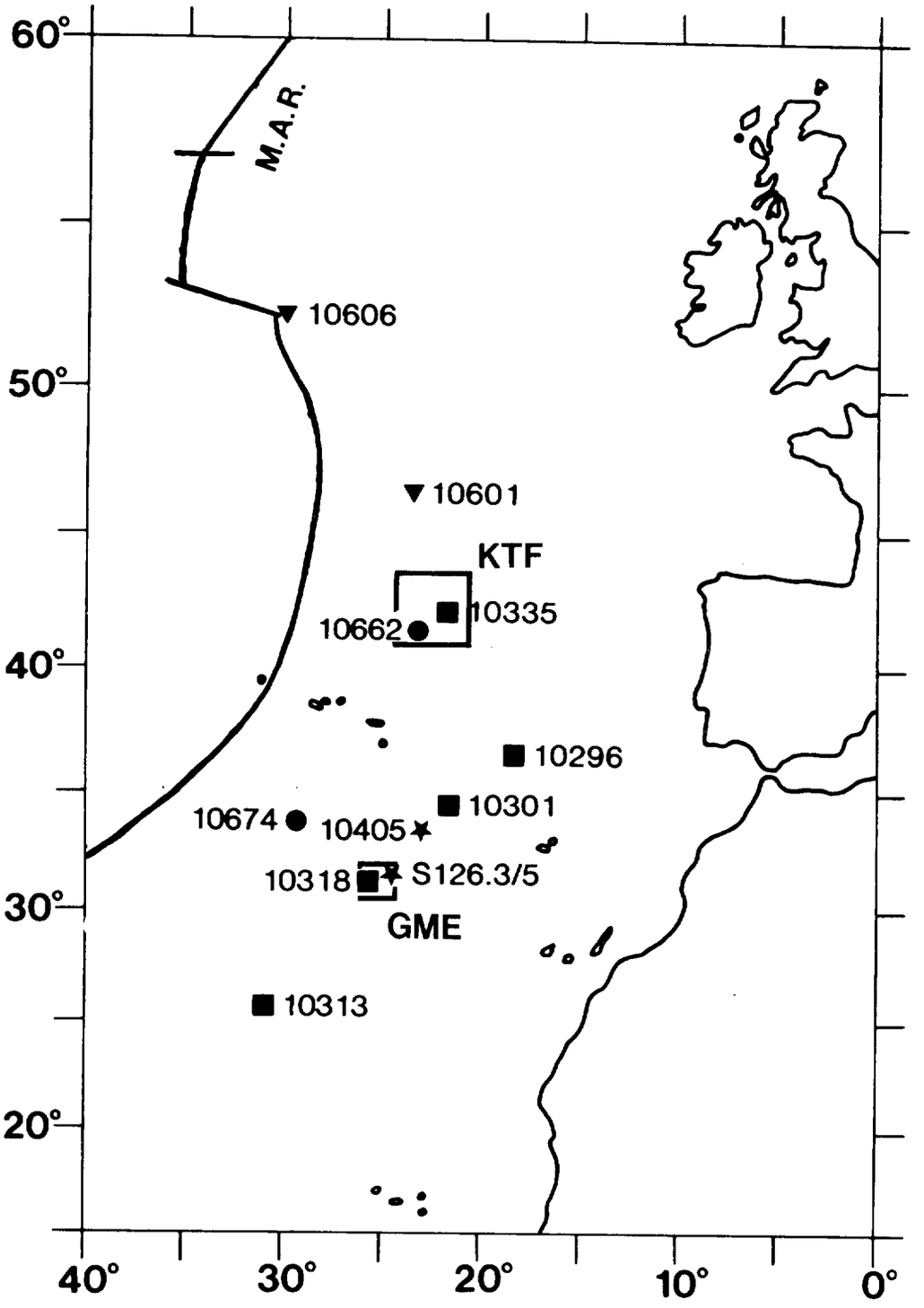

LOCATION OF HEAT FLOW STATIONS

CR 118 ■ CR 126 ★ CR 131 ▼ CR 134 ●

FIG. 2

HEAT FLOW vs. AGE

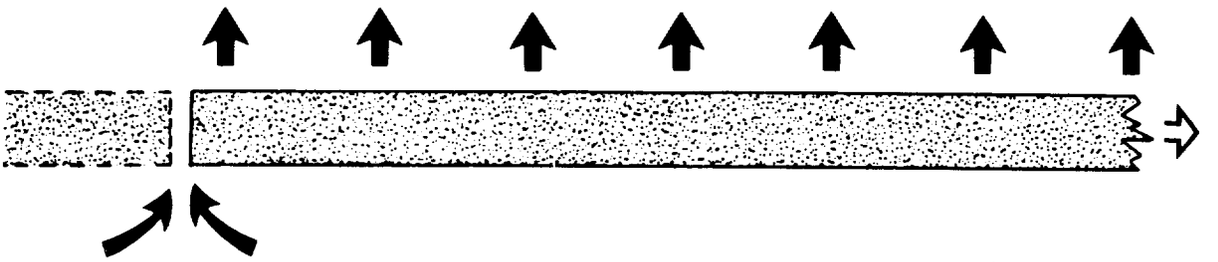

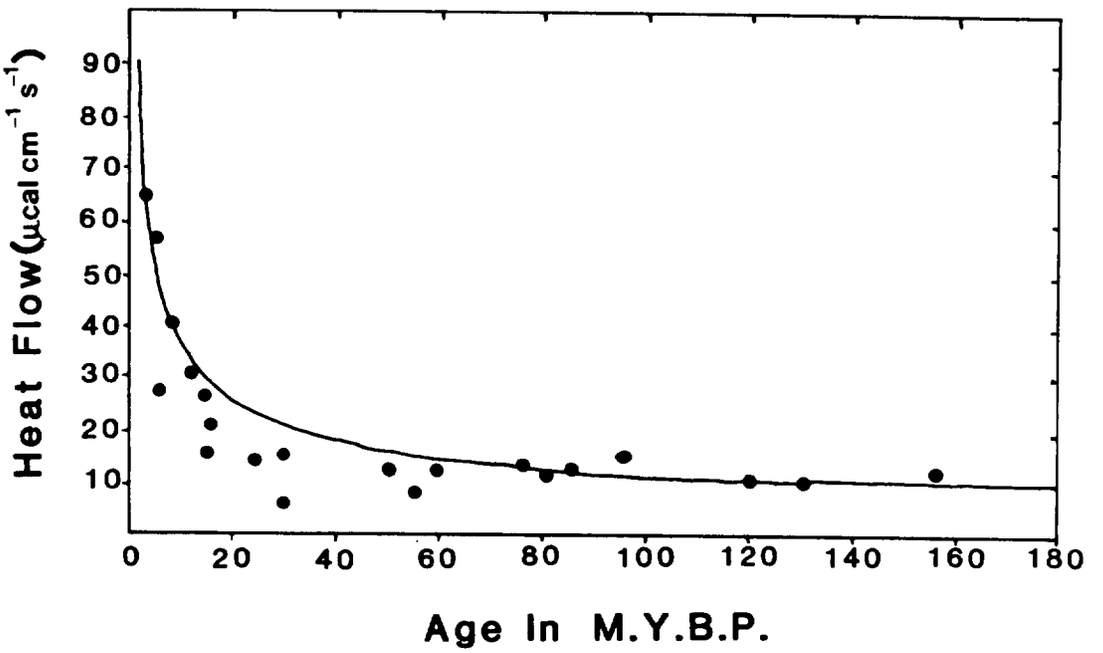

FIG. 3

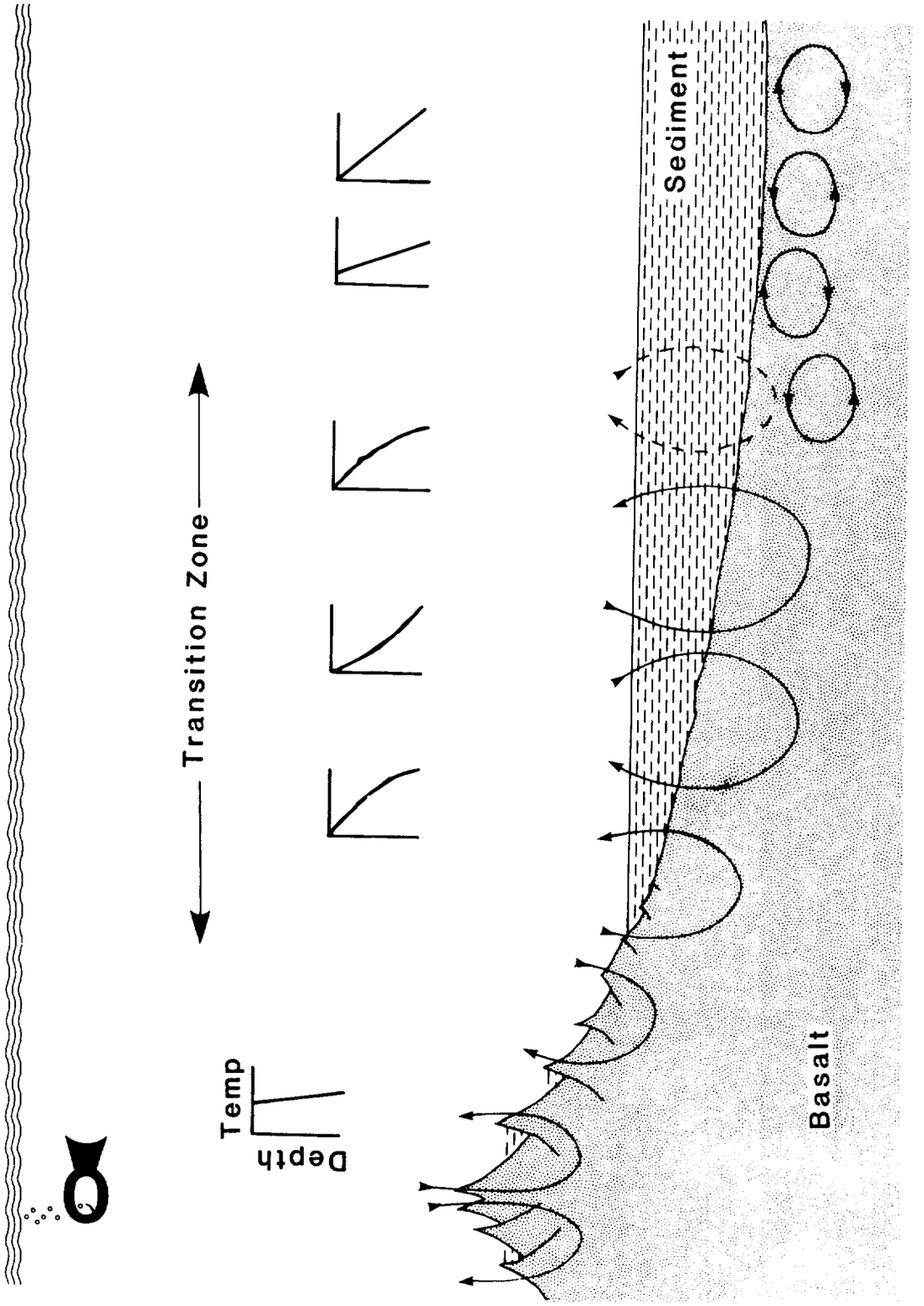

FIG. 4

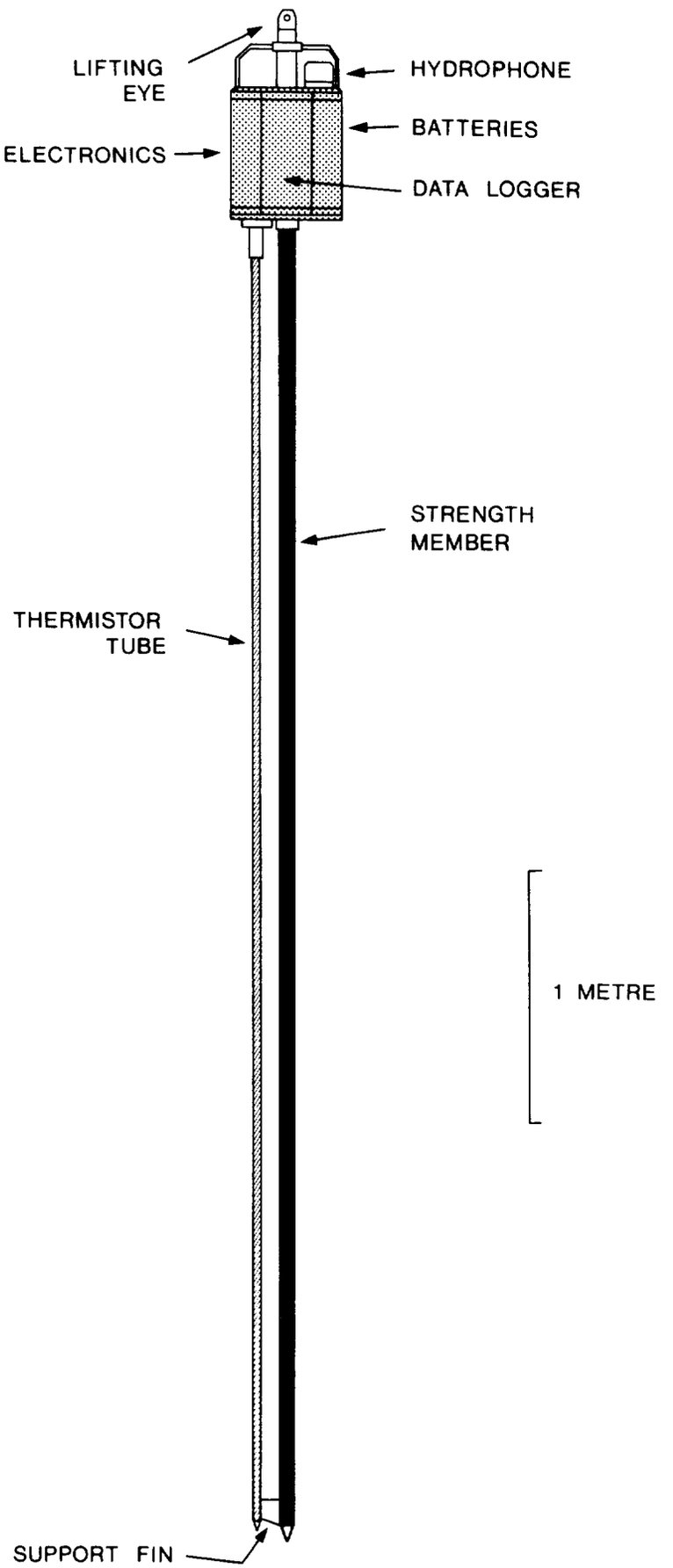
LIFTING EYE
HYDROPHONE
BATTERIES
ELECTRONICS
DATA LOGGER
STRENGTH MEMBER
THERMISTOR TUBE
1 METRE
SUPPORT FIN

FIG. 5

I.O.S. Cambridge Probe

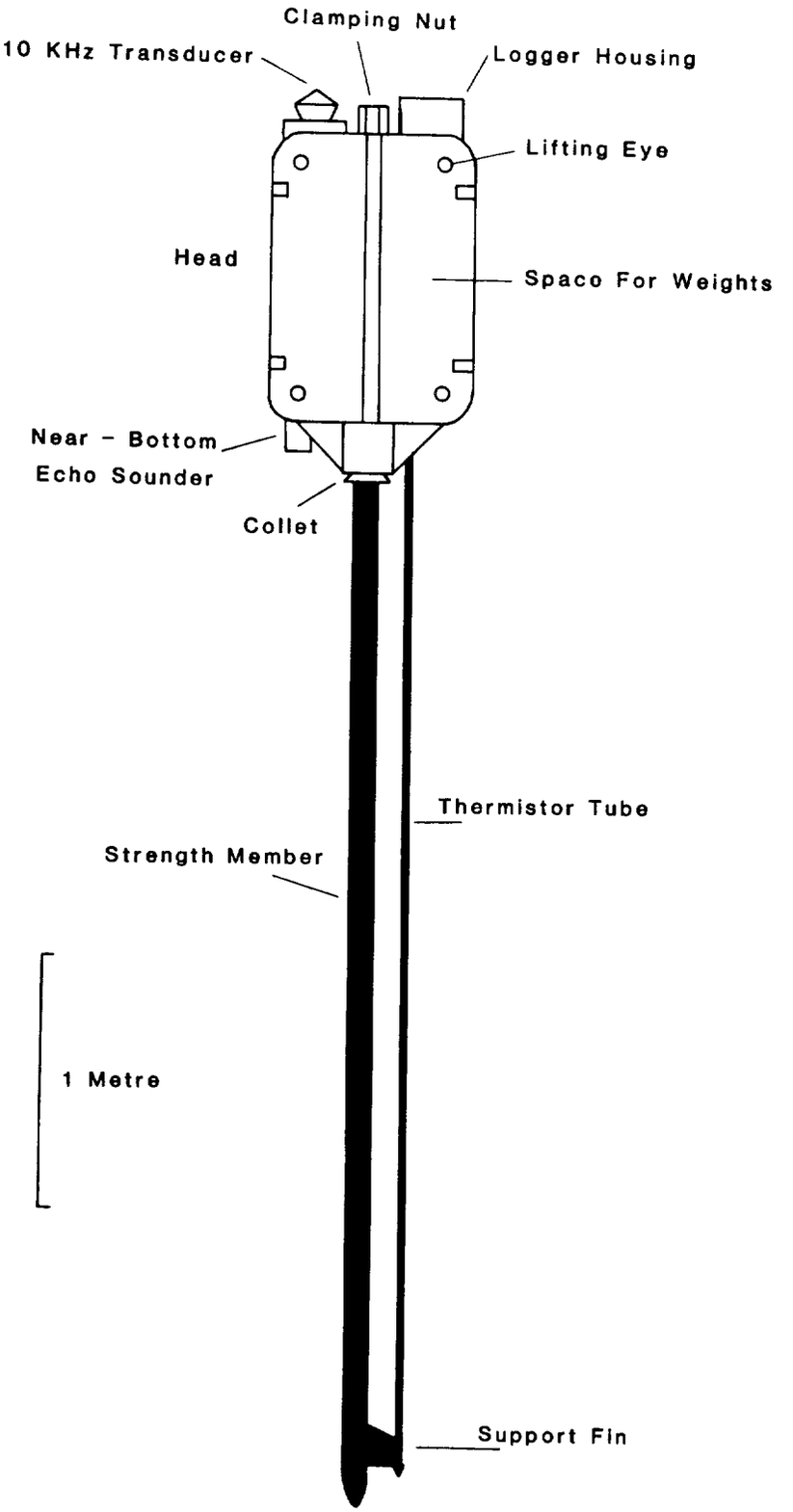

FIG. 6

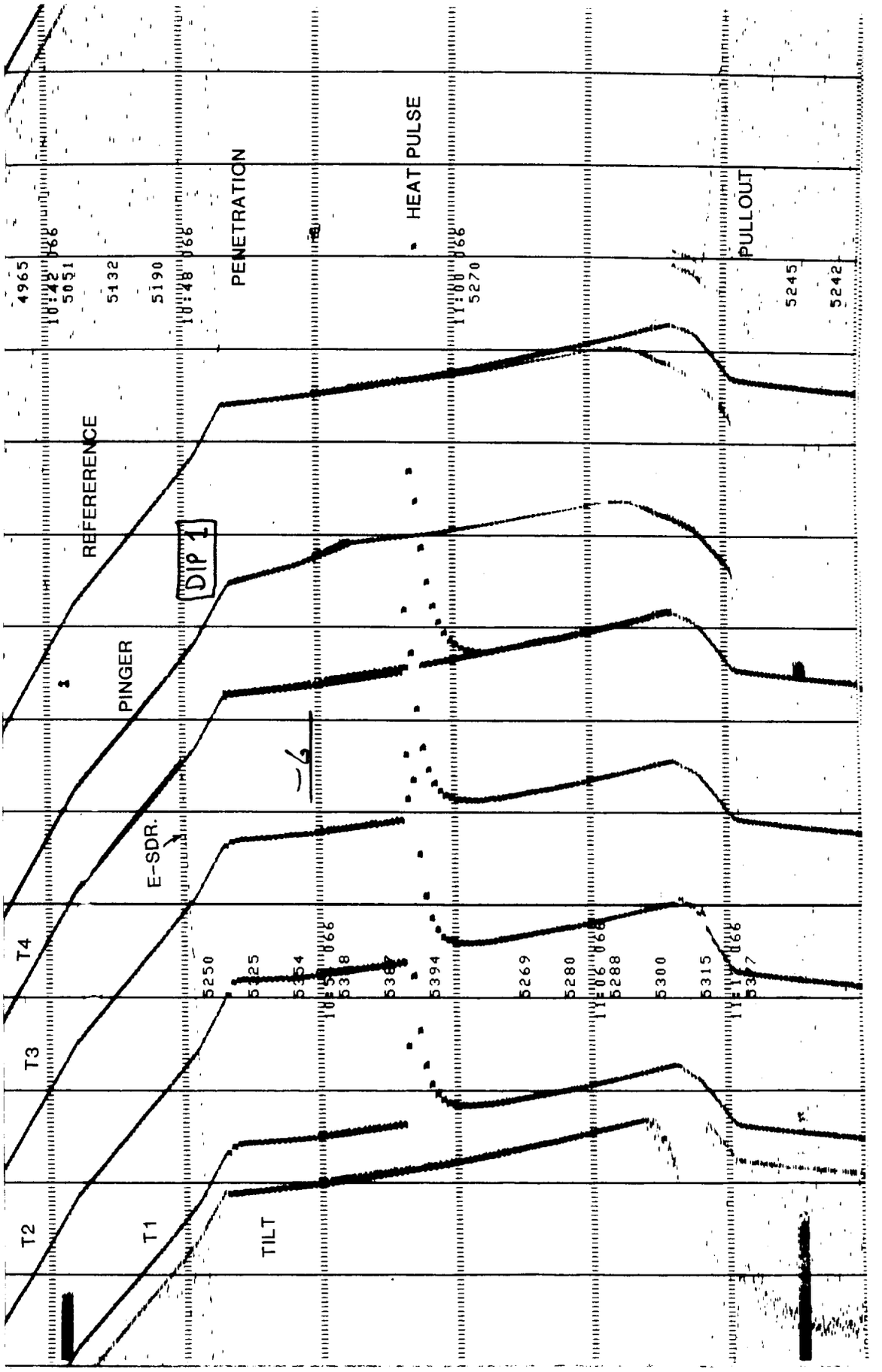
REFERENCE
PINGER
E-SDR.
T4
T3
T2
T1
TILT
PENETRATION
HEAT PULSE
PULLOUT
DIP 1
4965
5051
5132
5190
5270
5245
5242
5250
5325
5394
5269
5280
5288
5300
5315

FIG. 7

I.O.S. Needle Probe (Section)

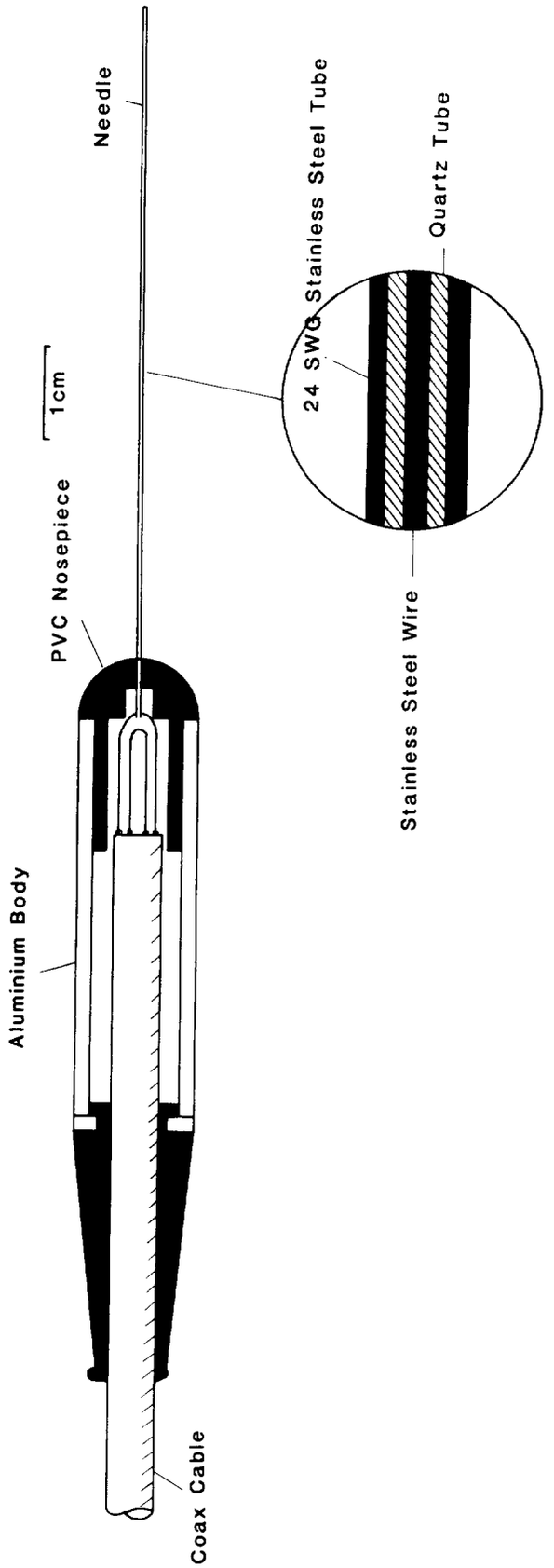

FIG. 8

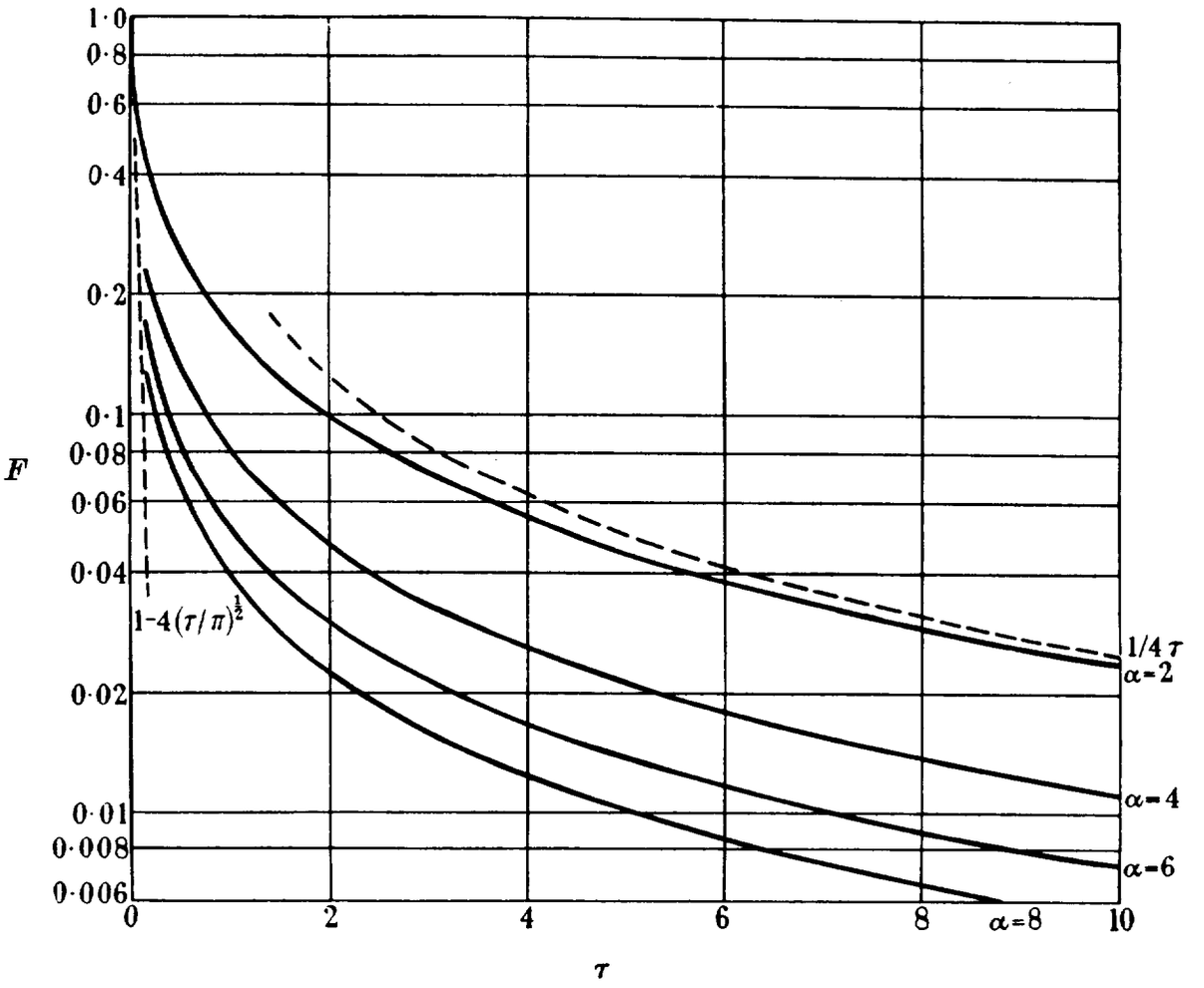
1·0
0·8
0·6
0·4
0·2
0·1
0·08
0·06
0·04
0·02
0·01
0·008
0·006
F
1-4(τ/π)^½
1/4 τ
α=2
α=4
α=6
α=8
0
2
4
6
8
10
τ

FIG.9

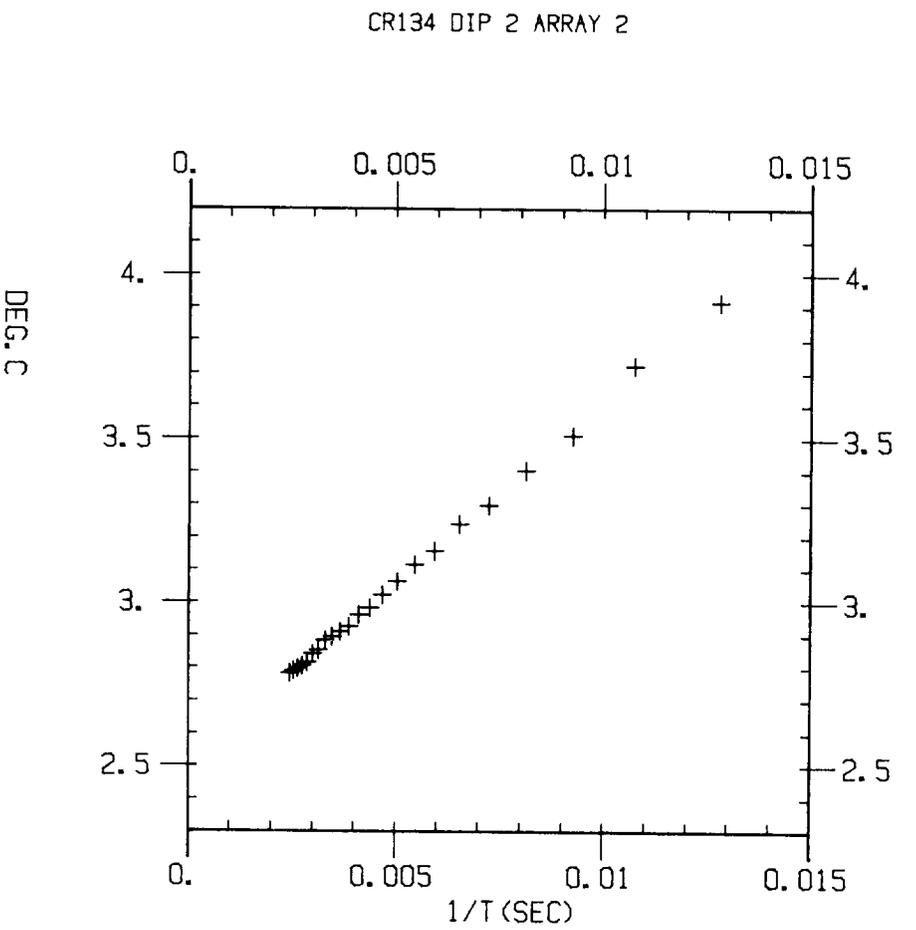

FIG. 10

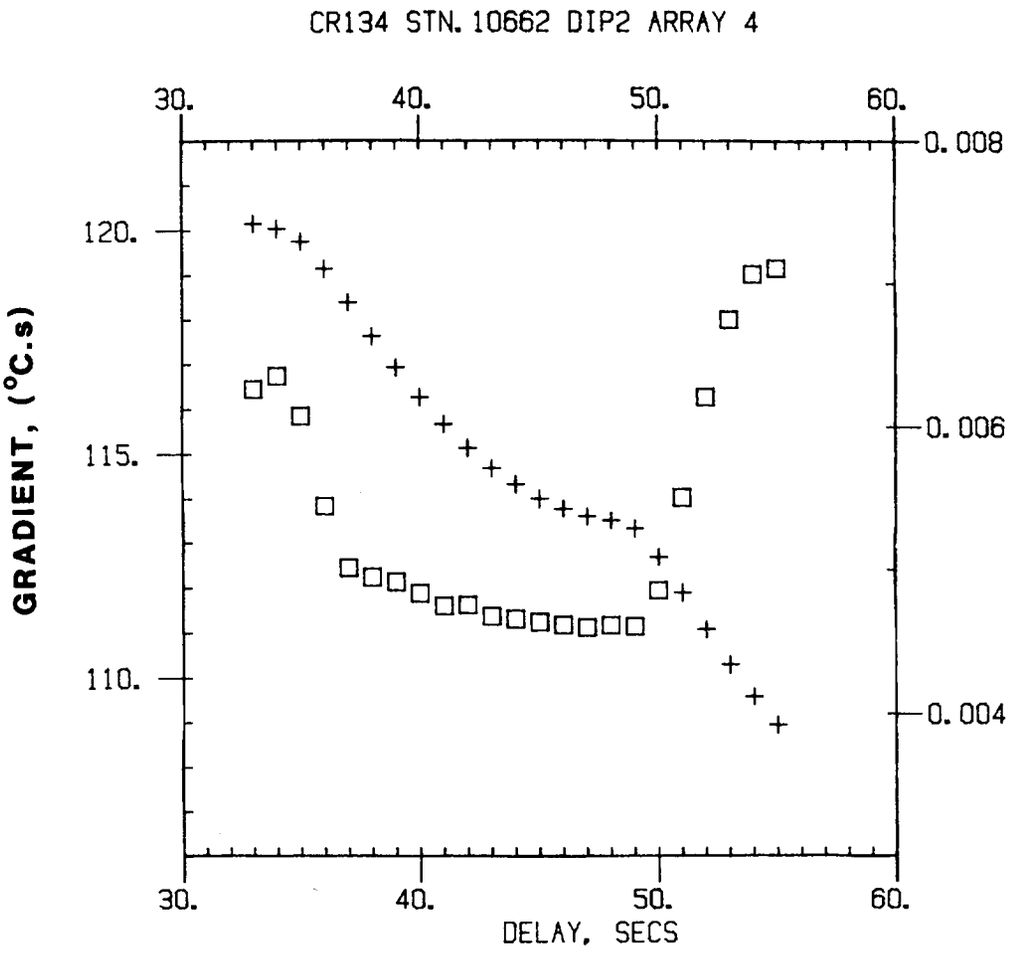
CR134 STN. 10662 DIP2 ARRAY 4
30.
40.
50.
60.
0.008
0.006
0.004
120.
115.
110.
GRADIENT, (°C.s)
DELAY, SECS

TYPICAL STATION TEMPERATURE RECORD

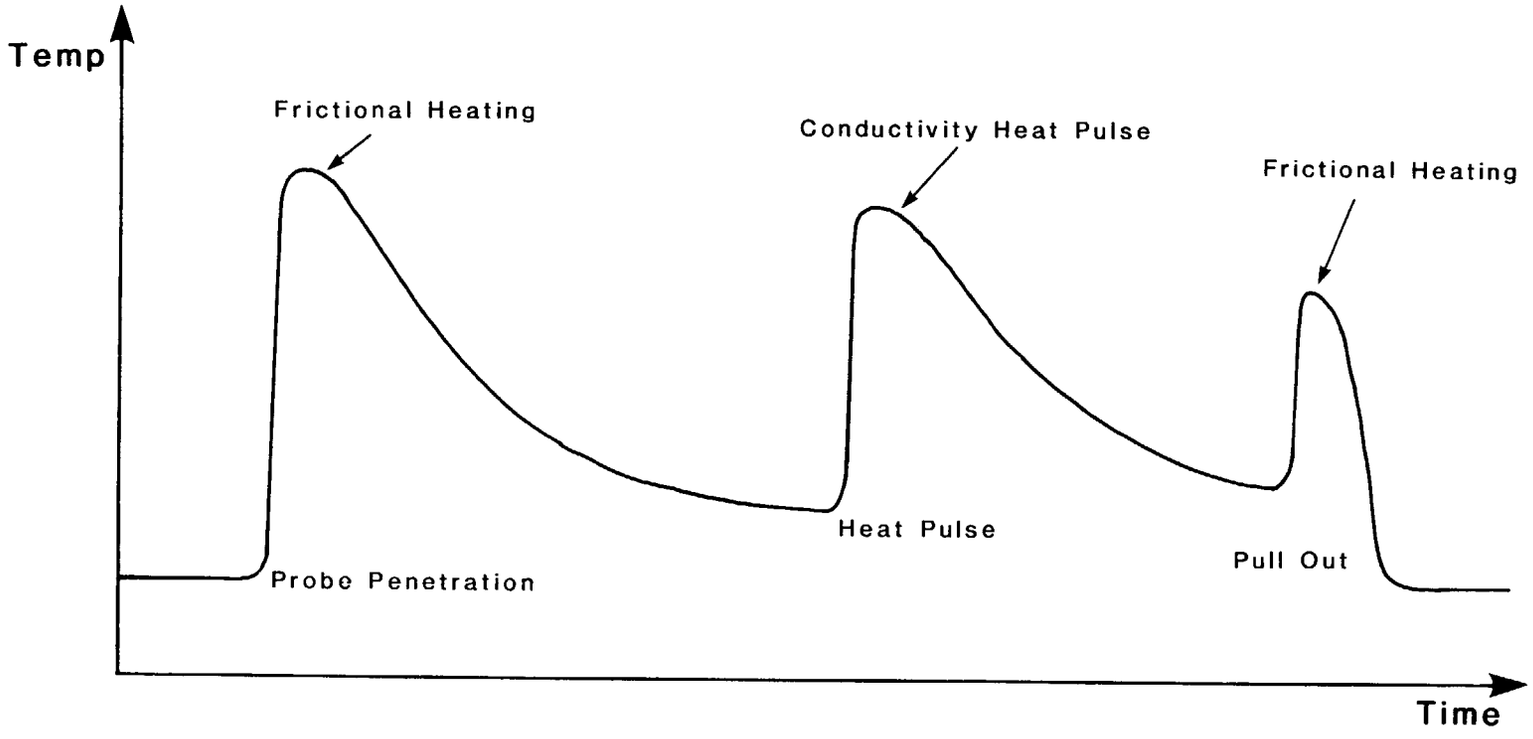

FIG. 11

FIG. 12

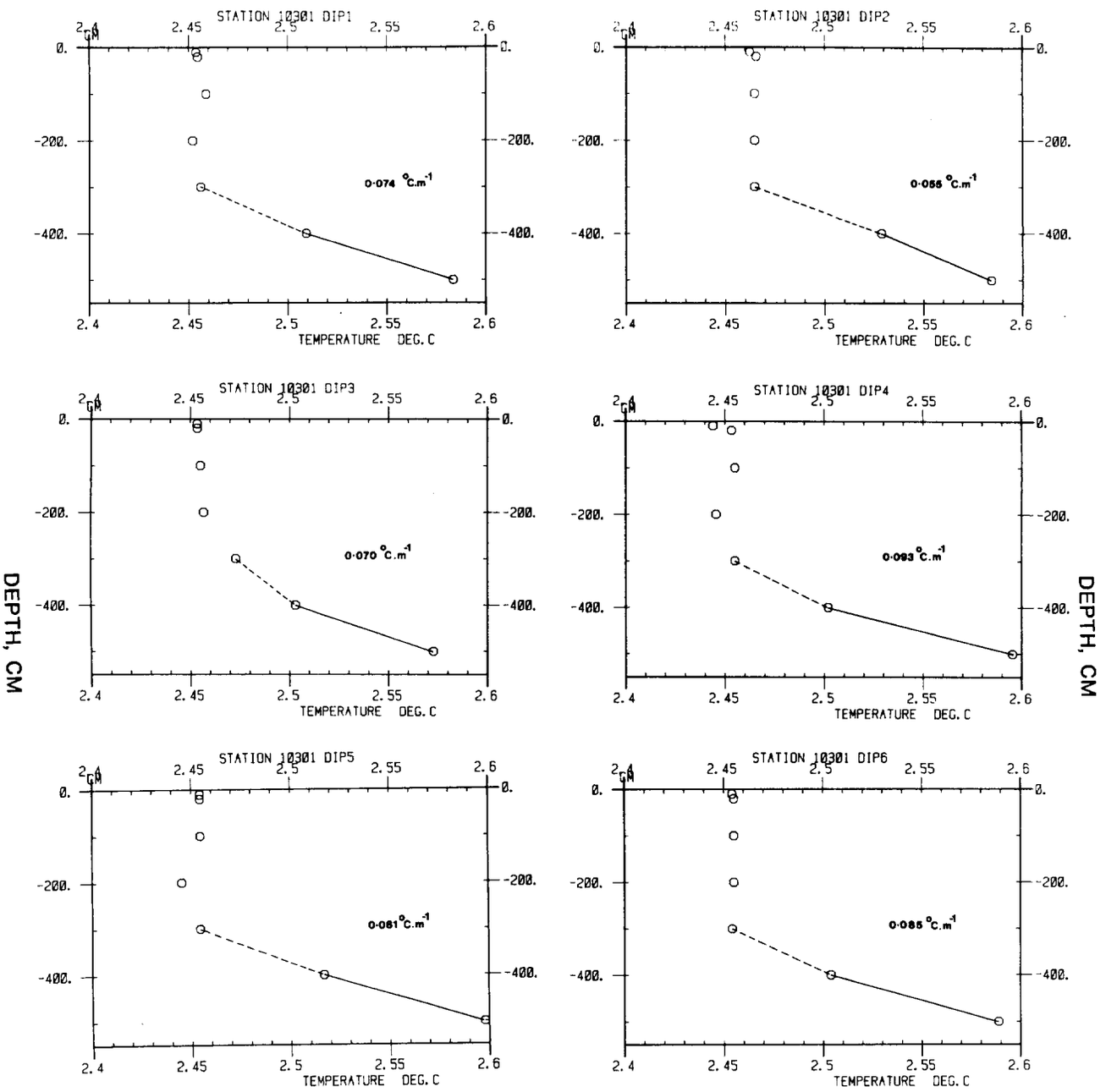
STATION 10301 DIP1
STATION 10301 DIP2
STATION 10301 DIP3
STATION 10301 DIP4
STATION 10301 DIP5
STATION 10301 DIP6
0.074 °C.m-1
0.055 °C.m-1
0.070 °C.m-1
0.093 °C.m-1
0.061 °C.m-1
0.085 °C.m-1
2.4
2.45
2.5
2.55
2.6
0.
-200.
-400.
TEMPERATURE DEG. C
DEPTH, CM

FIG. 13

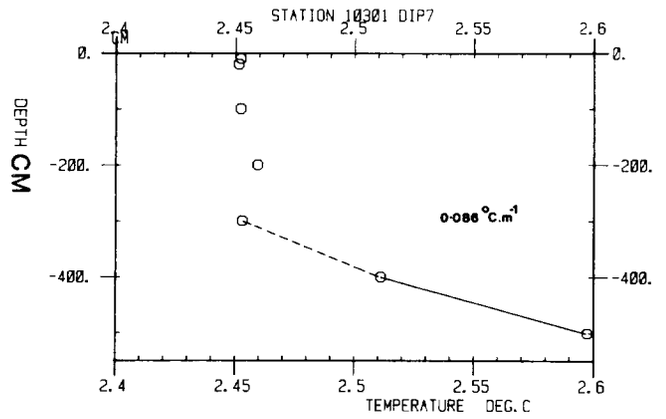
STATION 10301 DIP7
DEPTH CM
0.
-200.
-400.
2.4
2.45
2.5
2.55
2.6
0.086 °C.m⁻¹
TEMPERATURE DEG. C

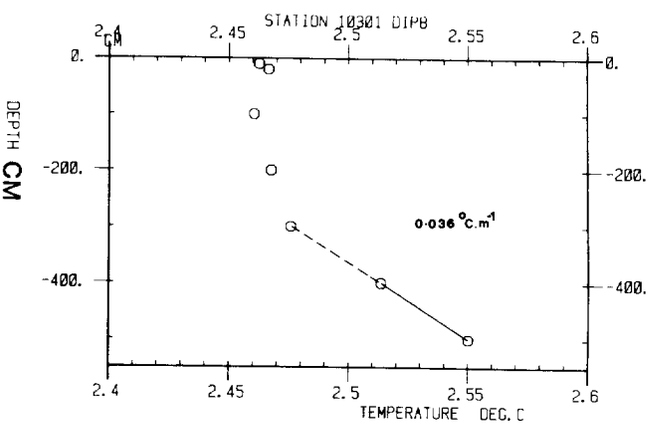
STATION 10301 DIP8
DEPTH CM
0.
-200.
-400.
2.4
2.45
2.5
2.55
2.6
0.036 °C.m⁻¹
TEMPERATURE DEG. C

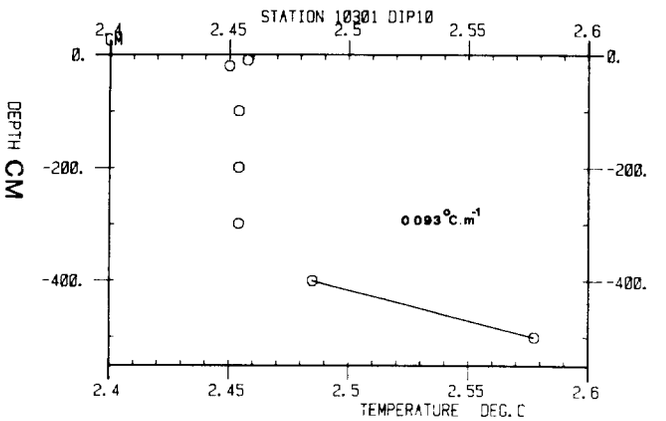
STATION 10301 DIP10
DEPTH CM
0.
-200.
-400.
2.4
2.45
2.5
2.55
2.6
0.093 °C.m⁻¹
TEMPERATURE DEG. C

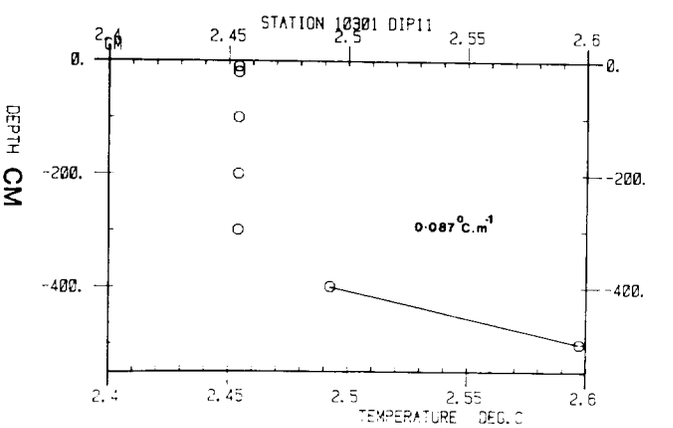
STATION 10301 DIP11
DEPTH CM
0.
-200.
-400.
2.4
2.45
2.5
2.55
2.6
0.087 °C.m⁻¹
TEMPERATURE DEG. C

FIG. 14

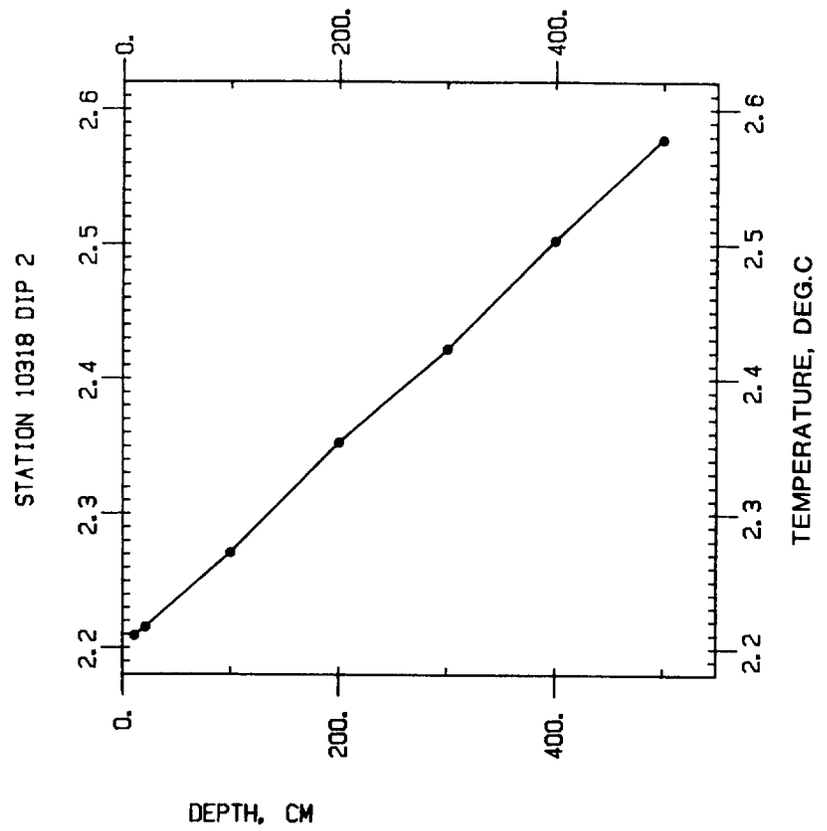
STATION 10318 DIP 2
0.
200.
400.
2.2
2.3
2.4
2.5
2.6
DEPTH, CM
TEMPERATURE, DEG.C

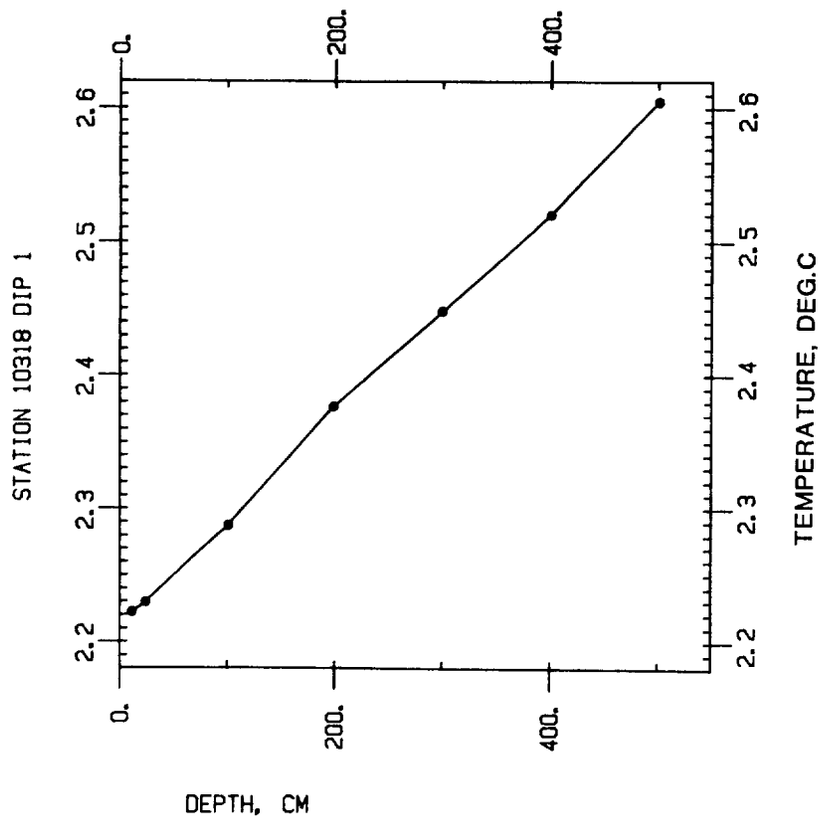
STATION 10318 DIP 1
0.
200.
400.
2.2
2.3
2.4
2.5
2.6
DEPTH, CM
TEMPERATURE, DEG.C

FIG. 15

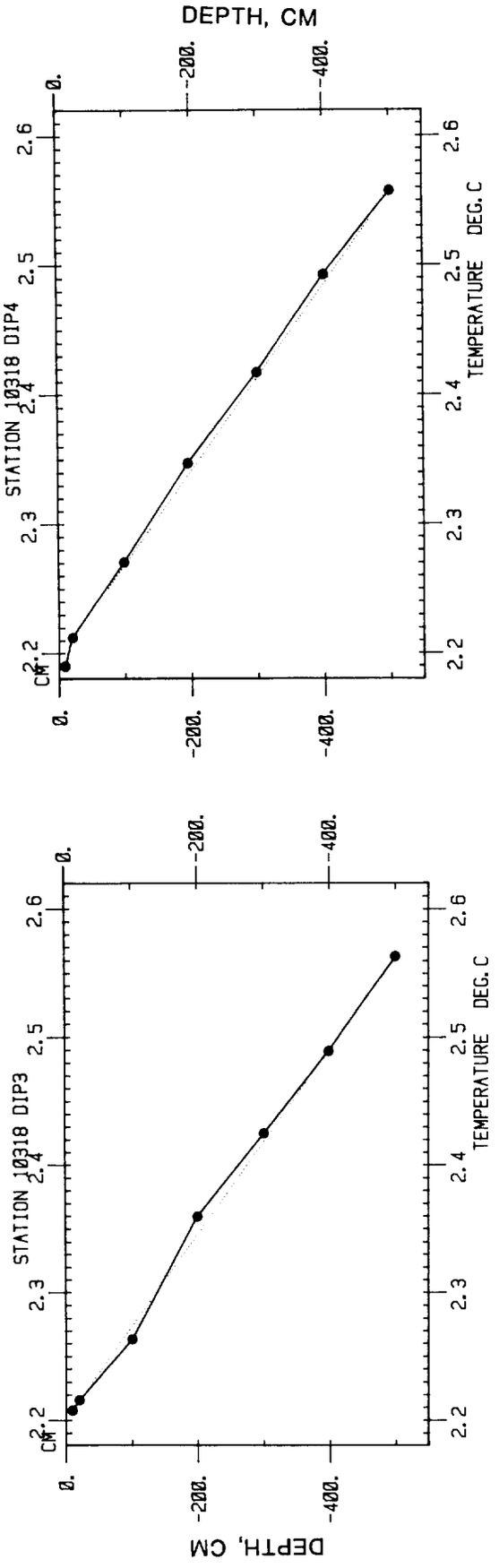
DEPTH, CM
0.
-200.
-400.
2.2
2.3
2.4
2.5
2.6
CM
STATION 10318 DIP4
TEMPERATURE DEG. C
STATION 10318 DIP3
TEMPERATURE DEG. C
DEPTH, CM

FIG. 16

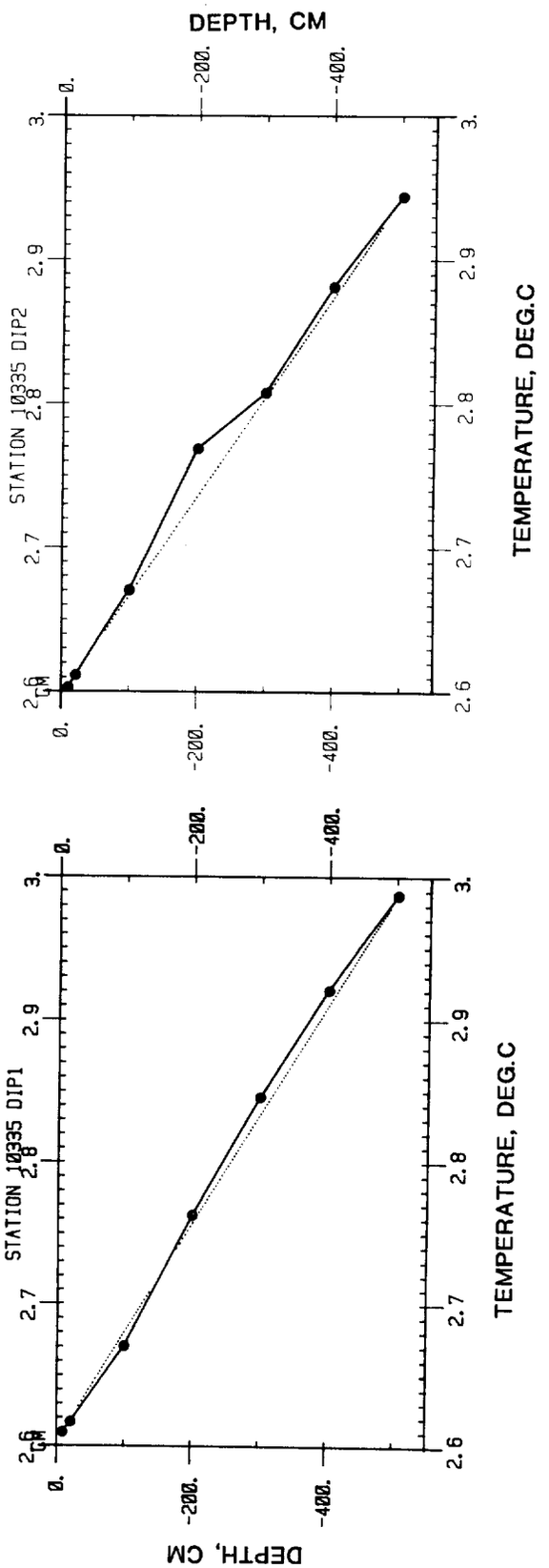
DEPTH, CM
0.
-200.
-400.
3.
2.9
2.8
2.7
2.6
TEMPERATURE, DEG.C
STATION 10335 DIP2
STATION 10335 DIP1

FIG. 17

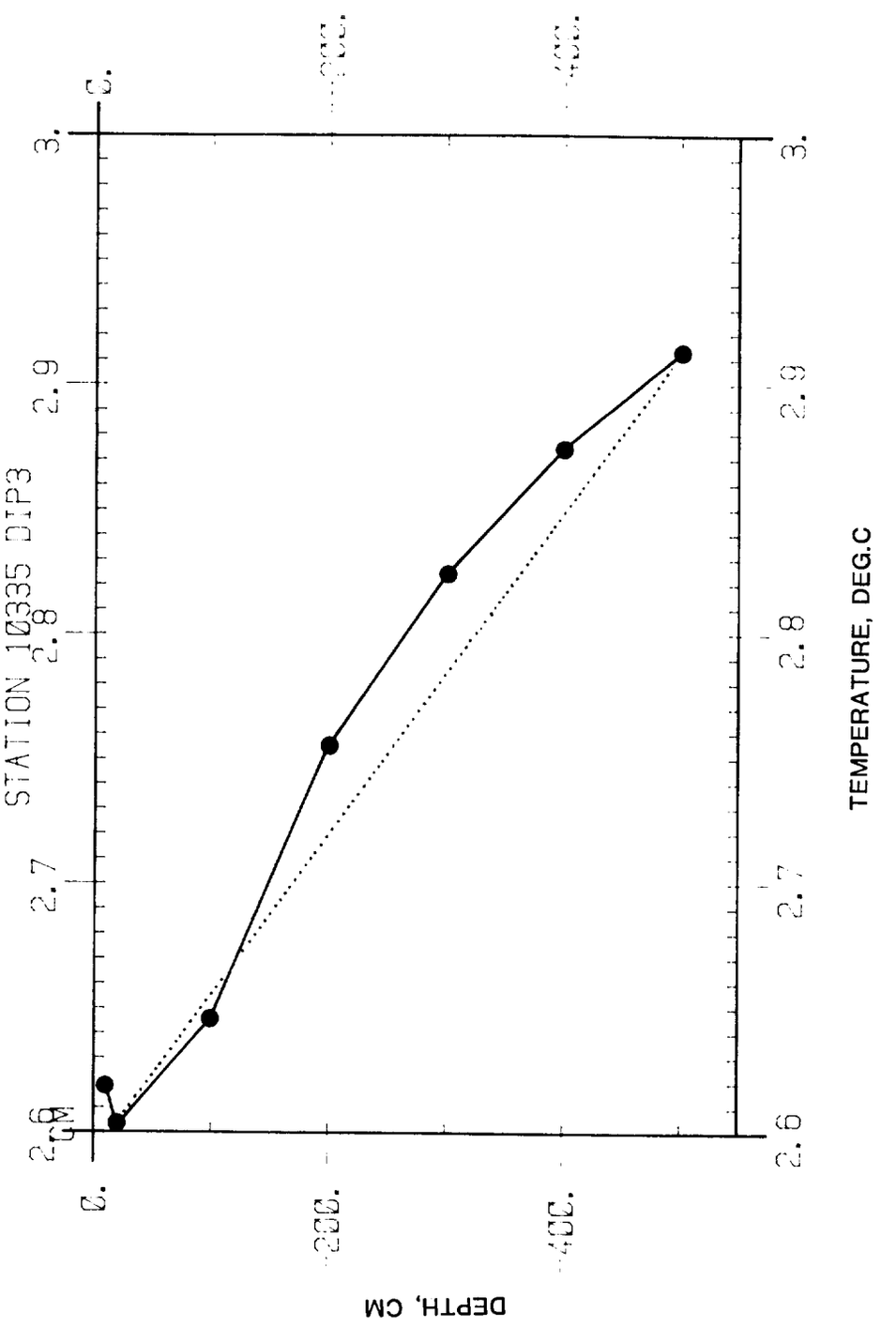
STATION 10335 DIP3
2.6
2.7
2.8
2.9
3.
0.
200.
400.
DEPTH, CM
TEMPERATURE, DEG.C

FIG. 18

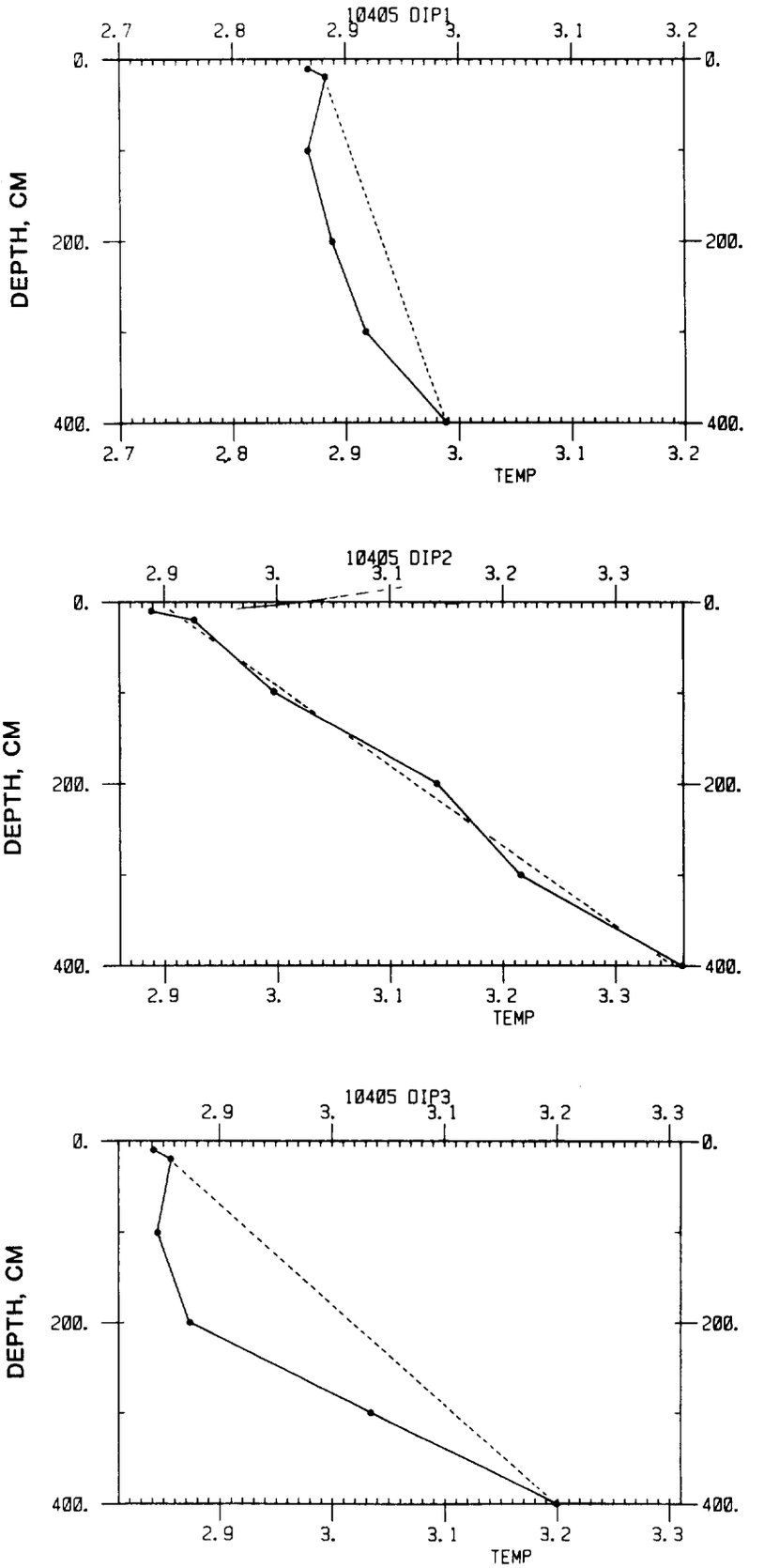
10405 DIP1
2.7
2.8
2.9
3.
3.1
3.2
0.
200.
400.
DEPTH, CM
TEMP
10405 DIP2
2.9
3.
3.1
3.2
3.3
0.
200.
400.
DEPTH, CM
TEMP
10405 DIP3
2.9
3.
3.1
3.2
3.3
0.
200.
400.
DEPTH, CM
TEMP

FIG. 19

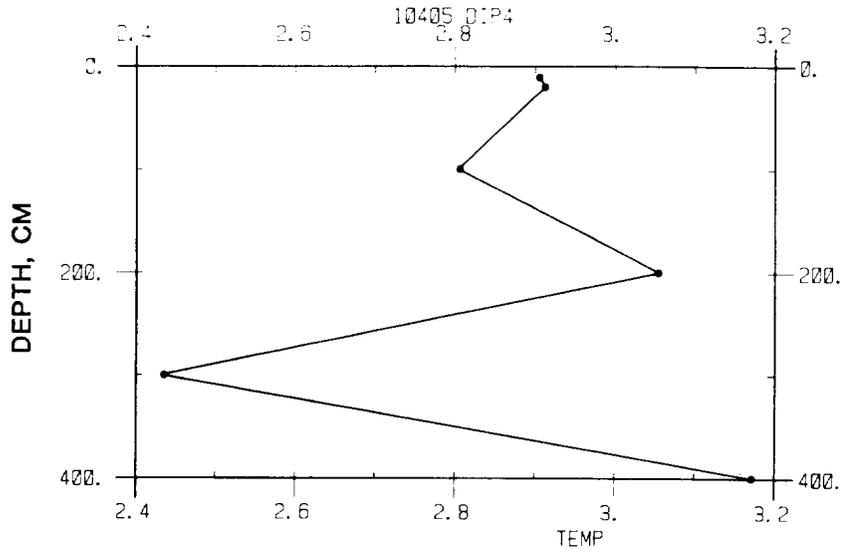
10405 DIP4
2.4
2.6
2.8
3.
3.2
0.
200.
400.
DEPTH, CM
TEMP

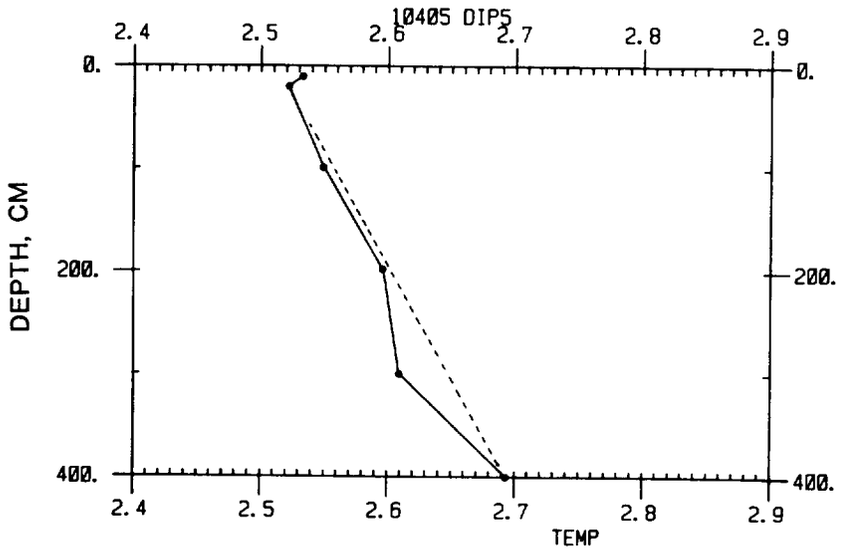
10405 DIP5
2.4
2.5
2.6
2.7
2.8
2.9
0.
200.
400.
DEPTH, CM
TEMP

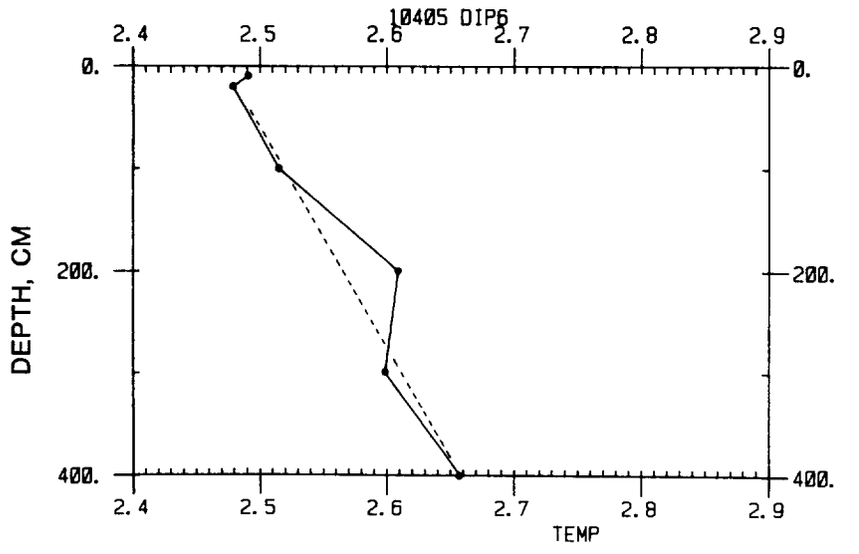
10405 DIP6
2.4
2.5
2.6
2.7
2.8
2.9
0.
200.
400.
DEPTH, CM
TEMP

FIG. 20

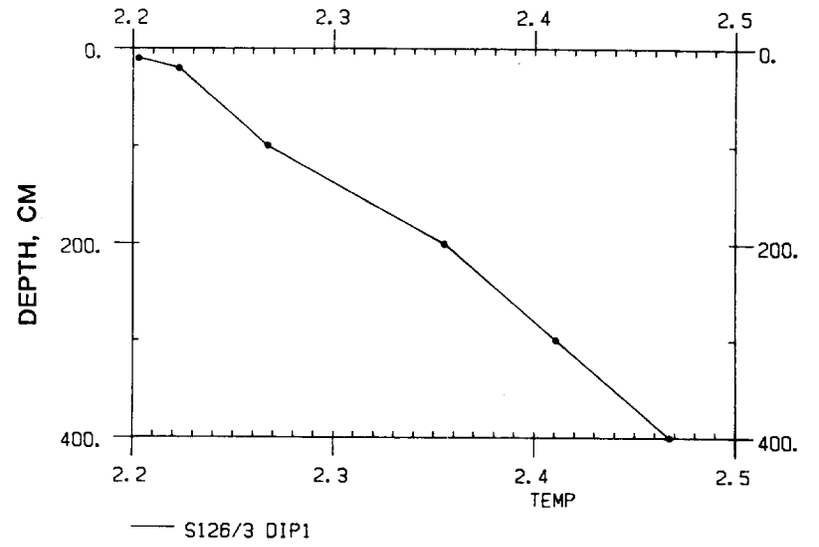
2.2
2.3
2.4
2.5
0.
200.
400.
DEPTH, CM
TEMP
S126/3 DIP1

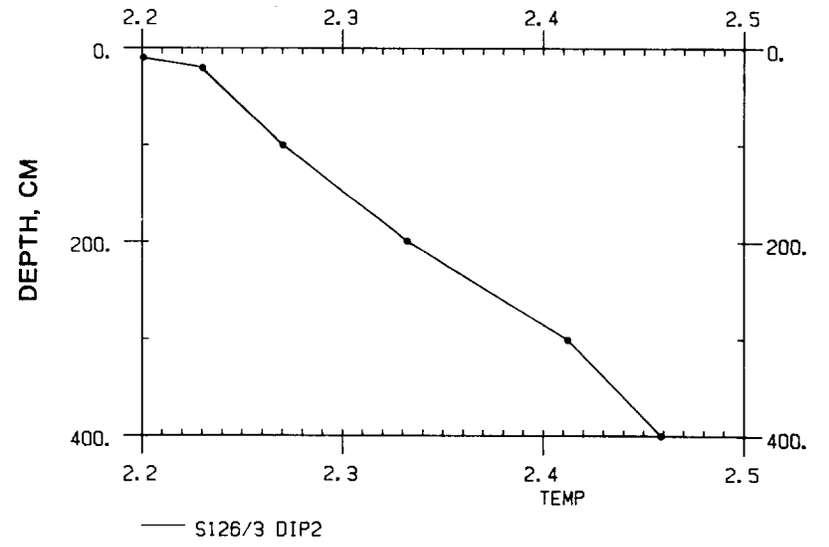
2.2
2.3
2.4
2.5
0.
200.
400.
DEPTH, CM
TEMP
S126/3 DIP2

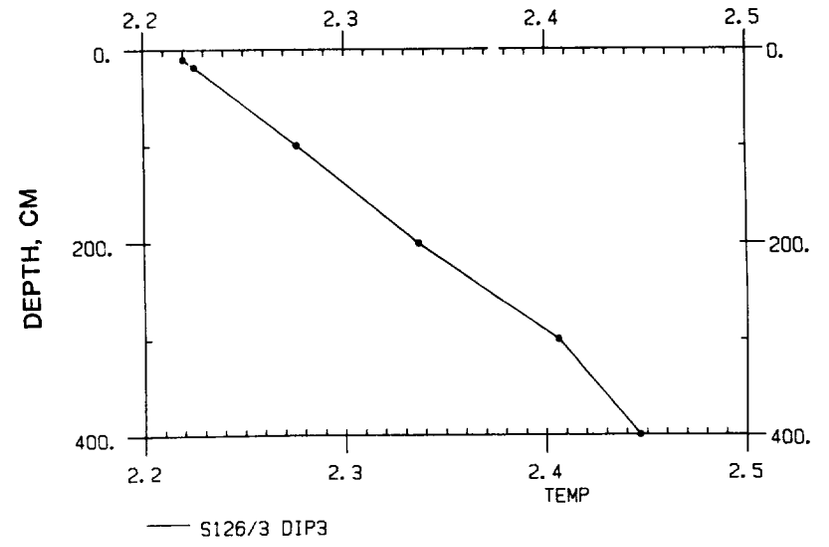
2.2
2.3
2.4
2.5
0.
200.
400.
DEPTH, CM
TEMP
S126/3 DIP3

FIG. 21

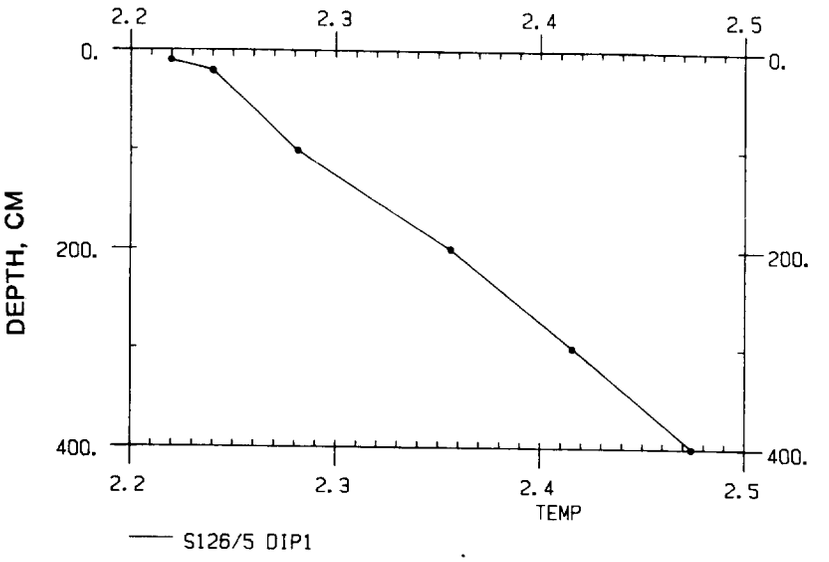
2.2
2.3
2.4
2.5
0.
200.
400.
DEPTH, CM
TEMP
S126/5 DIP1

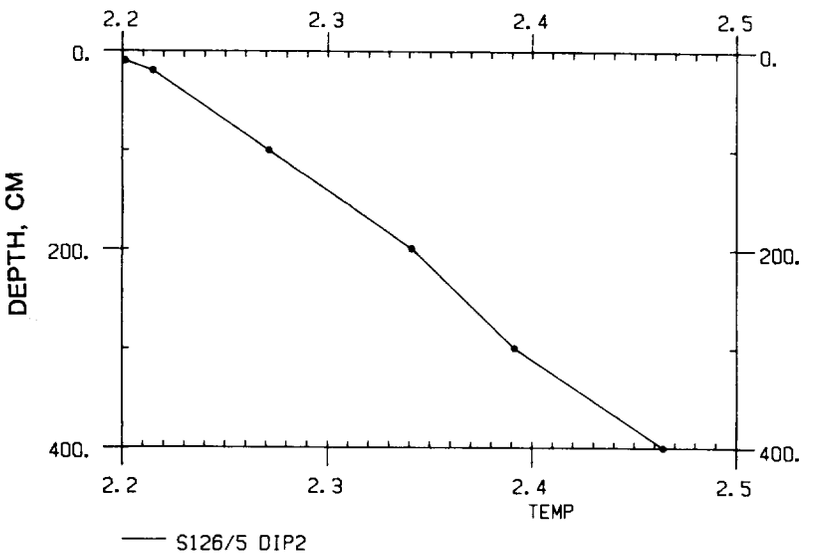
2.2
2.3
2.4
2.5
0.
200.
400.
DEPTH, CM
TEMP
S126/5 DIP2

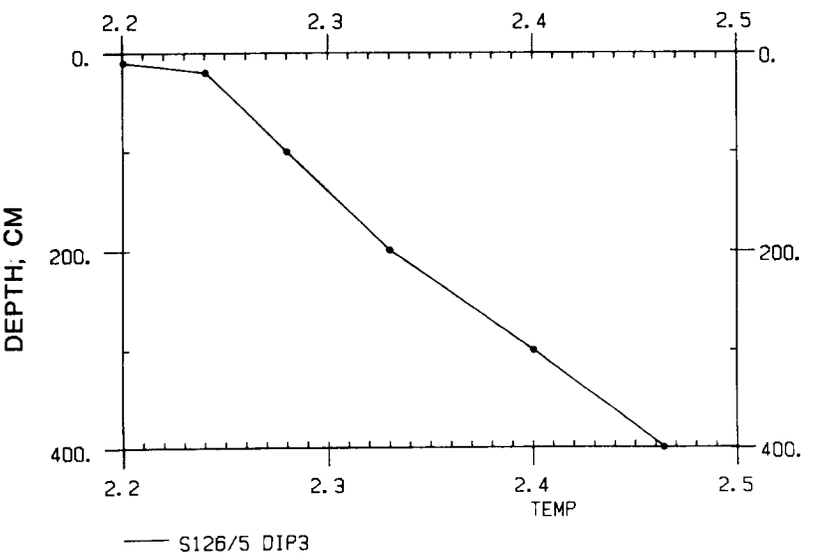
2.2
2.3
2.4
2.5
0.
200.
400.
DEPTH, CM
TEMP
S126/5 DIP3

FIG. 22

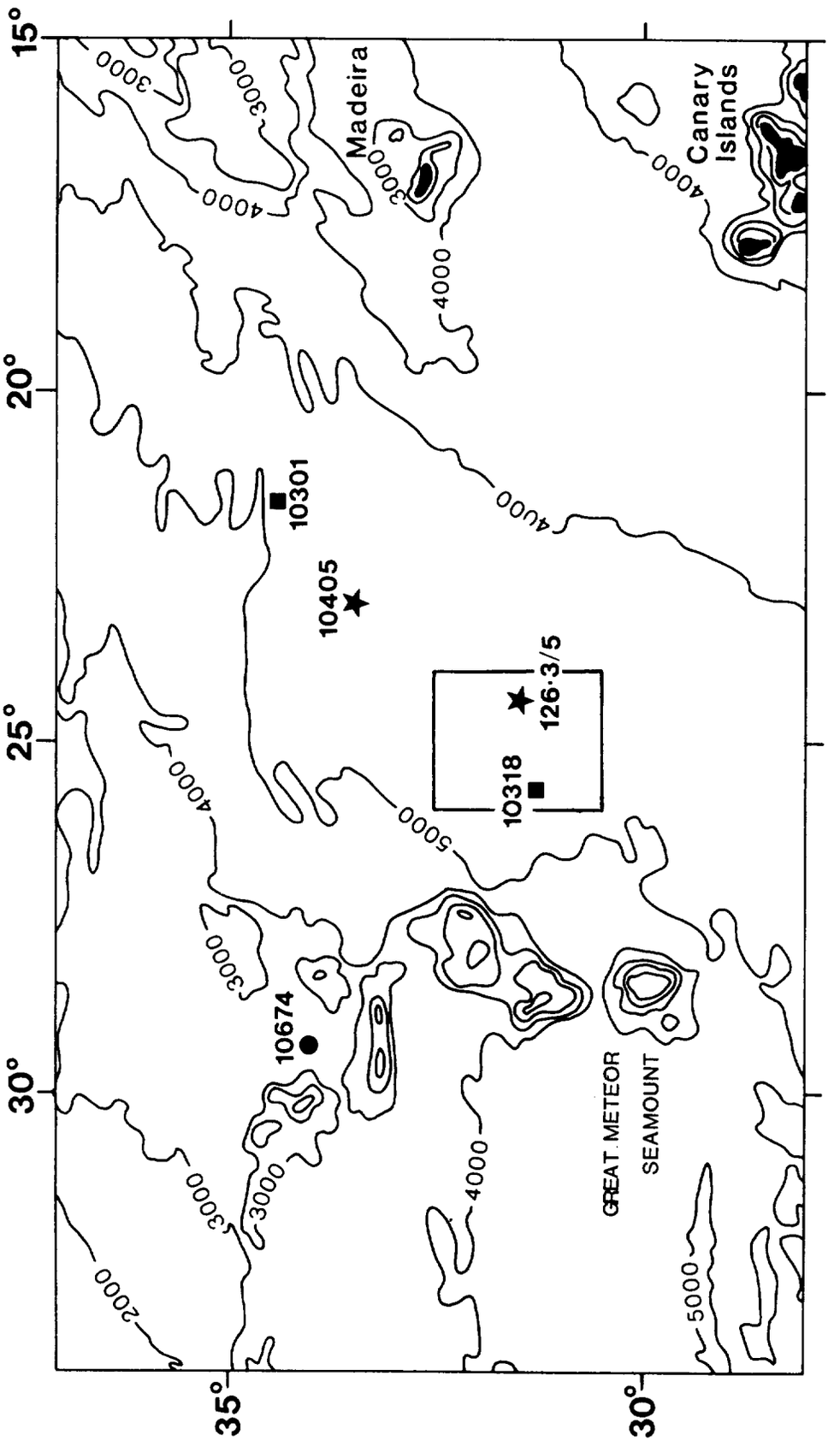
15°
20°
25°
30°
35°
30°
Madeira
Canary Islands
GREAT METEOR SEAMOUNT
10301
10405
10318
126·3/5
10674
2000
3000
4000
5000
CR 118 ■ CR 126 ★ CR 134 ●

FIG. 23

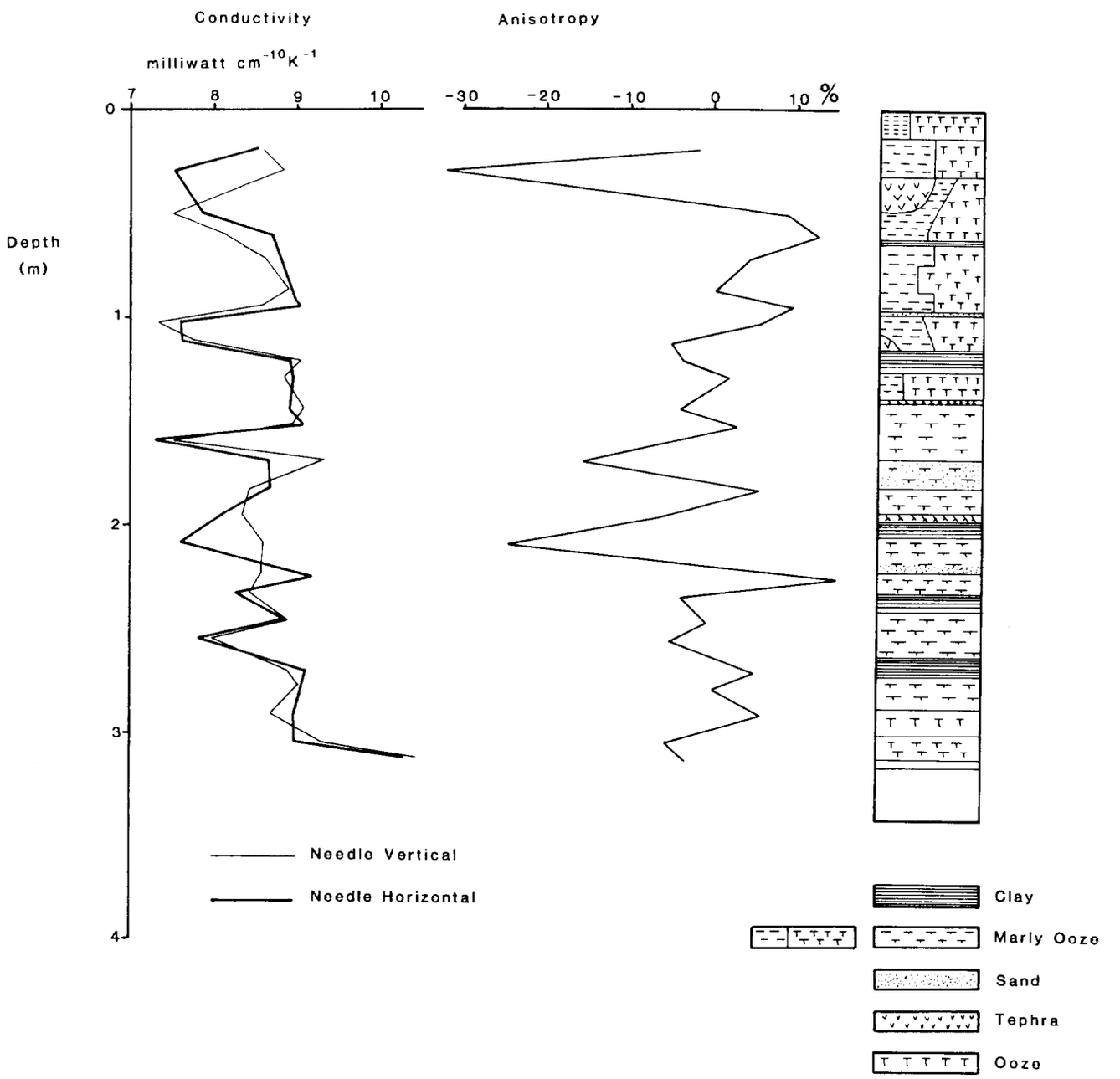
Core 10405 Eastern Madeira Abyssal Plain
Conductivity
milliwatt cm^{-1}K^{-1}
7
8
9
10
Anisotropy
-30
-20
-10
0
10
%
Depth
(m)
0
1
2
3
4
Needle Vertical
Needle Horizontal
Clay
Marly Ooze
Sand
Tephra
Ooze

FIG. 24

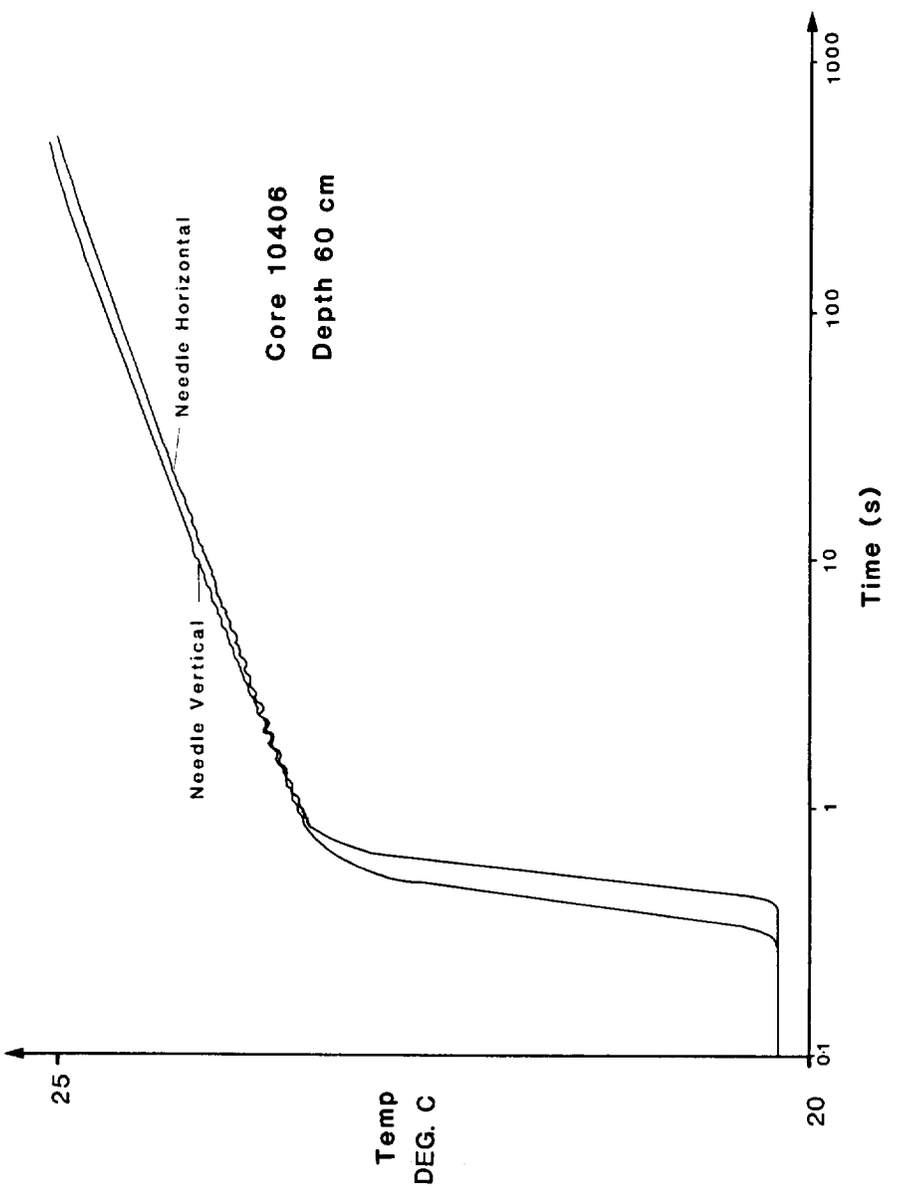
Core 10406
Depth 60 cm
Needle Horizontal
Needle Vertical
25
20
Temp
DEG. C
0.1
1
10
100
1000
Time (s)

FIG. 25

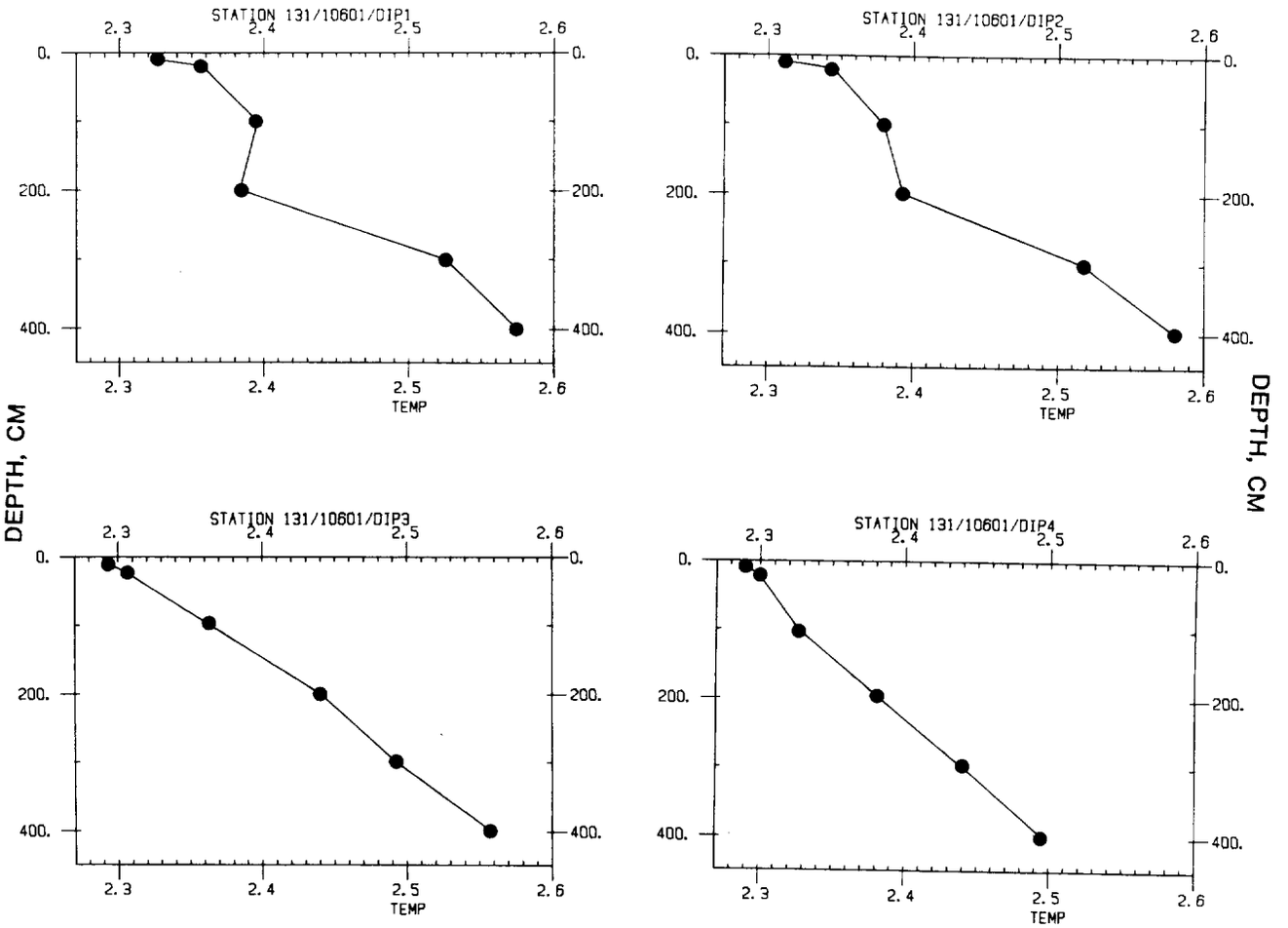
STATION 131/10601/DIP1
STATION 131/10601/DIP2
STATION 131/10601/DIP3
STATION 131/10601/DIP4
DEPTH, CM
DEPTH, CM
TEMP
2.3
2.4
2.5
2.6
0.
200.
400.

FIG. 26

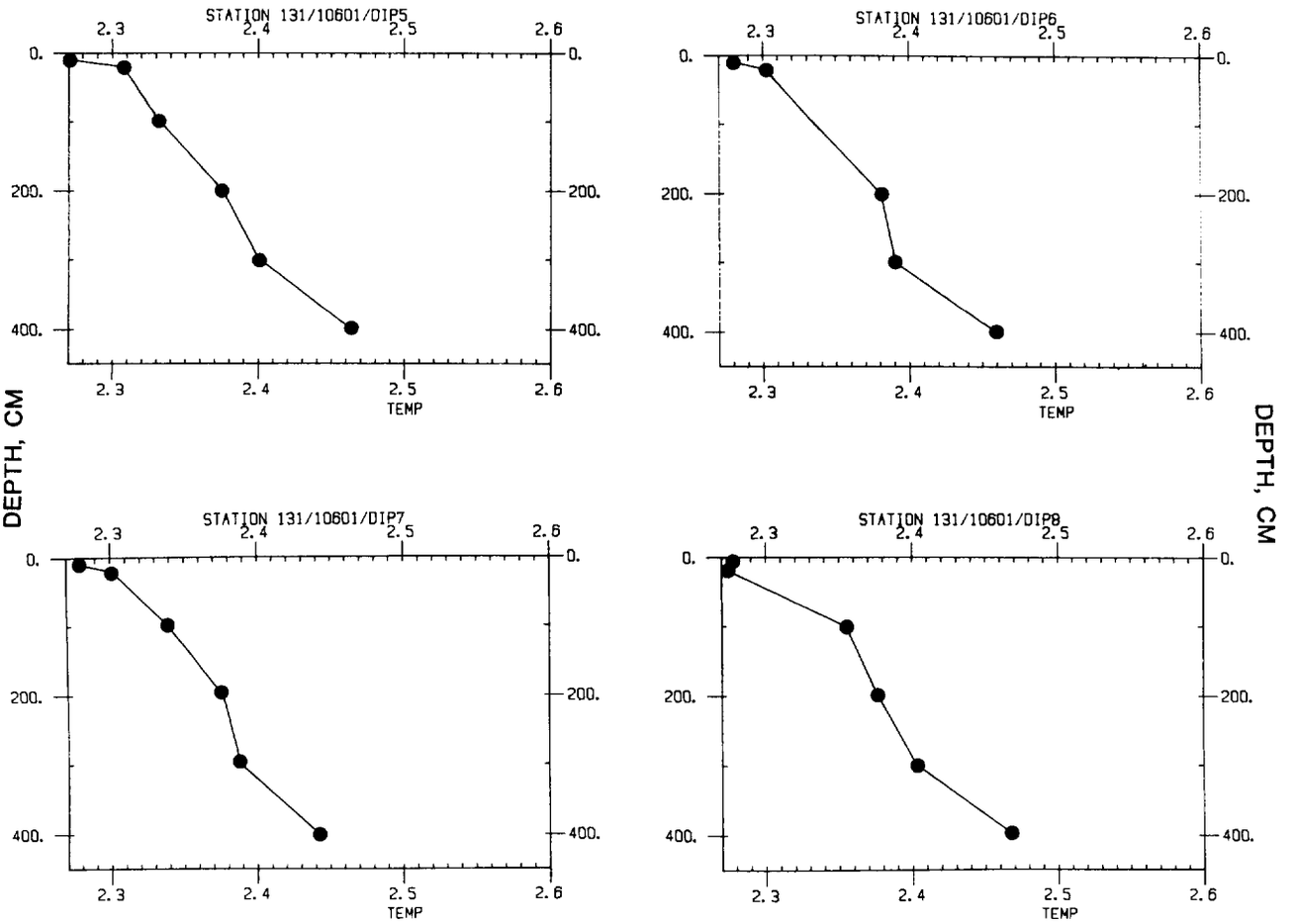
STATION 131/10601/DIP5
STATION 131/10601/DIP6
STATION 131/10601/DIP7
STATION 131/10601/DIP8
DEPTH, CM
DEPTH, CM
TEMP
TEMP
TEMP
TEMP
2.3
2.4
2.5
2.6
0.
200.
400.

FIG. 27

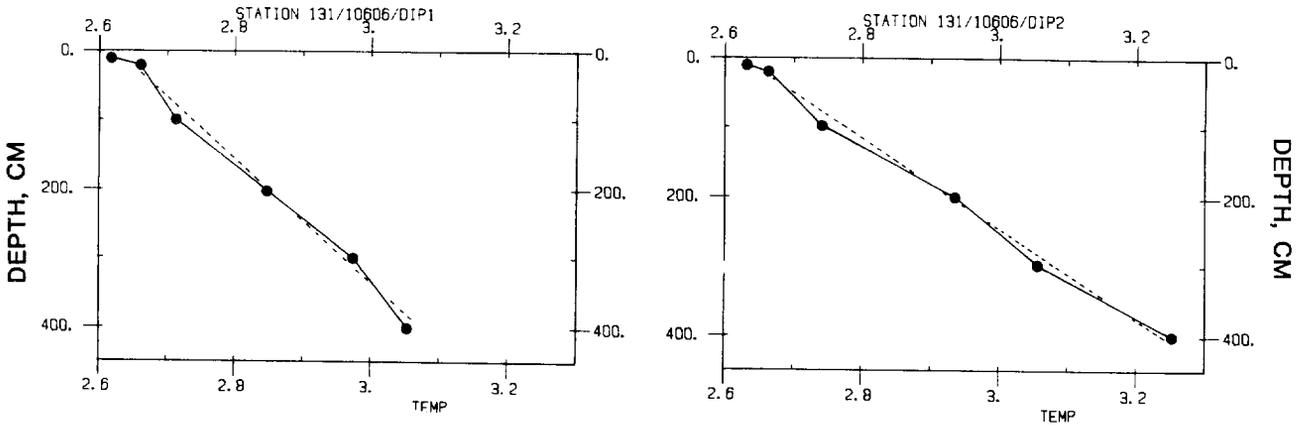
STATION 131/10606/DIP1
2.6
2.8
3.
3.2
0.
200.
400.
DEPTH, CM
TEMP
STATION 131/10606/DIP2
2.6
2.8
3.
3.2
0.
200.
400.
DEPTH, CM
TEMP

FIG. 28

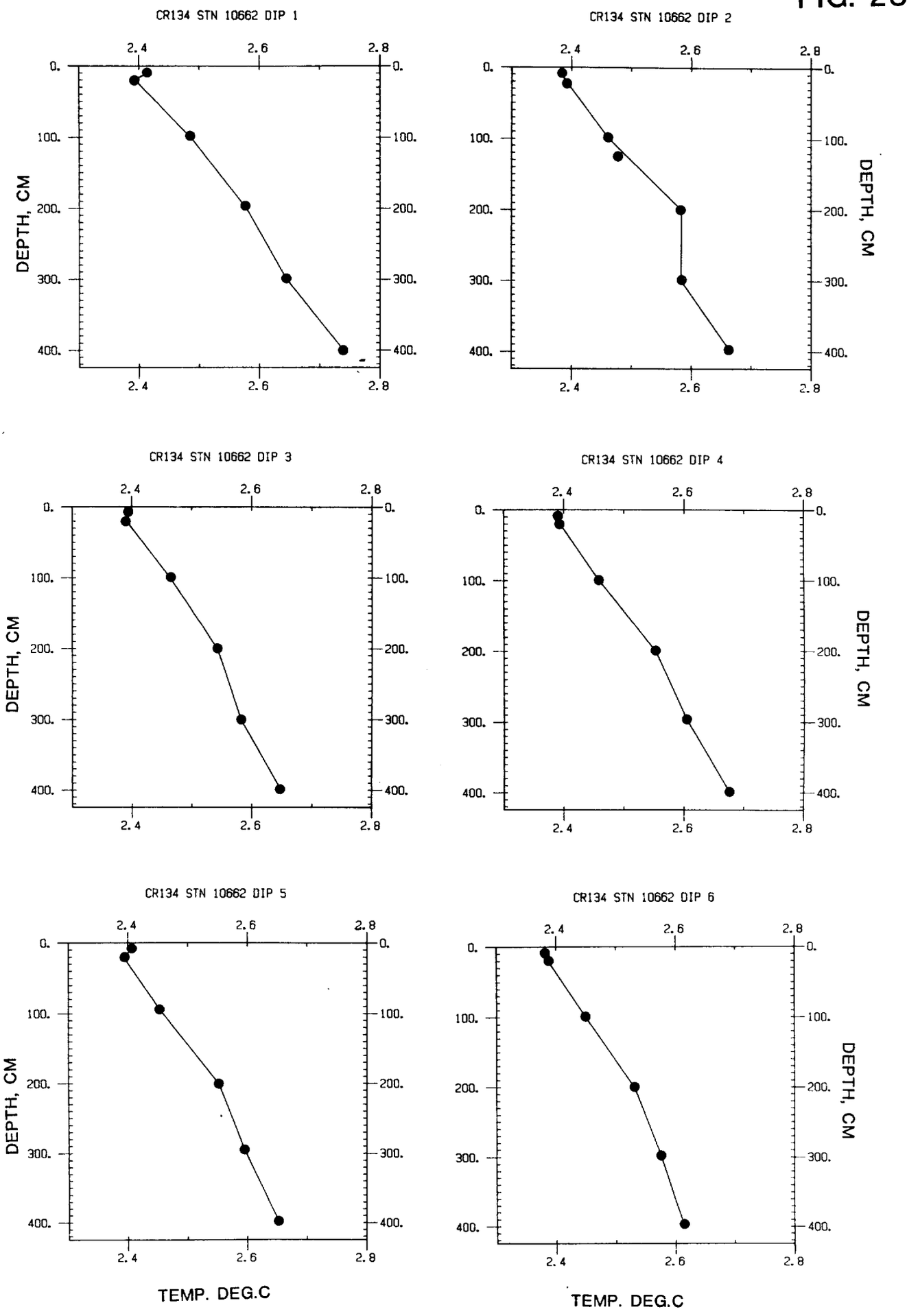
CR134 STN 10662 DIP 1
CR134 STN 10662 DIP 2
CR134 STN 10662 DIP 3
CR134 STN 10662 DIP 4
CR134 STN 10662 DIP 5
CR134 STN 10662 DIP 6
DEPTH, CM
TEMP. DEG.C
2.4
2.6
2.8
0.
100.
200.
300.
400.

FIG. 29

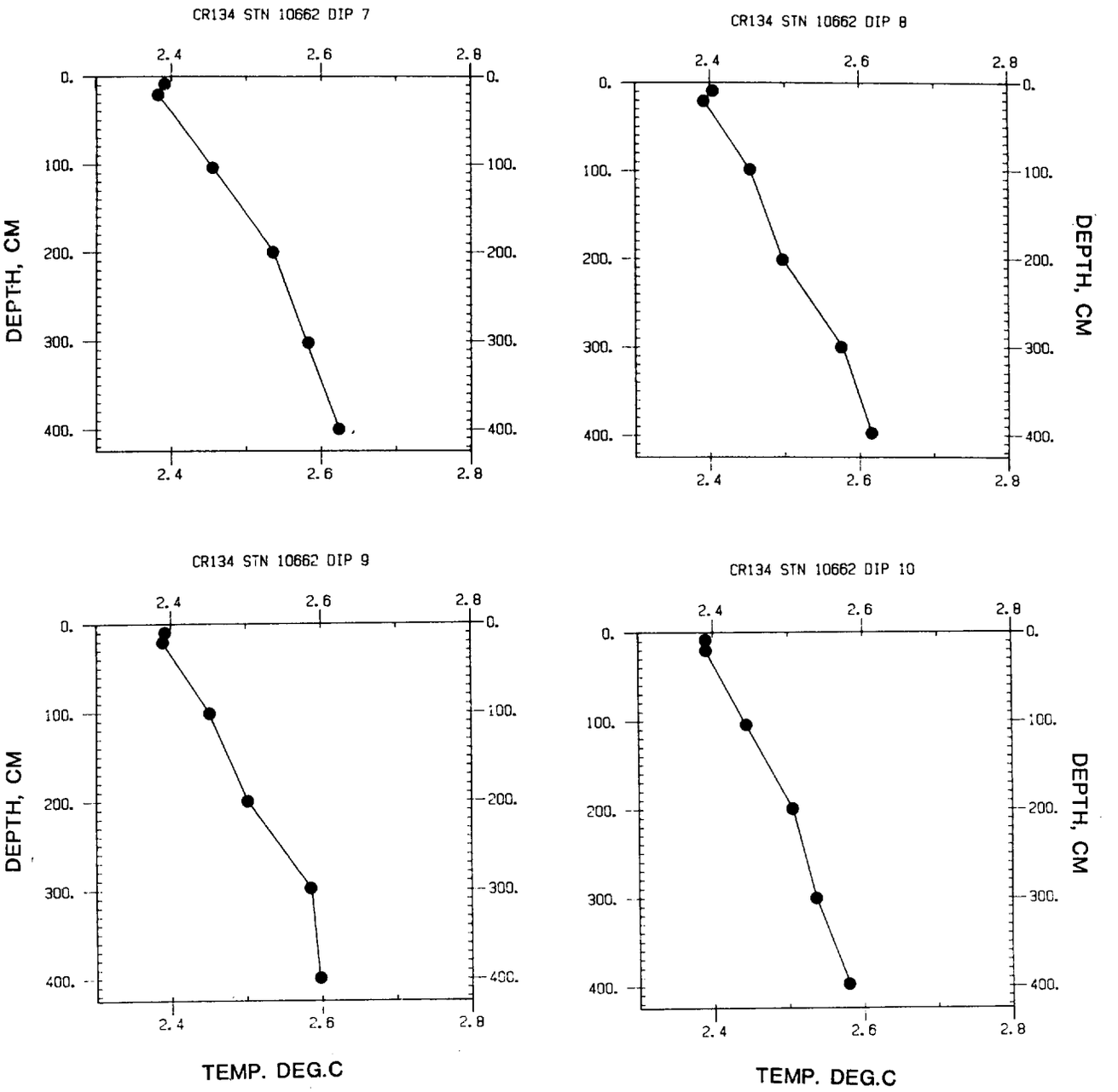
CR134 STN 10662 DIP 7
CR134 STN 10662 DIP 8
CR134 STN 10662 DIP 9
CR134 STN 10662 DIP 10
DEPTH, CM
TEMP. DEG.C
2.4
2.6
2.8
0.
100.
200.
300.
400.

FIG. 30

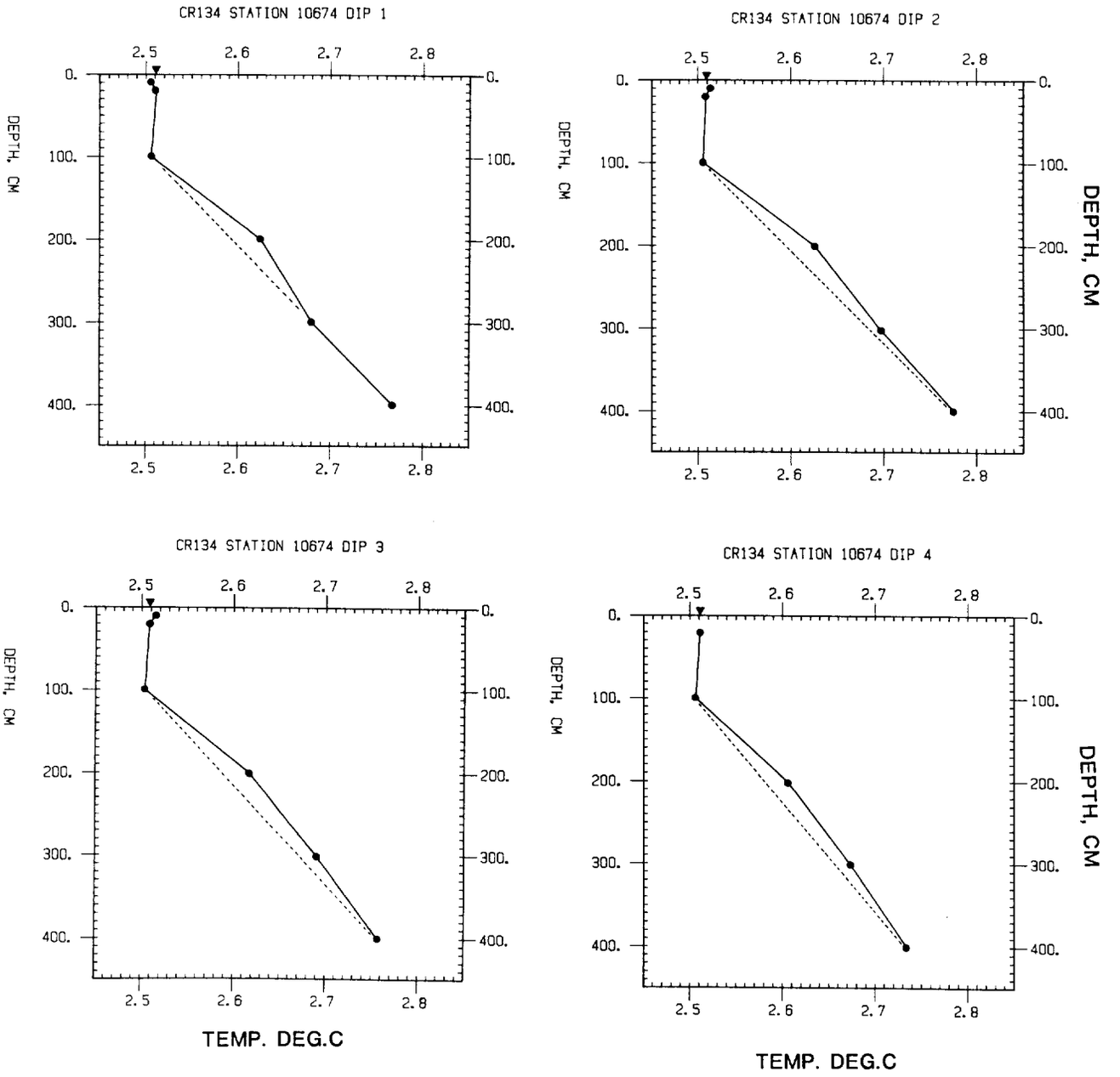
CR134 STATION 10674 DIP 1
CR134 STATION 10674 DIP 2
CR134 STATION 10674 DIP 3
CR134 STATION 10674 DIP 4
DEPTH, CM
TEMP. DEG.C
2.5
2.6
2.7
2.8
0.
100.
200.
300.
400.

FIG. 31

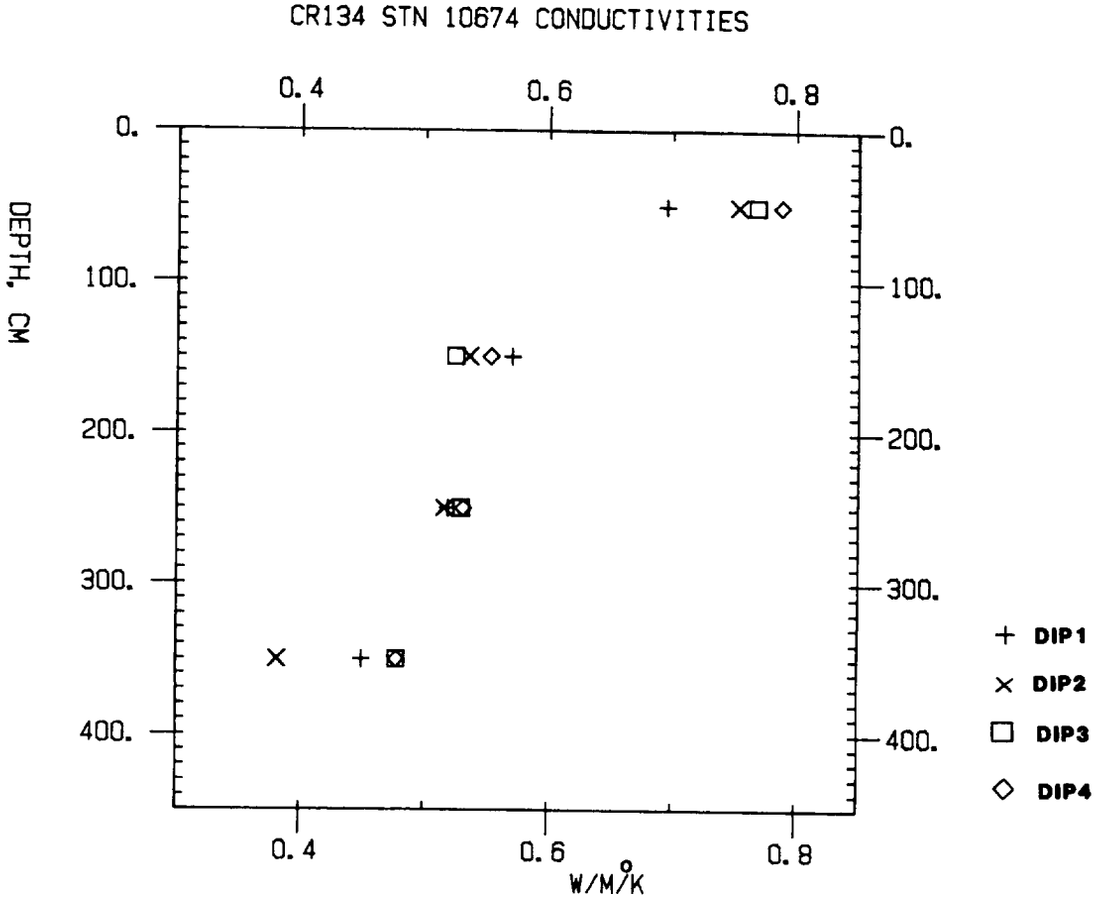
CR134 STN 10674 CONDUCTIVITIES
0.4
0.6
0.8
0.
100.
200.
300.
400.
DEPTH, CM
W/M/K°
DIP1
DIP2
DIP3
DIP4

FIG. 32

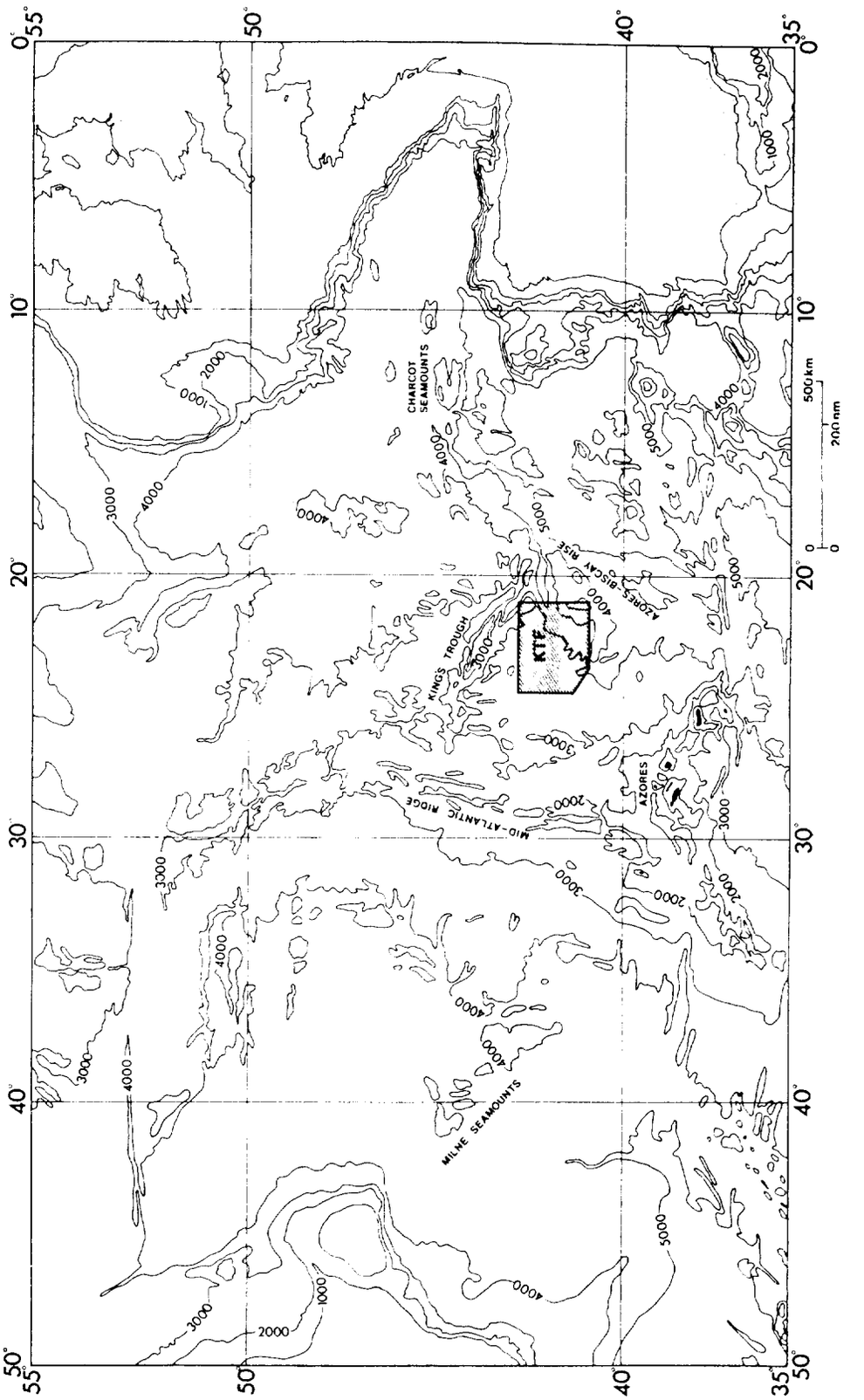
55°
50°
40°
35°
0°
10°
20°
30°
40°
50°
CHARCOT SEAMOUNTS
AZORES-BISCAY RISE
KINGS TROUGH
MID-ATLANTIC RIDGE
AZORES
MILNE SEAMOUNTS
KTF
500km
200nm
0
0
1000
2000
3000
4000
5000

FIG. 33

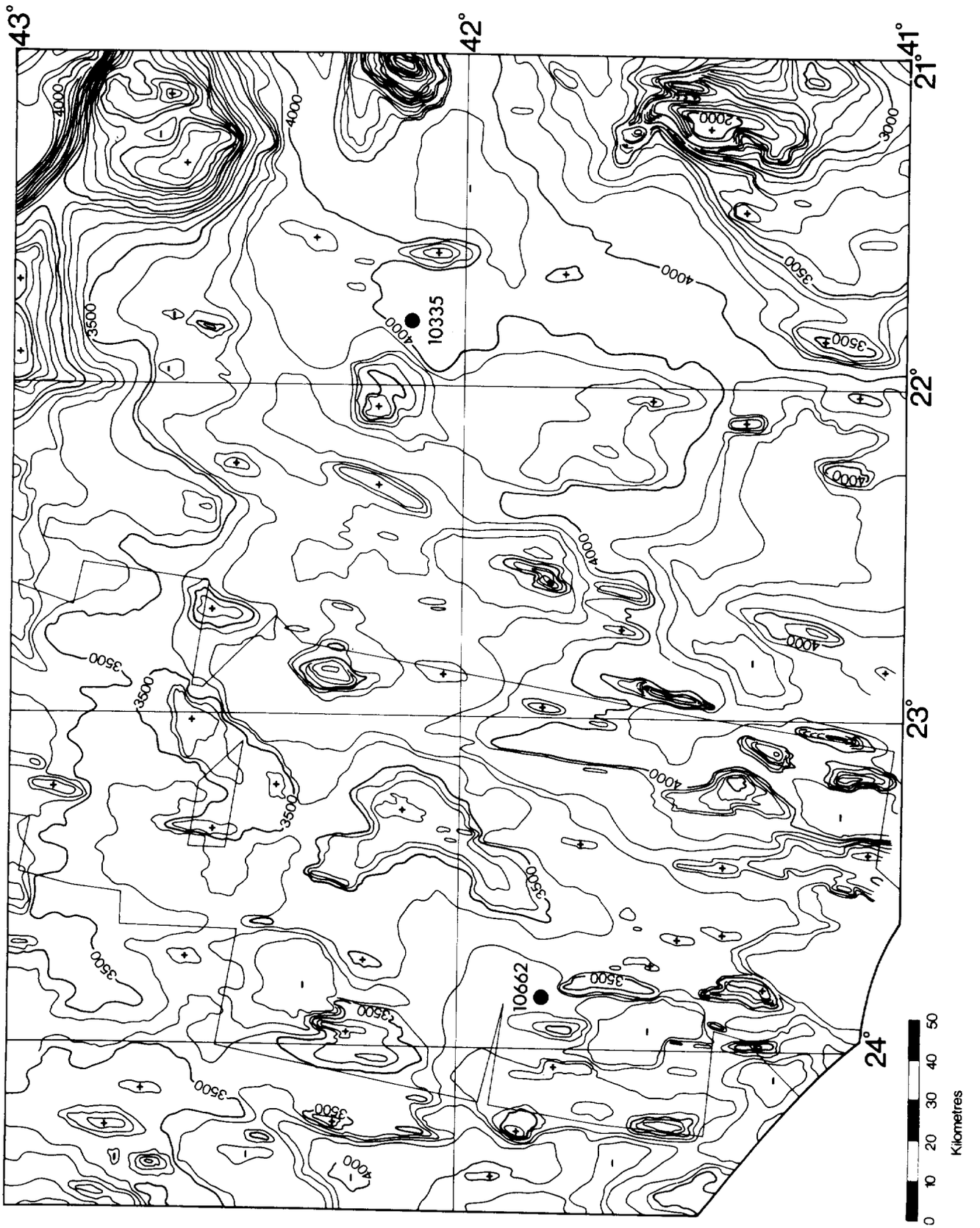
43°
42°
41°
21°
22°
23°
24°
10335
10662
4000
3500
3000
2000
0 10 20 30 40 50
Kilometres

GREAT METEOR EAST (GME)

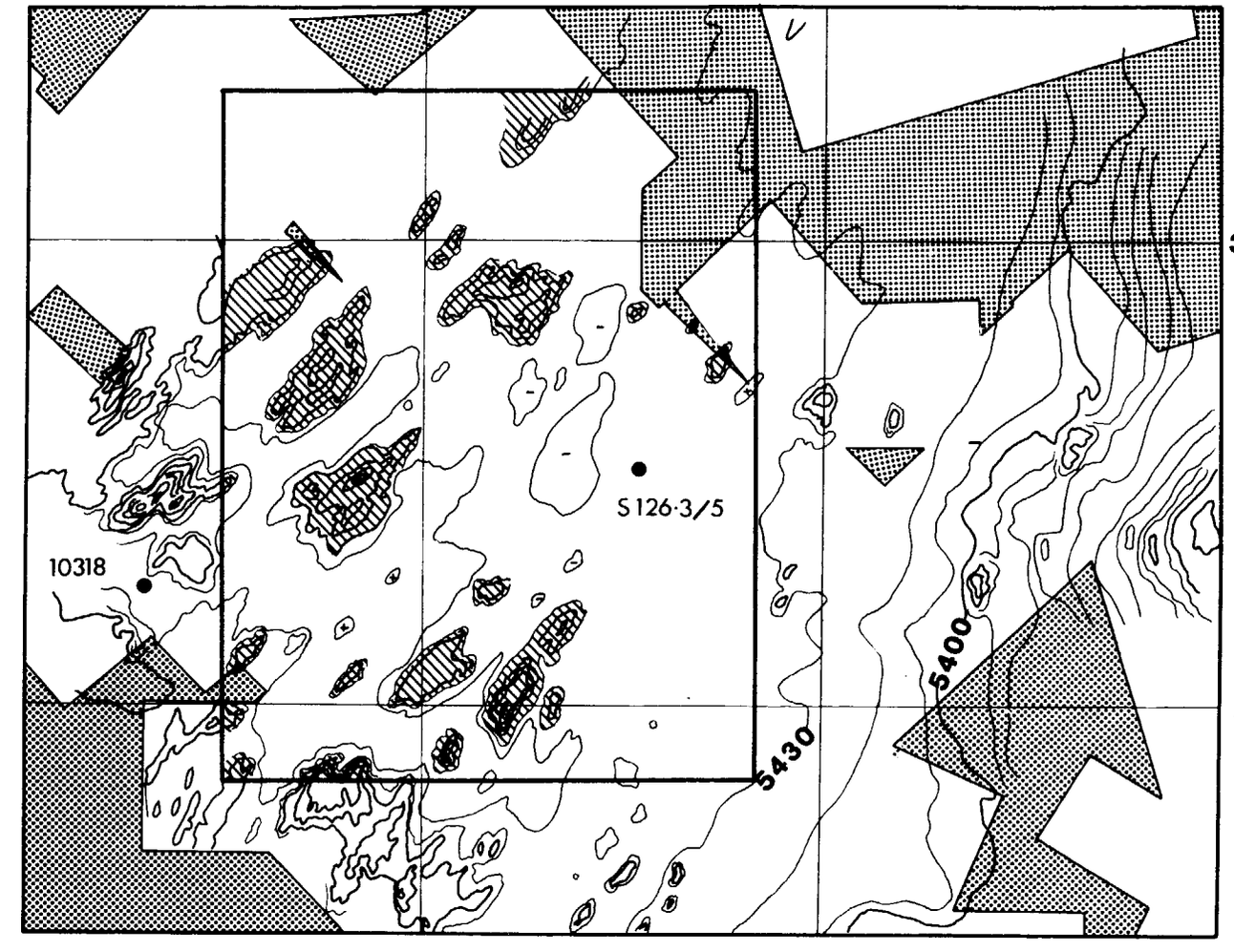

100m CONTOUR INTERVAL

10m CONTOUR INTERVAL

AREA SHALLOWER THAN 5430m

STIPPLED AREA - BEYOND RANGE OF GLORIA

FIG. 34